Report 76-0050

A PARAMETRIC SURVEY OF HYDROFOIL STRUT FLUTTER

DAVID W. TAYLOR NAVAL SHIP RESEARCH AND DEVELOPMENT CENTER

Bethesda, Md. 20084

A PARAMETRIC SURVEY OF HYDROFOIL STRUT FLUTTER

by

Peter K. Besch and
Edwin P. Rood, Jr.

SHIP PERFORMANCE DEPARTMENT
RESEARCH AND DEVELOPMENT REPORT

June 1976

Report 76-0050

MAJOR DTNSRDC ORGANIZATIONAL COMPONENTS

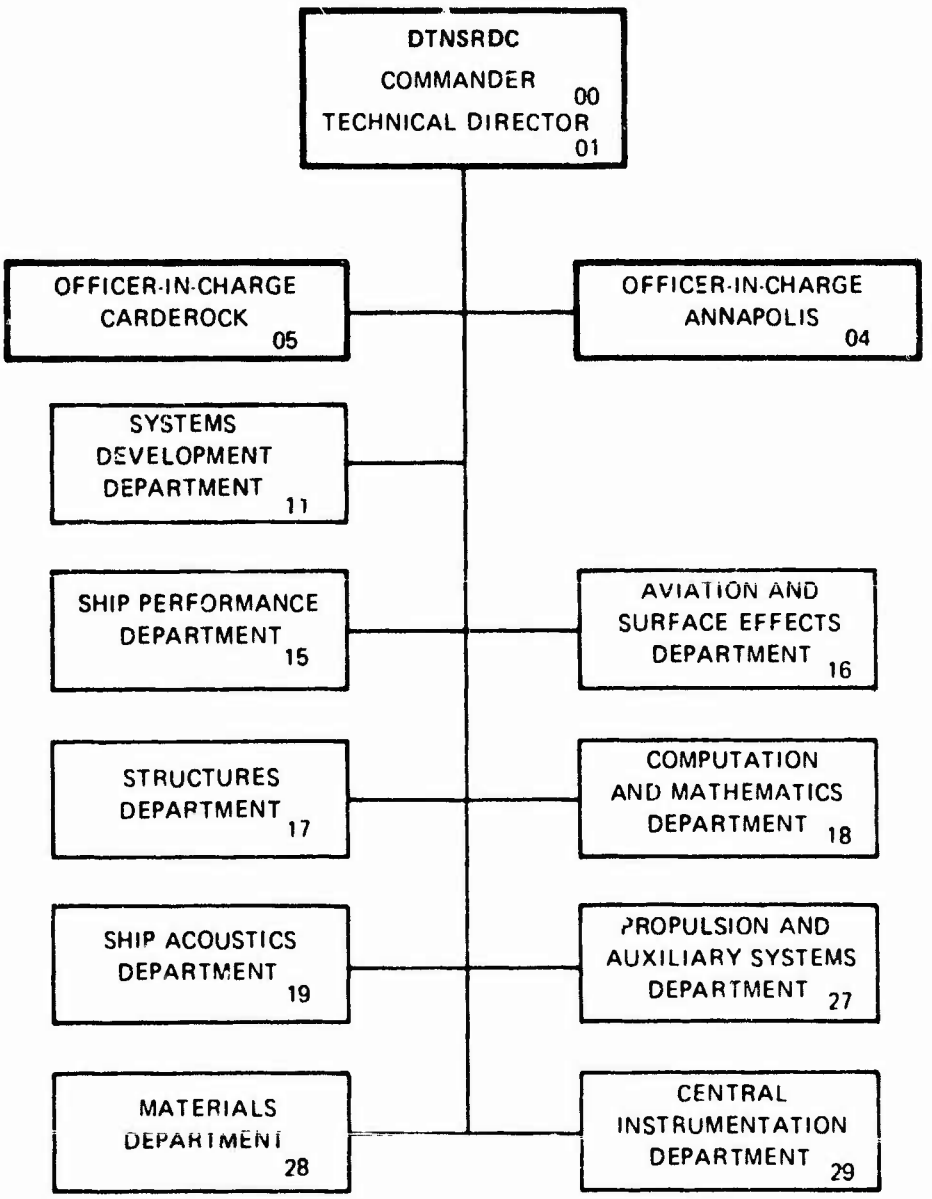

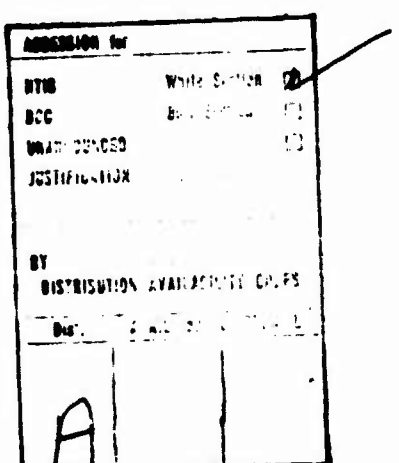

UNCLASSIFIED

SECURITY CLASSIFICATION OF THIS PAGE (When Data Entered)

REPORT DOCUMENTATION PAGE	READ INSTRUCTIONS BEFORE COMPLETING FORM
1. REPORT NUMBER: STNSRDC-76-0050	2. GOVT ACCESSION NO. / 3. RECIPIENT'S CATALOG NUMBER
4. TITLE (and Subtitle): A PARAMETRIC SURVEY OF HYDROFOIL STRUT FLUTTER	5. TYPE OF REPORT & PERIOD COVERED: Final rept.
	6. PERFORMING ORG. REPORT NUMBER
7. AUTHOR(s): Peter K. Besch and Edwin P. Rood, Jr.	8. CONTRACT OR GRANT NUMBER(s)
9. PERFORMING ORGANIZATION NAME AND ADDRESS: David W. Taylor Naval Ship Research and Development Center, Bethesda, Maryland 20084	10. PROGRAM ELEMENT, PROJECT, TASK AREA & WORK UNIT NUMBERS: (See reverse side)
11. CONTROLLING OFFICE NAME AND ADDRESS: (See reverse side)	12. REPORT DATE: June 1976 / 13. NUMBER OF PAGES: 116
14. MONITORING AGENCY NAME & ADDRESS(if different from Controlling Office): S4606, ZF43-421	15. SECURITY CLASS. (of this report): UNCLASSIFIED
	15a. DECLASSIFICATION/DOWNGRADING SCHEDULE

16. DISTRIBUTION STATEMENT (of this Report)

APPROVED FOR PUBLIC RELEASE: DISTRIBUTION UNLIMITED

ZF43-421-001

17. DISTRIBUTION STATEMENT (of the abstract entered in Block 20, if different from Report)

18. SUPPLEMENTARY NOTES

19. KEY WORDS (Continue on reverse side if necessary and identify by block number)

Hydrofoil - Strut - Flutter - Bending, Torsional - Divergence - Vibration - Hydrofoil - Strut - Damping - Model - Hydroelastic Hydrodynamics - Subcavitating, Supercavitating, Ventilation

20. ABSTRACT (Continue on reverse side if necessary and identify by block number)

In order to explore the fundamental nature of hydrofoil flutter, a hydroelastic instability which is a potential cause of structural failure of lifting surfaces operating at high speeds in water, a series of hydrofoil models was tested in a towing basin.

Flutter data were obtained from four surface-piercing hydrofoil strut

(Continued on reverse side)

DD FORM 1 JAN 73 1473 EDITION OF 1 NOV 65 IS OBSOLETE S/N 0102-014-6601

UNCLASSIFIED

SECURITY CLASSIFICATION OF THIS PAGE (When Data Entered)

387682

(Block 10)

NAVSHIPS Subproject S4606 (NAVSEA)
Task 1703
Work Units 1-1153-703 and 1-1153-003
NAVMAT Program Element 62754N
Task Area ZF43-421-001 ZF43-421-001
Work Unit 1-1520-001

(Block 11)

Naval Sea Systems Command
Washington, D.C. 20362

Naval Material Command
Washington, D.C. 20360

(Block 20 continued)

models with various pod and foil configurations. Flutter occurred in two independent hydroelastic modes having predominantly first bending and first torsion mode shapes, respectively. The unstable modes were found to exist simultaneously in at least one strut. Flutter inception speed of the bending flutter mode was affected by strut submergence and the presence or absence of a foil. Flutter inception speed of the torsional flutter mode was dependent on strut cavitation pattern, strut submergence, pod moment of inertia, pod length, and the presence or absence of a foil.

TABLE OF CONTENTS

LIST OF FIGURES

LIST OF TABLES

NOTATION

AR	Aspect ratio of submerged structure; (submerged span)^2/(submerged area)
a	Distance between the two bifilar pendulum suspension points, which were equidistant from pod center of gravity
c	Chord length of strut, measured perpendicular to elastic axis
c_{root}	Chord length of foil extended to pod centerline, measured parallel to free stream
c_s	Structural damping of a given vibration mode
c_{tip}	Chord length at tip of foil, measured parallel to free stream
EI	Bending stiffness of section normal to elastic axis
F_n	Froude number based on streamwise chord of strut, $U/\sqrt{gc/\cos \Lambda}$
f	Frequency of oscillation
f_f	Frequency of oscillation at flutter inception
GJ	Torsional stiffness of section normal to elastic axis
g	Acceleration due to gravity
h	Local depth at elastic axis
I_{cg}	Moment of inertia about center of gravity
I_{my}	Moment of inertia per unit span of strut, in air, about strut elastic axis
I_ϕ	Total moment of inertia of structure in air, about pod longitudinal axis
I_y	Total moment of inertia of strut, pod, or foil in air, about strut elastic axis
I_y^*	Total added moment of inertia of strut, pod, or foil due to rotation about strut elastic axis

k_{nf}	Reduced frequency at flutter inception; $c\omega_f/2U_{nf}$
L	Length of strut along elastic axis
ℓ	Submerged length of strut elastic axis
M	Total mass of structure in air
M*	Total added mass of strut or pod due to translation normal to strut chord plane
m	Mass per unit span, in air
p_a	Pressure of atmosphere above free surface
p_c	Pressure in a cavity
p_v	Water vapor pressure
R_{nf}	Reynolds number based on streamwise chord of strut; $U_f\ c/\nu \cos \Lambda$
s	Length of each of the lines suspending the pod as a bifilar pendulum
T	Period of bifilar pendulum oscillation
t	Ordinate of section profile measured normal to the axis of symmetry
t_0	Time at beginning of interval Δt over which decay curve is analyzed
Δt	Time interval over which decay curve is analyzed, chosen to span an integral number of cycles
U	Flow speed, or speed of structure through fluid
U_D	Flow speed at divergence instability
U_f	Flow speed at flutter inception
U_{nf}	Component of flow velocity at flutter inception, normal to strut elastic axis; $U_f \cos \Lambda$
x	Distance from centroid of section, measured along axis of symmetry
$\bar{x}$	Distance of elastic axis from section centroid, measured along axis of symmetry

x_{cg}	Distance from strut leading edge to center of gravity, measured perpendicular to strut elastic axis
x_{ea}	Distance from strut leading edge to strut elastic axis location, measured perpendicular to elastic axis
x_{foil}	Distance from leading edge of foil extended to midspan to leading edge of strut, measured along pod longitudinal axis, positive aft
x_{nose}	Distance from pod nose to leading edge of strut, measured along longitudinal axis of pod
y	Spanwise coordinate along strut elastic axis
y_1	Net displacement between local maximum at time t_0 and local minimum 1/2 cycle later
y_2	Net displacement between local maximum at time $t_0 + \Delta t$ and local minimum 1/2 cycle later
ζ (zeta)	Damping ratio; damping as a fraction of critical damping
ζ_s	Damping ratio due to structural damping
η (eta)	Poisson's ratio (approximately 0.3 for aluminum and steel)
κ (kappa)	Sweep parameter; $(c \tan \Lambda)/L$
Λ (lambda)	Sweep angle of quarter chord, positive for sweepback
$\mu_{bending}$ (mu)	Approximation to generalized mass ratio for bending motion
$\mu_{torsion}$	Approximation to generalized mass ratio for torsional motion
ν (nu)	Kinematic viscosity of water; 1.0×10^{-5} ft^2/sec
π (pi)	≈ 3.1416
ρ (rho)	Mass density of fluid in which structure is operated
σ (sigma)	Cavitation number based on water vapor pressure; $\dfrac{(p_a + \rho gh - p_v)}{1/2\ (\rho U^2)}$

σ_c	Cavitation number based on actual cavity pressure; $\frac{(p_a + \rho gh - p_c)}{1/2\ (\rho U^2)}$
τ (tau)	Taper ratio; (foil tip chord)/(foil root chord)
ω (omega)	Circular frequency of oscillation; $2\pi f$
ω_h	Circular frequency of first bending vibration mode in air
ω_α	Circular frequency of first torsional vibration mode in air

Subscripts

foil	Value associated with foil
pod	Value associated with pod
strut	Value associated with strut

ADMINISTRATIVE INFORMATION

This work was authorized and funded primarily under the Hydrofoil Development Program of the Naval Sea Systems Command, Subproject S4606, Task 1703, Work Units 1-1153-003 and 1-1153-703. Additional support was given by the Naval Material Command under Program Element 62754N, Task Area ZF43-421-001, Work Unit 1-1520-001.

This report was prepared prior to adoption of a policy requiring inclusion of metric units in Department of the Navy publications. In the interests of time and economy, metric units have not been added.

INTRODUCTION

Experimental and theoretical research into hydrofoil flutter has led to a good qualitative understanding of the flutter characteristics of strut systems.[1,2] Furthermore, usable quantitative predictions can now be made analytically when flutter occurs in the torsional flutter mode, although they still cannot be made for the bending flutter mode. Such predictions are possible only for subcavitating or base-vented flow conditions. Predictions in the remaining situations require a kinematically scaled model.

This degree of understanding has been developed on the basis of a large body of data which has not previously been documented in a detailed manner, although various results have been given.[1,2] The data supporting these previous publications pertain largely to simple hydrofoil strut systems and struts with attached tip pods. More recently, data have been acquired from a strut and attached foil that form a more realistic inverted-T configuration. The present report has been prepared to provide a complete description of all of the available data.

---

[1]Besch, P.K. and Y.-N. Liu, "Bending Flutter and Torsional Flutter of Flexible Hydrofoil Struts," Ninth Symposium on Naval Hydrodynamics, Paris, France (20-25 Aug 1972); also available as NSRDC Report 4012 (Feb 1973). A complete listing of references is given on page 100.

[2]Besch, P.K and Y.-N. Liu, "Hydroelastic Design of Subcavitating and Cavitating Hydrofoil Strut Systems," NSRDC Report 4257 (Apr 1974).

The objectives of the present experimental work were (1) to identify important flutter parameters and (2) to gain a working knowledge of the phenomenon of hydrofoil flutter, which had had a certain aura of mystery about it. Much of this mystery has been dispelled by better understanding of the two separate modes of flutter.[1] The broad nature of the objectives led to the use of several highly dissimilar models. Consequently, it will be observed that the data are incomplete for any one model or any one parameter. It is hoped that areas of particular importance will be pursued in future research.

This report describes the flutter characteristics of four surface-piercing strut models with various tip attachments (pods and a foil) and cavitation-producing profiles. Of special interest is the clear demonstration, for the first time, of the coexistence of two flutter modes in a strut system. Model parameters and experimental techniques of flutter testing are described in detail. It is hoped that these detailed descriptions and the reported strut behavior will give the reader some "feel" for the nature of the phenomenon of hydrofoil flutter.

DESCRIPTION OF THE MODELS

Two existing and two newly constructed strut models were used. In some instances, long, slender struts were combined with relatively large, heavy pods and foil to produce low flutter speeds and thus facilitate research.

All four struts were nearly the same size, having untapered chord lengths of approximately 12 in. and lengths of 4 to 5 ft. The struts differed primarily in profile (blunt base, blunt leading edge, or streamlined) and in stiffness (a function of material and profile). Pod diameters of 2 and 6 in. were used.

Model parameters in dimensional and nondimensional form are given in Tables 1 and 2, respectively. Geometrical parameters are indicated in Figure 1. The models are described in order of increasing complexity.

TABLE 1 - DIMENSIONED FLUTTER PARAMETERS FOR EXPERIMENTAL STRUT MODELS

TABLE 1a - MODEL A

Strut Parameters		Flutter Condition		
c, in.	12.0	ℓ, in.	42.9	32.0
L, in.	48.0	U_f, knots	35.5	39.8
Λ, deg	8.0	f_f, Hz	1.1	1.0
x_{ea}, in.	5.5	Mode Shape	Bending	Bending
x_{cg}, in.	7.2			
m, lb/in.	0.38			
I_{my}, lb-in.	4.5			
EI, lb-in.^{2}	1.7×10^5			
GJ, lb-in.^{2}	3.7×10^5			
Profile	Parabolic, 3.8% thick			

TABLE 1b - MODEL 2T

Strut Parameters		Pod Parameters						
		Pod Configuration	C	D	G			
c, in.	11.6	Length, in.	31.7	31.7	37.7			
L, in.	49.2	Max. diameter, in.	2.0	2.0	2.0			
Λ, deg	15	x_{nose}, in.	6.0	6.0	6.0			
x_{ea}, in.	7.9	$x_{cg,\ pod}$, in.	18.7	20.4	21.9			
x_{cg}, in.	6.8	M, lb	23.3	23.3	38.2			
m, lb/in.	1.07	$I_{y,\ pod}$, lb-in.^{2}	1620	2400	4680			
I_{my}, lb-in.	11.7	Flutter Condition						
EI, lb-in.^{2}	1.3×10^6	ℓ, in.	38.9	38.9	38.9	19.7	14.8	9.8
GJ, lb-in.^{2}	2.1×10^6	U_f, knots	37.0	27.7	18.3	17.0	19.6	25.0
Profile	Blunt base	f_f, Hz	8.0	7.9	6.4	7.6	7.9	8.0
	3.4% thick	Mode Shape	Torsion	Torsion	Torsion	Torsion	Torsion	Torsion

TABLE 1c - MODEL ALPHA

Strut Parameters		Pod Parameters		
		Pod Configuration	A	B
c, in.	12.0	Length, in.	44.0	44.0
L, in.	47.9	Max. diameter, in.	6.0	6.0
Λ, deg	15.0	x_{nose}, in.	16.2	16.2
x_{ea}, in.	10.3	$x_{cg,\ pod}$, in.	22.0	22.0
x_{cg}, in.	7.0*	M, lb	61.7	24.0
m, lb/in.	0.344*	$I_{y,\ pod}$, lb-in.^{2}	4760	2760
I_{my}, lb-in.	4.15*	Flutter Condition		
EI, lb-in.^{2}	4.83×10^5	ℓ	24.0	24.0
GJ, lb-in.^{2}	6.31×10^5	U_f, knots	6.5	18.6
Profile	Parabolic,	f_f, Hz	3.7	4.7
	3.9% thick	Mode Shape	Torsion	Torsion

*Values do not include shaker linkage and strut clamp located approximately 12.5 in. below strut root and weighing approximately 4 lb.

TABLE 1d - MODEL BETA WITH STREAMLINED PROFILE

Strut Parameters		Pod Parameters		
		Pod Configuration	A	B
c, in.	12.0	Length, in.	44.0	44.0
L, in.	58.4	Max. diameter, in.	6.0	6.0
Λ, deg	15.0	x_{nose}, in.	16.2	16.2
x_{ea}, in.	4.5	$x_{cg,\ pod}$, in.	22.0	22.0
x_{cg}, in.	6.2	M, lb	140.0	77.3
m, ib/in.	0.588	$I_{y,\ pod}$, lb-in.^{2}	15,700	7,070
I_{my}, lb-in.	8.21	Flutter Condition		
EI, lb-in.^{2}	7.58×10^5	ℓ, in.	30.4	30.4
GJ, lb-in.^{2}	10.4×10^5	U_f, knots	6.6	8.4
Profile	NACA 16-005	f_f, Hz	2.9	3.5
		Mode Shape	Torsion	Torsion

TABLE 1e - MODEL BETA WITH BLUNT BASE PROFILE

Strut Parameters		Pod Parameters			
		Pod Configuration	A	B	C
c, in.	12.0	Length, in.	44.0	44.0	44.0
L, in.	58.4	Max. diameter, in.	6.0	6.0	6.0
Λ, deg	15.0	x_{nose}, in.	16.2	16.2	16.2
x_{ea}, in.	4.5	$x_{cg,\ pod}$, in.	22.0	22.0	22.0
x_{cg}, in.	6.6*	M, lb	140.0	77.3	31.4
m, lb/in.	0.638*	$I_{y,\ pod}$, lb-in.^{2}	15,700	7,070	3,080
I_{my}, lb-in.	10.6*	Flutter Condition			
EI, lb-in.^{2}	7.34×10^5	ℓ	30.4	30.4	30.4
GJ, lb-in.^{2}	10.4×10^5	U_f, knots	5.9	7.0	12.7
Profile	Blunt base,	f_f, Hz	3.0	3.5	5.0
	5% thick	Mode Shape	Torsion	Torsion	Torsion

*Values do not include shaker linkage and strut clamp located 18 in. below strut root and weighing approximately 4 lb.

TABLE 1f - MODEL BETA WITH BLUNT LEADING EDGE PROFILE, WITHOUT FOIL

Strut Parameters		Pod Parameters						
		Pod Configuration	A	B	C	D	E	
c, in.	12.0	Length, in.	44.0	44.0	44.0	28.5	28.5	
L, in.	58.4	Max. diameter, in.	6.0	6.0	6.0	6.0	6.0	
Λ, deg	15.0	x_{nose}, in.	16.2	16.2	16.2	8.5	8.5	
x_{ea}, in.	4.5	$x_{cg,\ pod}$, in.	22.0	22.0	22.0	14.3	14.3	
x_{cg}, in.	6.5,* 6.8**	M, lb	140.0	77.3	31.4	59.4	33.9	
m, lb/in.	0.66,* 0.70**	$I_{y,\ pod}$, lb-in.^{2}	15,700	7,070	3,080	3,600	1,500	
I_{my}, lb-in.	11.6,* 13.6**	Flutter Condition						
EI, lb-in.^{2}	7.35×10^5	ℓ, in.	30.4	30.4	30.4	30.4	30.4	16.4
GJ, lb-in.^{2}	10.4×10^5	U_f, knots	6.2	7.5	8.2	10.7	12.2	12.1
Profile	Blunt leading	f_f, Hz	2.9	3.5	5.0	5.7	7.7	7.9
	edge	Mode Shape	Torsion	Torsion	Torsion	Torsion	Torsion	Torsion

*Pod Configurations A, B, and C; values do not include shaker linkage and strut clamp located 18 in. below strut root and weighing approximately 4 lb.

**Pod Configurations D and E, tested with air line attached to strut trailing edge; shaker linkage and strut clamp not included (see note above).

TABLE 1g - MODEL BETA WITH BLUNT LEADING EDGE PROFILE AND FOIL WITH HEAVIER WEIGHT POD

Strut Parameters		Foil Parameters	
c, in.	12.0	Area, $in.^2$	298
L, in.	58.4	c_{root}, in.	14.4
Λ, deg	15.0	c_{tip}, in.	10.0
x_{ea}, in.	4.5	Full span, in.	24.4
x_{cg}, in.	6.8†	Λ, deg	12.0
m, lb/in.	0.70†	x_{foil}, in.	1.4
I_{my}, lb-in.	13.6†	M, lb	31.9
EI, $lb\text{-}in.^2$	7.35×10^5	$x_{cg,\ pod + foil}$, in.	††
GJ, $lb\text{-}in.^2$	10.4×10^5	$I_{\phi,\ pod + foil}$, $lb\text{-}in.^2$	619†††
Profile	Blunt leading edge	$I_{y,\ pod + foil}$, $lb\text{-}in.^2$	4,950
		Profile	NACA 16-012 with vent. trip
Pod DF Parameters		Angle of attack, deg	0.0
Length, in.	28.5	**Flutter Condition**	
Max. dia., in.	6.0	ℓ, in.	30.4 16.4
x_{nose}, in.	8.5	U_f, knots	11.2 9.5
x_{cg}, in.	14.3	f_f, Hz	4.9 1.3
M, lb	61.8	Mode Shape	Torsion Bending

†Air line attached to strut trailing edge; values do not include shaker linkage and strut clamp located 18 in. below strut root and weighing 5.8 lb.

††Not measured; value is between 14.25 and 14.6 in.

†††Calculated.

TABLE 1h - MODEL BETA WITH BLUNT LEADING EDGE PROFILE AND FOIL WITH LIGHTER WEIGHT POD

Strut Parameters		Foil Parameters	
c, in.	12.0	Area, $in.^2$	298
L, in.	58.4	c_{root}, in.	14.4
Λ, deg	15.0	c_{tip}, in.	10.0
x_{ea}, in.	4.5	Full span, in.	24.4
x_{cg}, in.	6.8†	Λ, deg	12.0
m, lb/in.	0.70†	x_{foil}, in.	1.4
I_{my}, lb-in.	13.6	M, lb	31.9
EI, $lb\text{-}in.^2$	7.35×10^5	$x_{cg,\ pod + foil}$, in.	14.6
GJ, $lb\text{-}in.^2$	10.4×10^5	$I_{\phi,\ pod + foil}$, $lb\text{-}in.^2$	527††
Profile	Blunt leading edge	$I_{y,\ pod + foil}$, $lb\text{-}in.^2$	2,890
		Profile	NACA 16-012 with vent. trip
Pod EF Parameters		Angle of attack, deg	0.0
Length, in.	28.5	Flutter Condition	
Max. diameter, in.	6.0	ℓ, in.	30.4 16.4
x_{nose}, in.	8.5	U_f, knots	11.5 9.7
x_{cg}, in.	14.3	f_f, Hz	6.1 1.3
M, lb	36.5	Mode Shape	Torsion Bending

†Air line attached to strut trailing edge; values do not include shaker linkage and strut clamp located 18 in. below strut root and weighing 5.8 lb.

††Calculated.

TABLE 2 - NONDIMENSIONAL FLUTTER PARAMETERS FOR EXPERIMENTAL STRUT MODELS

TABLE 2a - MODEL A

Strut Parameters		Flutter Condition		
L/c	4.0	AR (wetted area)	3.51	2.61
AR (to root)	4.0	k_{nf}	0.058	0.047
κ	0.0351	$4\ EI/\pi\ \rho\ c^2\ \omega_f^2\ L^4$	0.63	0.77
x_{ea}/c	0.46	$16\ GJ/\pi\ \rho\ L^2\ \omega_f^2\ c^4$	88	110
x_{cg}/c	0.60	R_{nf}	6.0×10^7	6.7×10^7
$4\ m/\pi\ \rho\ c^2$	0.093	F_{nf}	10.5	11.8
$16\ I_{my}/\pi\ \rho\ c^4$	3.1×10^{-2}	$\mu_{bending}$	0.104	0.138
		ζ_s (mode 1)	0.07	Not avail.
		σ_f (at surface)	0.59	0.47

TABLE 2b - MODEL 2T

Strut Parameters		Pod Parameters						
		Pod Configuration	C	D	G			
L/c	4.24	Fineness ratio	15.9:1	15.9:1	18.9:1			
AR (to root)	3.96	Diameter/c	0.17	0.17	0.17			
κ	0.0632	x_{nose}/c	0.52	0.52	0.52			
x_{ea}/c	0.69	$x_{cg,\ pod}/c$	1.61	1.76	1.89			
x_{cg}/c	0.50	M_{pod}/M_{strut}	0.44	0.44	0.73			
$4\ m/\pi\ \rho\ c^2$	0.274	$I_{y,\ pod}/I_{y,\ strut}$	2.81	4.17	8.13			
$16\ I_{my}/\pi\ \rho\ c^4$	8.9×10^{-2}	Flutter Condition						
		AR (wetted area)	3.1	3.1	3.1	1.6	1.2	0.79
		k_{nf}	0.40	0.53	0.65	0.83	0.75	0.60
		$4\ EI/\pi\ \rho\ c^2\ \omega_f^2\ L^4$	8.9×10^{-3}	9.1×10^{-3}	1.4×10^{-2}	9.9×10^{-3}	9.1×10^{-3}	8.9×10^{-3}
		$16\ GJ/\pi\ \rho\ L^2\ \omega_f^2\ c^4$	1.0	1.1	1.6	1.1	1.1	1.0
		R_{nf}	5.1×10^6	3.8×10^6	2.5×10^6	2.3×10^6	2.7×10^6	3.5×10^6
		F_{nf}	11	8.3	5.5	5.1	5.8	7.5
		$\mu_{torsion}$	0.87	1.2	2.0	3.6	4.6	6.2
		ζ_s (mode 2)	0.02	0.02	0.01	0.009	0.02	0.02
		σ_f (at surface)	0.55	0.97	2.2	2.6	1.9	1.2

TABLE 2c - MODEL ALPHA

Strut Parameters		Pod Parameters		
		Pod Configuration	A	B
L/c	3.99	Fineness ratio	7.33:1	7.33:1
AR (to root)	3.72	Diameter/c	0.50	0.50
κ	0.0671	x_{nose}/c	1.35	1.35
x_{ea}/c	0.86	$x_{cg,\ pod}/c$	1.83	1.83
x_{cg}/c	0.58	M_{pod}/M_{strut}	3.74	1.46
$4\ m/\pi\ \rho\ c^2$	0.0842	$I_{y,\ pod}/I_{y,\ strut}$	23.9	13.9
$16\ I_{my}/\pi\ \rho\ c^4$	2.82×10^{-2}	Flutter Condition		
		AR (wetted area)	1.87	1.87
		k_{nf}	1.10	0.49
		$4\ EI/\pi\ \rho\ c^2\ \omega_f^2\ L^4$	1.6×10^{-2}	9.9×10^{-3}
		$16\ GJ/\pi\ \rho\ L^2\ \omega_f^2\ c^4$	1.3	0.83
		R_{nf}	9.3×10^5	2.7×10^6
		F_{nf}	1.9	5.4
		$\mu_{torsion}$	1.02	0.61
		ζ_s (mode 2)	0.02	0.03
		σ_f (at surface)	18	2.2

TABLE 2d - MODEL BETA WITH STREAMLINED PROFILE

Strut Parameters		Pod Parameters		
		Pod Configuration	A	F
L/c	4.87	Fineness ratio	7.33:1	7.33:1
AR (to root)	4.54	Diameter/c	0.50	0.50
κ	0.0551	x_{nose}/c	1.35	1.35
x_{ea}/c	0.375	x_{cg}/c	1.83	1.83
x_{cg}/c	0.52	M_{pod}/M_{strut}	4.08	2.25
$4\ m/\pi\ \rho\ c^2$	0.144	$I_{y,\ pod}/I_{y,\ strut}$	32.7	14.7
$16\ I_{my}/\pi\ \rho\ c^4$	0.0559	Flutter Condition		
		AR (wetted area)	2.36	2.36
		k_{nf}	0.846	0.802
		$4\ EI/\pi\ \rho\ c^2\ \omega_f^2\ L^4$	0.0186	0.0127
		$16\ GJ/\pi\ \rho\ L^2\ \omega_f^2\ c^4$	2.41	1.66
		R_{nf}	9.5×10^5	1.2×10^6
		F_{nf}	1.9	2.5
		ζ_s (mode 2)	0.02	0.02
		$\mu_{torsion}$	4.75	2.21
		σ_f (at surface)	17	11

TABLE 2e - MODEL BETA WITH BLUNT BASE PROFILE

Strut Parameters		Pod Parameters			
		Pod Configurations	A	B	C
L/c	4.87	Fineness ratio	7.33:1	7.33:1	7.33:1
AR (to root)	4.54	Diameter/c	0.50	0.50	0.50
κ	0.0551	x_{nose}/c	1.35	1.35	1.35
x_{ea}/c	0.38	$x_{cg,\ pod}/c$	1.83	1.83	1.83
x_{cg}/c	0.55	M_{pod}/M_{strut}	3.76	2.07	0.843
$4\ m/\pi\ \rho\ c^2$	0.156	$I_{y,\ pod}/I_{y,\ strut}$	25.4	11.4	4.99
$16\ I_{my}/\pi\ \rho\ c^4$	7.21×10^{-2}	Flutter Condition			
		AR (wetted area)	2.36	2.36	2.36
		k_{nf}	0.98	0.96	0.76
		$4\ EI/\pi\ \rho\ c^2\ \omega_f^2\ L^4$	1.7×10^{-2}	1.2×10^{-2}	6.0×10^{-3}
		$16\ GJ/\pi\ \rho\ L^2\ \omega_f^2\ c^4$	2.3	1.7	0.81
		R_{nf}	8.5×10^5	1.0×10^6	1.8×10^6
		F_{nf}	1.7	2.0	3.7
		$\mu_{torsion}$	4.75	2.21	1.08
		ζ_s (mode 2)	0.007	0.009	0.008
		σ_f (at surface)	21	15	4.6

TABLE 2f - MODEL BETA WITH BLUNT LEADING EDGE PROFILE, WITHOUT FOIL

Strut Parameters		Pod Parameters						
		Pod Configuration	A	B	C	D	E	
L/c	4.87	Fineness ratio	7.33:1	7.33:1	7.33:1	4.75:1	4.75:1	
AR (to root)	4.54	Diameter/:	0.5	0.5	0.5	0.5	0.5	
κ	0.0551	x_{nose}/c	1.35	1.35	1.35	0.71	0.71	
x_{ea}/c	0.38	$x_{cg,\ pod}/c$	1.83	1.83	1.83	1.19	1.19	
x_{cg}/c	0.57	M_{pod}/M_{strut}	3.62	2.00	0.811	1.46	0.83	
$4\ m/\pi\ \rho\ c^2$	0.171	$I_{y,\ pod}/I_{y,\ strut}$	23.2	10.4	4.55	4.52	1.88	
$16\ I_{ay}/\pi\ \rho\ c^4$	9.28×10^{-2}	Flutter Condition						
		AR (wetted area)	2.36	2.36	2.36	2.36	2.36	1.32
		k_{af}	0.90	0.90	1.3	1.0	1.2	1.3
		$4\ EI/\pi\ \rho\ c^2\ \omega_f^2\ L^4$	1.8×10^{-2}	1.2×10^{-2}	6.1×10^{-3}	4.7×10^{-3}	2.6×10^{-3}	2.4×10^{-3}
		$16\ GJ/\pi\ \rho\ L^2\ \omega_f^2\ c^4$	2.4	1.7	0.81	0.63	0.34	0.33
		R_{af}	8.9×10^5	1.1×10^6	1.2×10^6	1.5×10^6	1.8×10^6	1.7×10^6
		P_{af}	1.8	2.2	2.4	3.1	3.6	3.5
		$\nu_{torsion}$	4.81	2.27	1.10	3.19	1.67	2.31
		ζ_a (mode 2)	0.007	0.01	0.01	0.009	0.02	Not avail.
		σ_f (at surface)	19	13	11	6.5	5.0	5.1

TABLE 2g - MODEL BETA WITH BLUNT LEADING EDGE PROFILE AND FOIL WITH HEAVIER WEIGHT POD

Strut Parameters		Foil Parameters		
L/c	4.87	c_{root}/c	1.2	
AR (to root)	4.54	AR	2.0	
κ	0.0551	Λ	12.0	
x_{ea}/c	0.38	τ	0.69	
x_{cg}/c	0.57	M_{foil}/M_{strut}	0.78	
$4\ m/\pi\ \rho\ c^2$	0.17	$x_{cg,\ pod\ +\ foil}/c$	1.19-1.22	
$16\ I_{my}/\pi\ \rho\ c^4$	0.093	$I_{y,\ pod\ +\ foil}/I_{y,\ strut}$	6.21	
Pod DF Parameters		**Flutter Condition**		
Fineness ratio	4.75:1	AR (strut wetted area)	2.36	1.28
Diameter/c	0.5	k_{nf}	0.84	0.26
x_{nose}/c	0.71	$4\ EI/\pi\ \rho\ c^2\ \omega_f^2\ L^4$	6.3×10^{-3}	9.0×10^{-2}
x_{cg}/c	1.19	$16\ GJ/\pi\ \rho\ L^2\ \omega_f^2\ c^4$	0.85	12
M_{pod}/M_{strut}	1.52	R_{nf}	1.6×10^6	1.4×10^6
		F_{nf}	3.3	2.8
		ζ_s	0.01 (mode 2)	0.02 (mode 1)
		σ_f (at surface)	6.0	8.3

TABLE 2h - MODEL BETA WITH BLUNT LEADING EDGE PROFILE AND FOIL WITH LIGHTER WEIGHT POD

Strut Parameters		Foil Parameters		
L/c	4.87	c_{root}/c	1 2	
AR (to root)	4.54	AR	2.0	
κ	0.0551	Λ	12.0	
x_{ea}/c	0.38	τ	0.69	
x_{cg}/c	0.57	M_{foil}/M_{strut}	0.78	
$4\ m/\pi\ \rho\ c^2$	0.17	$x_{cg,\ pod\ +\ foil}/c$	1.2	
$16\ I_{my}/\pi\ \rho\ c^4$	0.093	$I_{y,\ pod\ +\ foil}/I_{y,\ strut}$	3.6	
Pod EF Parameters		**Flutter Condition**		
Fineness ratio	4.75:1	AR (strut wetted area)	2.36	1.28
Diameter/c	0.5	k_{nf}	1.0	0.26
x_{nose}/c	0.71	$4\ EI/\pi\ \rho\ c^2\ \omega_f^2\ L^4$	4.1×10^{-3}	9.0×10^{-2}
x_{cg}/c	1.19	$16\ GJ/\pi\ \rho\ L^2\ \omega_f^2\ c^4$	0.55	12
M_{pod}/M_{strut}	0.90	R_{nf}	1.7×10^6	1.4×10^6
		F_{nf}	3.4	2.8
		ζ_s	Not avail.	0.06 (mode 1)
		σ_f (at surface)	5.7	7.9

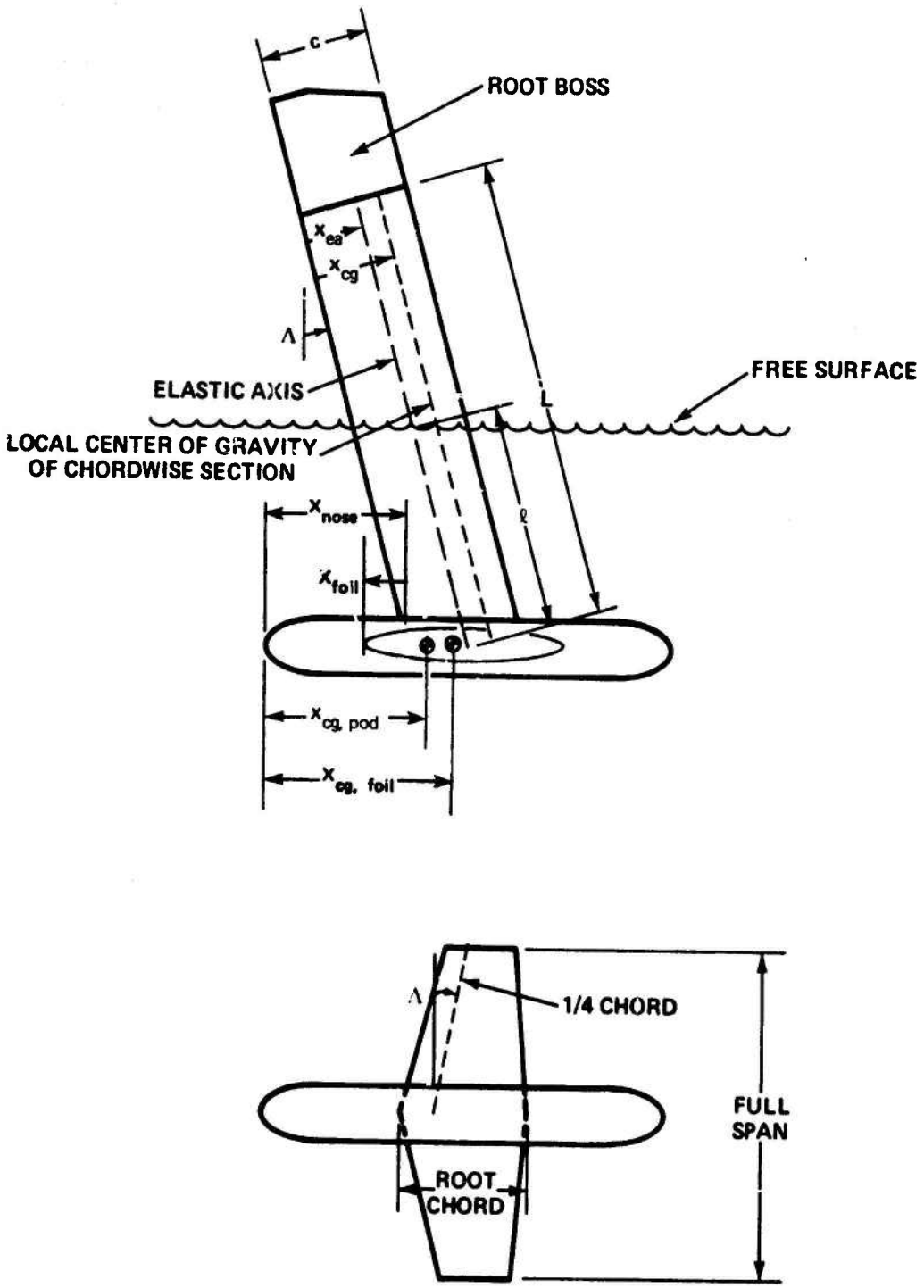

Figure 1 - Geometrical Parameters of Strut System

MODEL A

Model A (Figure 2) was originally constructed and flutter tested by Squires.[3] It was available to DTNSRDC in the 48-in. length to which it had been reduced in the course of studying the effects of strut length on flutter speed.

The Model A strut was constructed of solid aluminum with a parabolic profile; the maximum thickness of 3.8 percent of the chord occurred at the trailing edge. Chordwise cuts 1/8 in. wide had been made in the leading and trailing edges every 4 in. along the span. The cuts extended into the leading edge to a depth of 1.5 in. and into the trailing edge to a depth of 4.5 in.; all cuts were filled with a rubber compound. The cuts moved the elastic axis of the section forward from 86 to 46 percent of the chord but reduced strut stiffness by only about 10 percent.

Structural characteristics of Model A are given in Tables 1a and 2a. The bending and torsional stiffnesses and elastic axis location were measured and found to be in excellent agreement with values given by Squires.[3]

MODEL 2T

Model 2T (Figure 3) was a reconstructed version of the original Model 2T configuration which had been flutter tested by Baird et al.[4] in the High-Speed Hydrodynamics Facility at Langley Field, Virginia.[5] The original Model 2T had been structurally deformed by large-amplitude oscillation during the previous experiment. It was reconstructed by cutting the pod off the deformed Model 2T strut and welding it to the

---

[3]Squires, C.E., Jr., "Hydrofoil Flutter, Small Sweep Angle Investigation--Final Report," Grumman Aircraft Engineering Corporation Report DA Nonr-3989.3 (Nov 1963).

[4]Baird, E.F. et al., "Investigation of Hydrofoil Flutter--Final Report," Grumman Aircraft Engineering Corporation Report DA 10-480-3 (Feb 1962).

[5]Olson, R.E. and W.F. Brownell, "Facilities and Research Capabilities--High Speed Phenomena Division, David Taylor Model Basin, Langley Field, Va.," David Taylor Model Basin Report 1809 (Apr 1964).

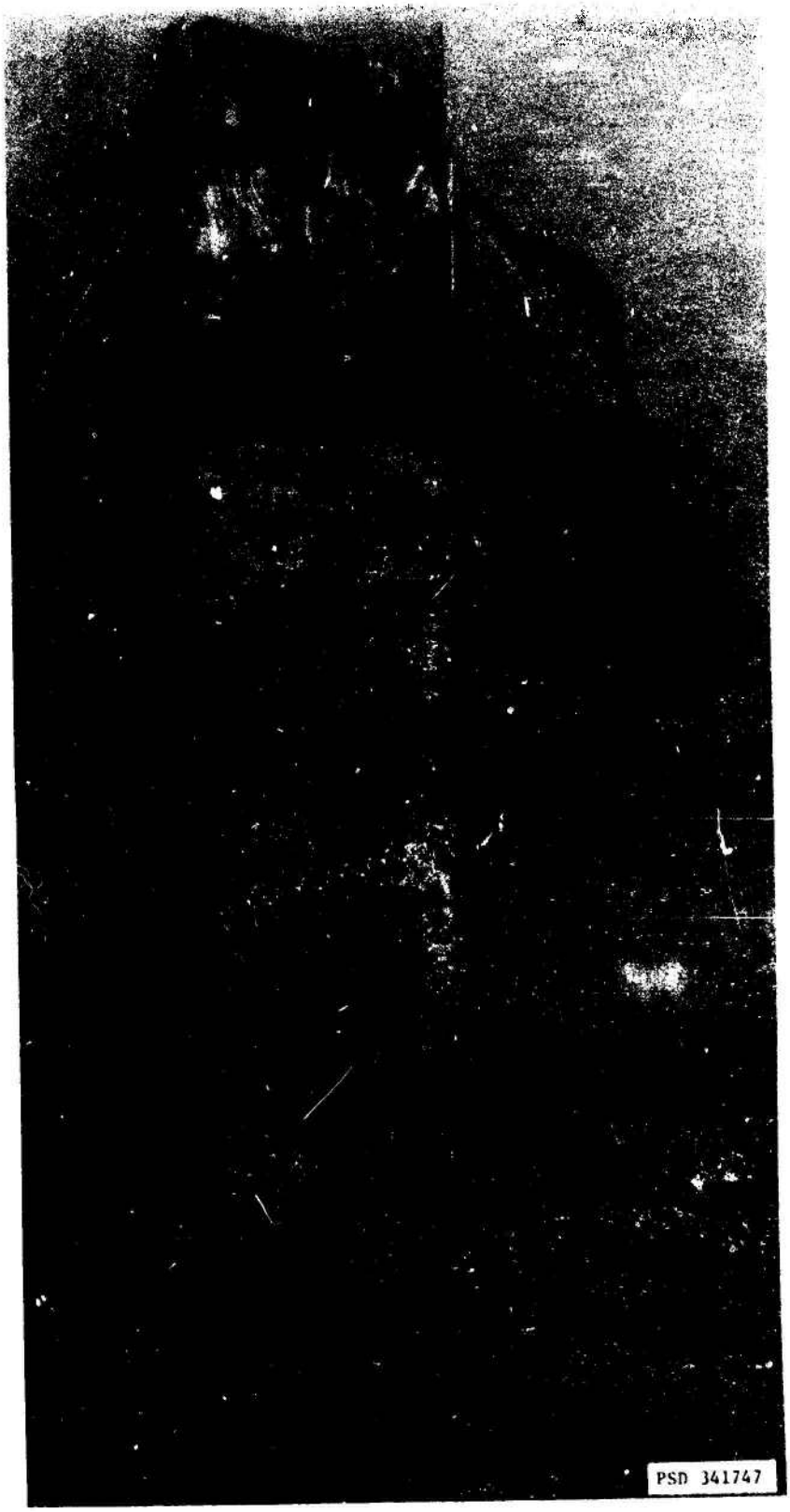

Figure 2 - Model A

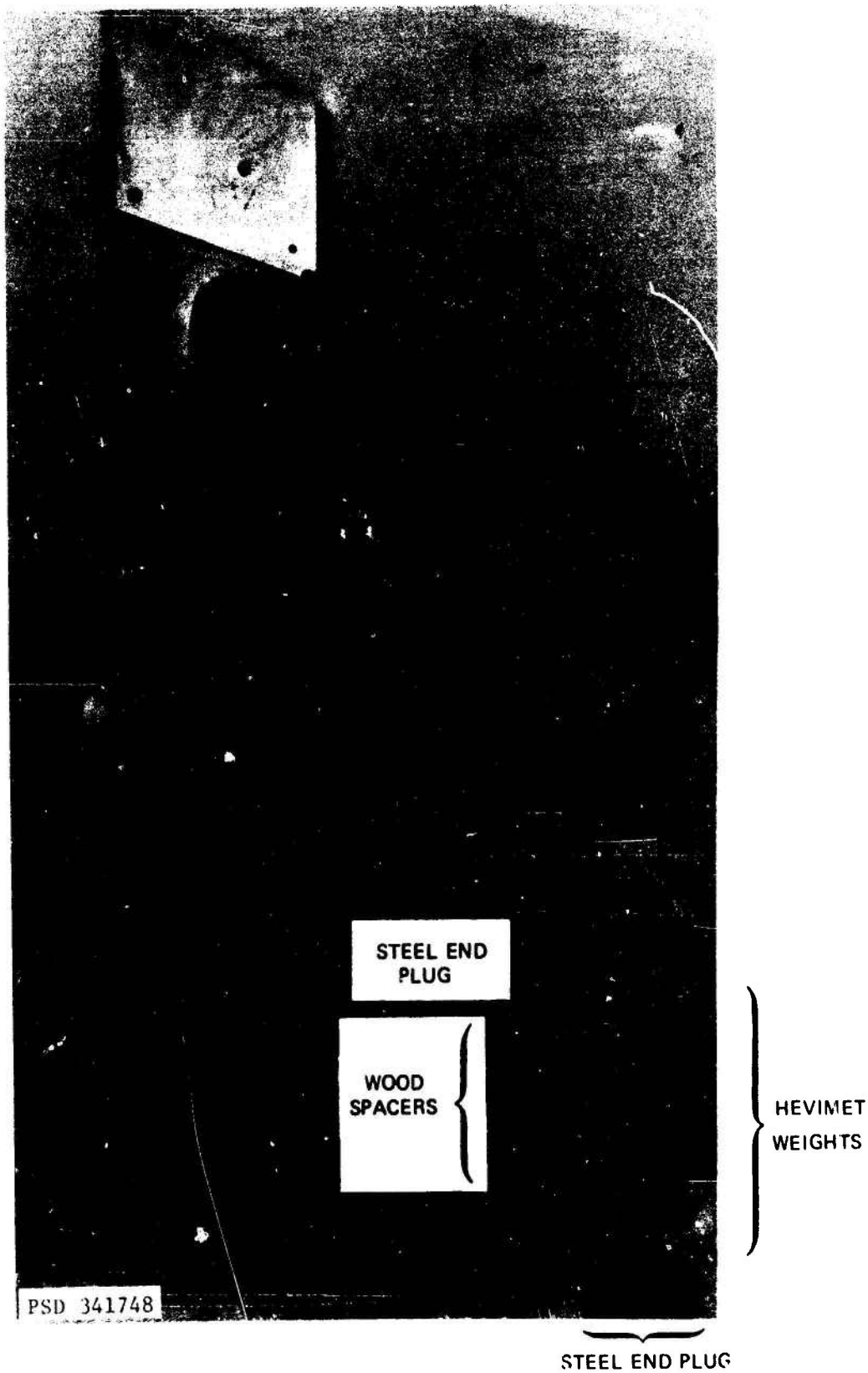

Figure 3 - Model 2T with Ballast Weights

strut of another model used during the previous experiment (designated Model 2 in that experiment and built to the same specifications as the Model 2T strut).

Model 2T consisted of a solid steel strut with a long, thin pod attached to its tip. The strut was swept 15 deg, with the axis of the pod aligned parallel to the flow. The strut had a blunt-based, symmetric profile composed of a circular arc from the leading edge to the midchord and a constant thickness (3.4 percent) section from the midchord aft. The tip pod had a solid nose section and a hollow cylindrical aft section constructed of 2-in. OD steel pipe. Various combinations of ballast weights and wood spacers, shown in Figure 3, were used to produce wide variations in the inertial characteristics of the pod. The ballast weights were made of either stainless steel or Hevimet (a tungsten-nickel-copper alloy manufactured by the General Electric Company) which has a specific gravity of 16.7 or 2.1 times that of steel.

Structural characteristics for the model are listed in Tables 1b and 2b. These characteristics correspond to the three lowest flutter speed configurations studied by Baird et al. (and designated by them as 2T-C, 2T-D, and 2T-G). Measurements of strut stiffness were made, but the values were somewhat imprecise because only small deflections could be obtained. Therefore the originally reported values are given in this report. For the same reason, the strut elastic axis location was calculated (rather than measured) by using the following formula:[6]

$$\bar{x} = \frac{(1 + 3\eta) \int x t^3 \, dx}{(1 + \eta) \int t^3 \, dx}$$

The resulting elastic axis location of 68 percent of the chord aft of the leading edge agreed with the estimate of 69 percent given by Baird.

Measured values of pod mass and moment of inertia, made prior to welding the pod to the strut, were in excellent agreement with the

[6]Duncan, W.J., "The Flexural Centre or Centre of Shear," J. Royal Aeronautical Society, Vol. 57, pp. 594-597 (Sep 1953).

original values. Pod moment of inertia $I_{cg,\ pod}$ was determined by suspending the pod as a bifilar pendulum, giving

$$I_{cg,\ pod} = r^2 M_{pod}$$

$$r = \frac{Ta}{4\pi \sqrt{\frac{s}{g}}}$$

MODEL ALPHA

Model Alpha (Figure 4) was a relatively flexible, lightweight strut with a large, variable-mass pod. The 3.9-percent-thick parabolic strut profile was similar to that of Model A except that no chordwise cuts were made in the strut. The resulting far aft location of the elastic axis was expected to produce relatively low flutter speeds in both bending and torsional flutter modes, according to calculations made with the simplified flutter theory of Caporali and Brunelle.[7]

The model strut was machined of solid 6061 aluminum. Two pods were used with the strut. One was machined from solid mahogany, with a slot for the strut. The other consisted of an aluminum center section with a slot for the strut, openings at both ends for ballast weights, and interchangeable elliptical end sections of aluminum and mahogany. The aluminum end sections also had weight compartments. Three close-fitting bolts were used to attach the pods to the strut; the center of the pod was on the extended midchord line of the strut. Cover plates enclosed the openings around the struts. The ballast weights were made of foam, mahogany, steel, or lead and were securely held in the weight compartments with set screws, tie rods, or wood screws.

Two pod configurations were used with Model Alpha; one employed the mahogany pod and the other an aluminum center section with mahogany end sections. The weight configurations were symmetrical about the pod midpoint.

---

[7] Caporali, R.L. and E.J. Brunelle, "Hydrofoil Instability at Low Mass Density Ratios," Princeton University Aerospace and Mechanical Sciences Report 670 (Mar 1964).

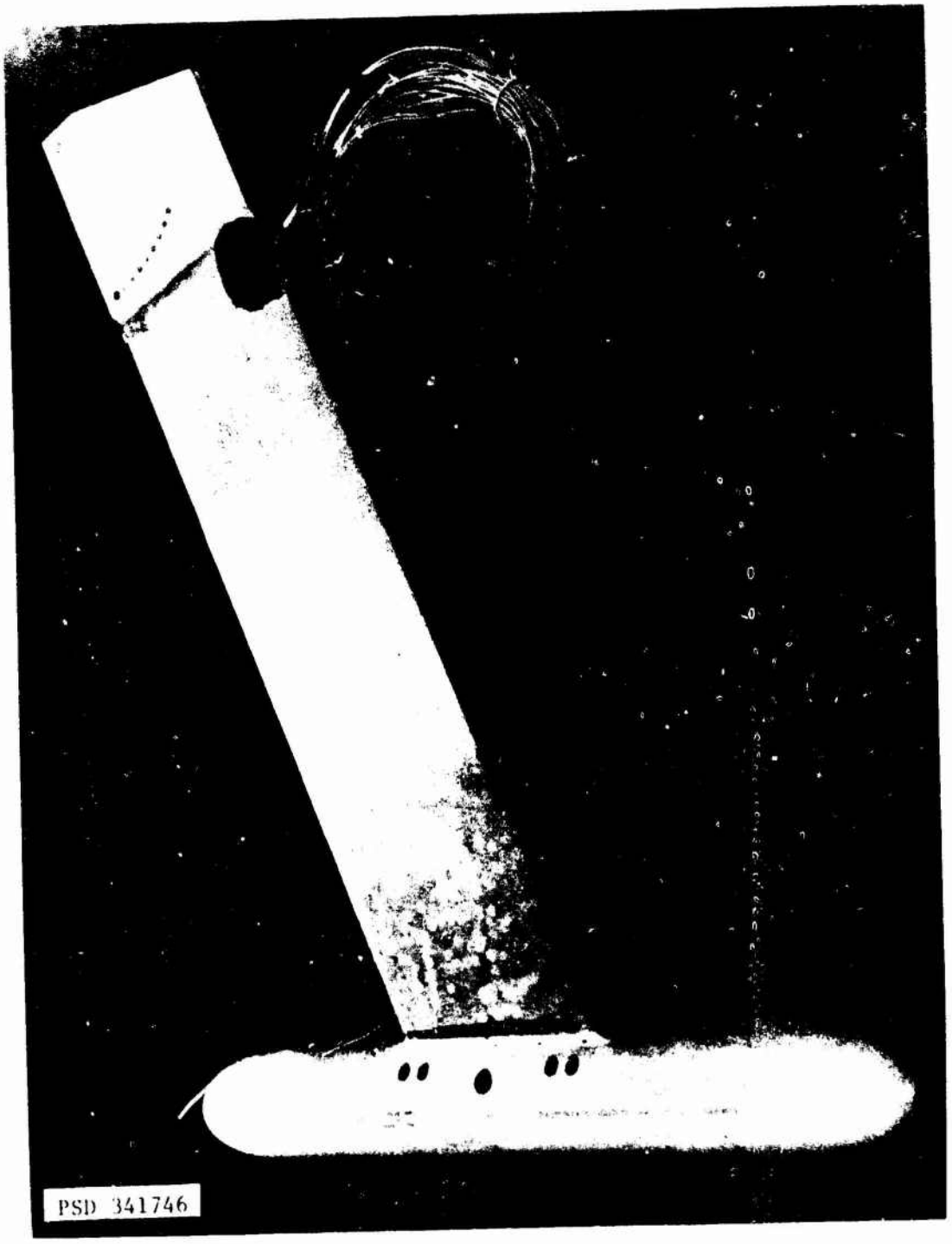

Figure 4 - Model Alpha with Pod A

Model parameters are given in Tables 1c and 2c. To obtain accurate strut stiffness measurements, the root end of the strut was rigidly mounted between plates bolted to a strongback, clamps were placed around the strut at several spanwise positions, and Bourns infinite resolution deflection potentiometers were attached to the ends of the clamps. The potentiometers were connected to a 12-channel potentiometer balance unit for excitation and readout. Bending and torsional loadings were applied near the tip of the model to produce deflections. A small electromagnetic oscillator was attached to the beam holding the potentiometer coils and operated throughout all loading cycles to reduce the effect of friction in the potentiometers. Strain measurements obtained from the root strain gages showed that deflections due to friction were virtually eliminated by this procedure. Uncertainty in the measured stiffness values is estimated to be less than 2 percent.

Pod moment of inertia was determined for each configuration using the bifilar pendulum method previously described.

MODEL BETA

Model Beta (Figure 5) was designed with the unusual characteristic of a changeable strut profile in order to study the effects of cavitation pattern on flutter speed. Three different profiles were produced with minimal structural changes by attaching pieces of lightweight, flexible plastic to the strut.

The strut was machined from solid 6061 aluminum with a nominal NACA 16-005 profile. However, just aft of midchord, the profile was interrupted by spanwise channels 3.5 in. wide and approximately 0.1 in. deep. The resulting shape was fitted with pieces of Lexan plastic to produce the three profiles shown in Figure 6. The first profile was an NACA 16-005 section obtained by continuing the basic strut contour across the spanwise channels. For the second profile (designated the blunt base profile), the strut thickness at midchord was continued aft

Figure 5 - Model Beta in High Speed Basin

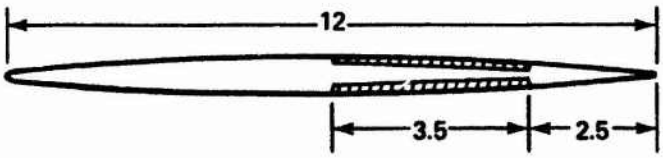

NACA 16-005 PROFILE

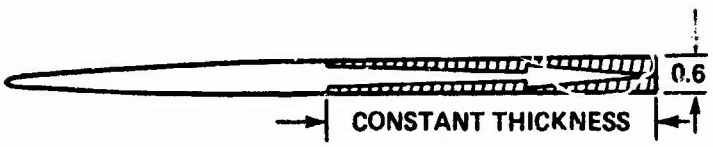

BLUNT BASE PROFILE

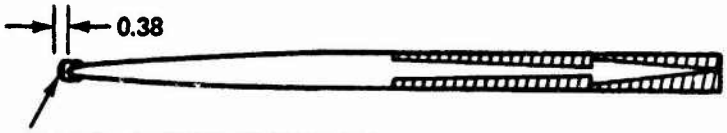

BLUNT LEADING EDGE PROFILE

NOTE: DIMENSIONS IN INCHES

Figure 6 - Model Beta Profiles

to the trailing edge, producing a combined NACA 16-005 and constant-thickness section. The third profile (designated as the blunt leading edge profile) was obtained by adding blunt nose pieces with bevelled edges. Although this modification increased the chord slightly, results are presented in terms of the original chord length of 12.0 in.

The Lexan pieces were approximately 4 in. long and were separated by 1/8-in. spaces to reduce the stress on the adhesive bond between the plastic and the strut. Silastic 732 RTV adhesive/sealant was used to attach the plastic and to fill the gaps between the pieces. This adhesive formed a moderately strong bond to Lexan and had the desirable qualities of curing on exposure to water or water vapor and of remaining flexible after curing to minimize its stiffness contribution.

The pods used on Model Alpha were also used on Model Beta, but with different inertial configurations. Additionally, the aluminum pod was shortened and fitted with a foil in an inverted-T configuration, shown in Figure 5. The otherwise noncavitating shapes of pod and foil were altered by attaching both a 1/4-in. square ventilation trip to the foil 10 percent of the foil chord aft of the leading edge and a 1/2-in. square ventilation trip to the pod between the foil trip and the surface of the strut. The combined system of ventilation trips was used in conjunction with the blunt leading edge strut profile in anticipation of producing a foil cavity which was fully ventilated by air flowing down along and behind the strut.

An artificial air supply was installed to assist in ventilating the foil cavity. Air was supplied through 1/2-in. OD copper tubing held against the trailing edge of the strut by steel brackets. Flexible plastic tubing carried the air through the pod to air passages which opened on the upper foil surfaces at the intersection of the foil and pod ventilation trips. Air was supplied to the foil at a pressure of 50 to 80 psig. The air line is visible in Figure 5.

Parametric values for pod and pod-foil configurations of Model Beta are given in Tables 1d-1h and 2d-2h. Inertial characteristics include the effects of the air supply system where applicable, except

as noted. Structural stiffnesses and pod moments of inertia were measured as described for Model Alpha. Moments of inertia for the two pod-foil combinations were also determined by the bifilar pendulum method.

Differences in structural characteristics caused by changing the strut profile on Model Beta were considered sufficiently small to permit meaningful comparisons of flutter characteristics. Although the strut inertial parameters showed substantial percentage differences, the strut inertia was much smaller than that of the pod, particularly in torsional motion.

VIBRATION MODES OF THE MODELS

Vibration mode shapes, either in air or in water at zero speed, have been found to provide an accurate indication of the flutter mode shape of a strut. These were determined as part of the present experiment together with frequencies.

MODEL A

In-air nodal line measurements previously made by Rowe and Marvin[8] had indicated that Model A was a bending-type strut. These measurements were accepted and not repeated. This type of strut has a second vibration mode (i.e., resonant mode with the next-to-lowest frequency) with a predominantly second bending mode shape, with mode shapes being referred to uncoupled cantilever beam modes. The first and third modes are predominantly first bending and first torsion, respectively. Flutter normally occurs in a first bending mode shape for this type of strut, and bending flutter did occur for Model A.

MODEL 2T

Model 2T was a torsion-type system with the pod configuration tested; the second vibration modes had predominantly first torsion

---

[8] Rowe, W.S. and T.G.B. Marvin, "A Program of Theoretical Research on Hydroelastic Stability," The Boeing Company, Contract N00014-67-C-0248 (Nov 1968).

mode shapes, and the first and third modes were primarily first and second bending, respectively. Substantial coupling was present between bending and torsional modes, as can be seen in the nodal lines for one configuration given in Figure 7. In-air nodal lines were determined by excitation with a lightweight coil that was attached to the model and acted against a fixed permanent magnet. Resonance frequencies were determined by peak accelerometer output; nodal lines were defined by phase shifts between a fixed and a roving accelerometer. Flutter in a first torsion mode shape has come to be associated with this vibration mode sequence, and torsional flutter was observed.

MODEL ALPHA

Also a torsion-type system, Model Alpha exhibited torsion-type vibration modes both in air and in water. In-air vibration modes were determined as for Model 2T; sample nodal lines are shown in Figure 8. Very little coupling between bending and torsional motion was present. The in-water modes were determined with the vibration equipment described later in connection with flutter testing procedures. Approximate nodal line characteristics in water were obtained by observing the relative phase of the two velocity sensor outputs and by visual observations of the water wave pattern. In-phase velocities indicated a bending mode with a nodal line passing outside the two sensors; out-of-phase velocities indicated a torsional mode with a nodal line passing between the sensors. In keeping with its torsion-type mode characteristics, Model Alpha underwent torsional flutter in each tested configuration.

MODEL BETA

Model Beta had a torsion-type vibration mode sequence in each configuration, but it cannot be classified as a purely torsion-type strut because bending flutter occurred in two instances. The vibration modes were determined in air both with the lightweight coil used for Models 2T and Alpha and with the vibration equipment used for flutter

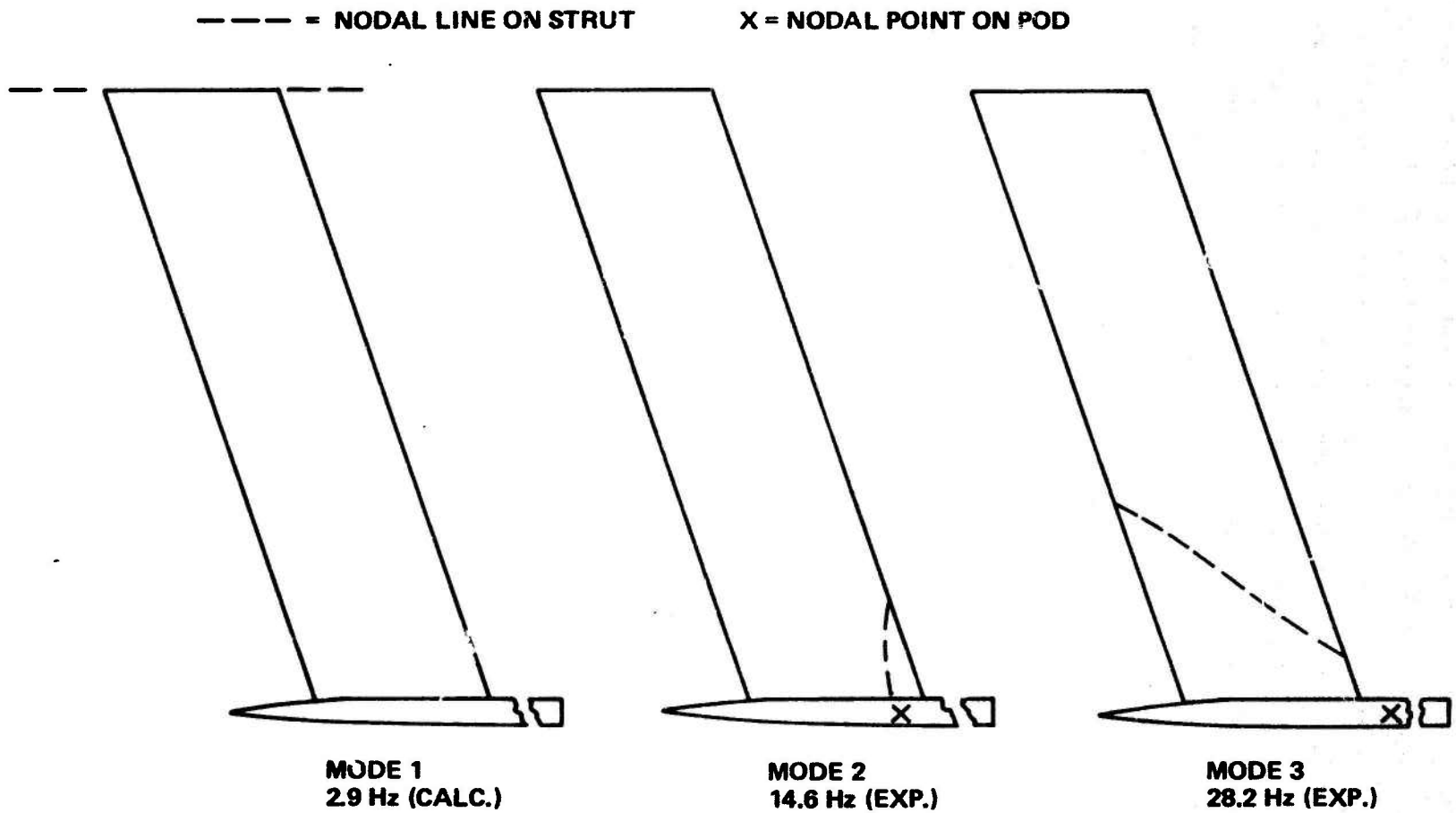

Figure 7 - Nodal Lines and Resonant Frequencies for Model 2T with Pod C in Air

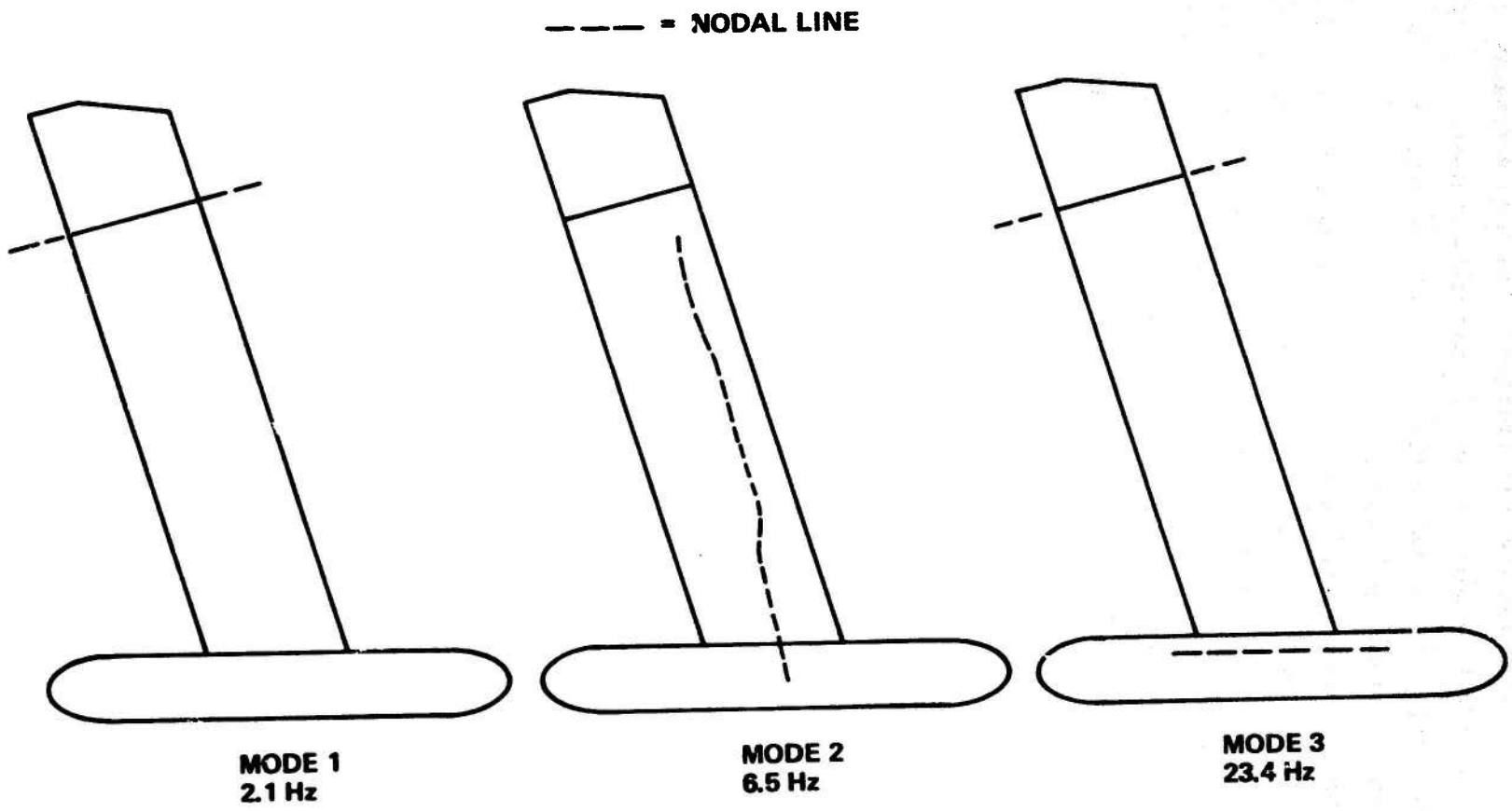

Figure 8 - Experimental Nodal Lines and Resonant Frequencies for Model Alpha with Pod B in Air

testing. The resulting resonant frequencies were in agreement, indicating satisfactory operation of the vibration equipment. Note that the sample nodal lines shown in Figure 9 exhibited virtually uncoupled bending and torsional mode shapes.

In-water resonant frequencies and approximate nodal lines for Model Beta were obtained as described for Model Alpha. Of particular interest is the fact that the second and third in-water resonant frequencies were often extremely close together; see Table 3. This frequency spacing was as close as 0.7 Hz (or 10 percent of the torsional frequency) when no foil was present and as close as 0.3 Hz (or 5 percent of the torsional frequency) when a foil was attached. Reducing pod mass, increasing strut submergence, and attaching the foil all reduced the frequency interval between the second and third modes. The relationship of the vibration and flutter modes of Model Beta will be examined in a later section of this report.

PROCEDURE FOR FLUTTER TESTING

INSTRUMENTATION

Model instrumentation consisted of sensors for measuring strut motion, excitation systems for generating oscillations, and associated equipment for recording and analysis.

Each strut had two or more sets of strain gage bridges, each set consisting of a bending-sensitive bridge and a torsion-sensitive bridge. The strain gages were mounted near the strut elastic axis, just below the enlarged root section. Models Alpha and Beta were also monitored by two velocity transducers mounted perpendicular to the plane of the strut, 14 in. apart and equidistant from the leading and trailing edges; they were respectively 12.5 and 18 in. below the root for Models Alpha and Beta. These velocity transducers, attached between a fixed bracket and clamps placed around the strut (as shown in Figure 5), were Hewlett-Packard Sanborn LVsyn Models 3LVA5 or 3LVI Linear Velocity Transducers. A Computer Instruments Corporation Type III Rectilinear Potentiometer was used in place of one of the velocity transducers during a portion of the experiment.

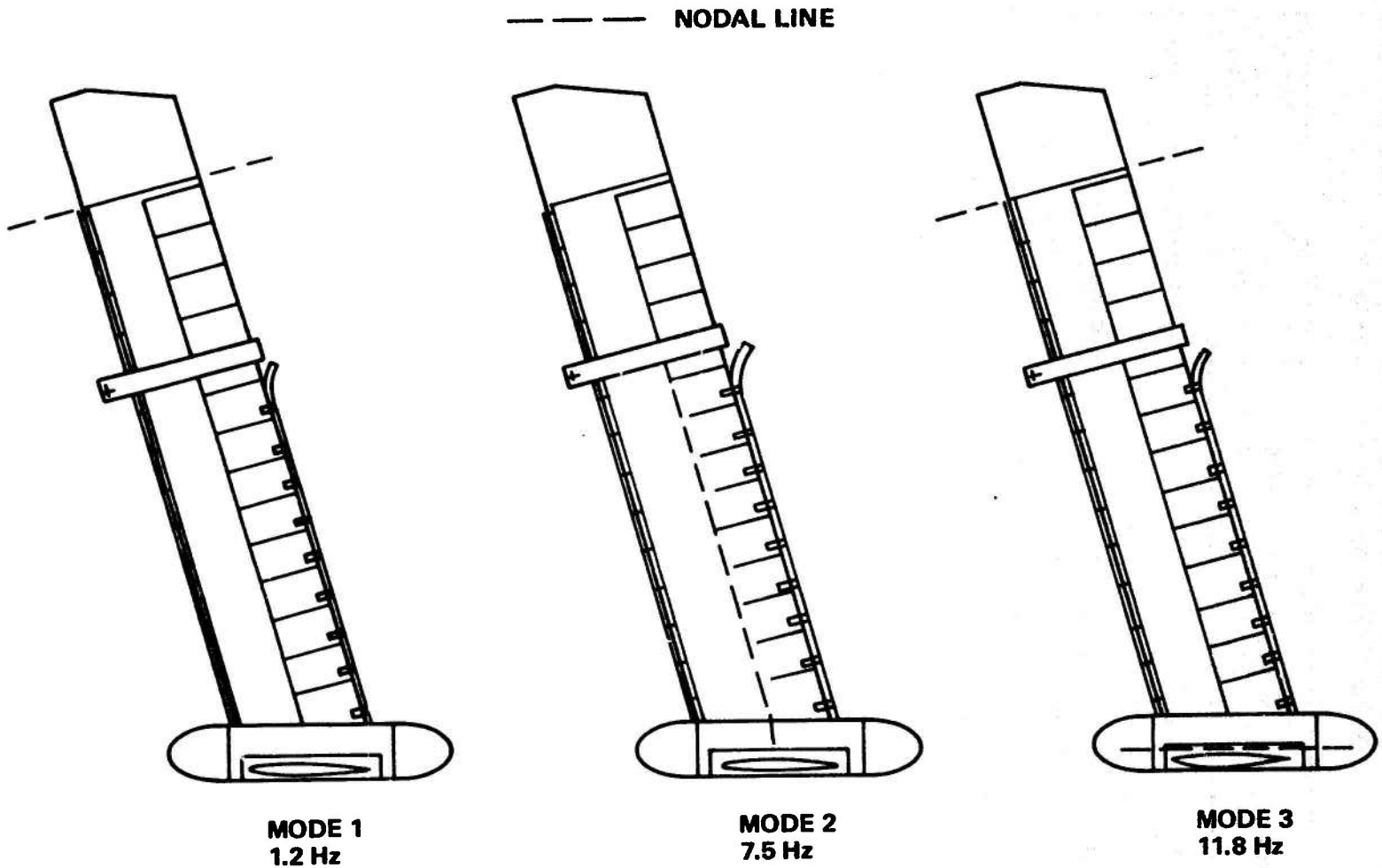

Figure 9 - Experimental Nodal Lines and Resonant Frequencies for Model Beta with Blunt Leading Edge Profile and Pod-Foil EF, in Air

TABLE 3 - IN-WATER VIBRATION MODE CHARACTERISTICS FOR MODEL BETA WITH BLUNT LEADING EDGE PROFILE AT ZERO SPEED

Pod	Foil	Strut Submergence ℓ/L	Mode No.	Frequency Hz	Vibration Mode Shape	Flutter Mode Shape
A	No	0.52	1	0.70	First bending	Torsion
			2	3.0	First torsion	
			3	7.1	Second bending	
B		0.52	1	0.77	First bending	
			2	3.6	First torsion	
			3	7.5	Second bending	
C		0.52	1	0.89	First bending	
			2	4.8	First torsion	
			3	8.2	Second bending	
D		0.52	1	0.85	First bending	
			2	5.8	First torsion	
			3	7.5	Second bending	
E		0.52	1	0.9	First bending	
			2	7.3	First torsion	
			3	8.0	Second bending	
		0.28	1	0.9	First bending	
			2	7.7	First torsion	
	No		3	-	-	
DF	Yes	0.52	1	0.8	First bending	
			2	5.1	First torsion	
			3	6.2	Second bending	Torsion
		0.28	1	0.7	First bending	
			2	5.1	First torsion	Bending
			3	8.3	Second bending	
EF	Yes	0.52	1	0.8	First bending	
			2	6.0	First torsion	Torsion
			3	6.3	Second bending	
		0.28	1	0.8	First bending	
			2	6.2	First torsion	Bending
			3	8.2	Second bending	

Excitation was provided for Model 2T by attaching a 200-lb test monofilament line to the aft end of the pod. The line was run through a pulley above the water surface to one side of the strut and forward to the carriage instrumentation area. Oscillation of the model was induced by drawing the line taut and cutting it. No excitation was used for Model A because excessive deflections resulted.

The excitation system used for Models Alpha and Beta (and shown in Figure 5) utilized an electromagnetic shaker to produce the desired excitations. This much more versatile excitation system permitted a detailed study of individual hydroelastic mode characteristics. A Pye-Ling Type V50 MK 1 Vibration Generator was rigidly mounted on the starboard side of the strut. Constant-amplitude driving current (approximating constant force amplitude) was obtained from a Spectral Dynamics Model SD104A-2 Sweep Oscillator and amplified by a Kepco Model BOP 36-5M Power Amplifier. A specially constructed control box made it possible to automatically zero the driving current on completion of a desired sweep range.

The driving spindle of the vibration generator was linked to a clamp bolted around the strut. The linkage contained a close-fitting ball joint and a Tyco Bytrex 100-lb load cell. The clamp location and the weight of the entire assembly that moved with the strut are given in Table 1.

Output from all force and motion sensors was recorded on magnetic tape in analog form and was visually monitored on a Sanborn 8-channel oscillograph. Various photographic records were made, including above- and below-surface photographs, and video tapes were recorded for a number of test conditions.

Two types of electronic data analysis equipment were used. Transfer functions were determined from rapid-sweep excitation with the Time/Data TD 1923-C FFT Analyzer. Mechanical impedances were obtained with the Spectral Dynamics Model SD-1002 Automatic Mechanical Impedance Measuring System in conjunction with a multiple-speed tape recorder which was used to increase experiment[illegible] frequencies by a factor of 4.

FLUTTER TEST TECHNIQUE

Flutter speeds were determined by towing the strut models in the high-speed basin[9] at DTNSRDC. A sufficient speed range was covered to obtain indications of flutter inception from one or both of the methods of damping measurement.

The strut model under investigation was clamped at the desired sweep angle in a support bracket constructed of heavy steel plate. The bracket was attached to a platform which permitted variations in strut angle of attack and submergence. The platform was attached to Carriage 5.

The models were towed in the following manner. The struts were placed at zero angle of attack with the pods horizontal. The towing carriage was accelerated to a selected speed, held at a constant speed for a damping determination, and then either brought to a stop or accelerated to a higher speed. Several speeds were often obtained on a single carriage run. Run speeds were increased until flutter occurred. Small speed increments were used when flutter was considered imminent.

Damping was measured by using rapid sweep excitation and, occasionally, line cut excitation. Flutter inception occurred when the model exhibited zero damping. The excitation methods are described in the following sections along with the measurement technique for mechanical impedance. Mechanical impedance can be used to determine damping, but the present results were unsatisfactory for determining flutter inception.

Rapid Sweep Excitation

This method of excitation, employed on Models Alpha and Beta, utilized a special type of impulse to selectively excite a single hydroelastic mode. Both direct visual analysis and electronic spectral analysis were employed.

---

[9] Brownell, W.F. and M.L. Miller, "Hydromechanics Cavitation Research Facilities and Techniques in Use at the David Taylor Model Basin," Symposium on Cavitation Research Facilities and Techniques, American Society of Mechanical Engineers (May 1964); also available as David Taylor Model Basin Report 1856 (Oct 1964).

The technique was based on a transient excitation approach developed by Skingle,[10] Kandianis,[11,12] and White.[13-15] The vibration generator attached to the model applied sinusoidal force of rapidly varying frequency. The frequency was swept over a narrow frequency range, 1 to 2 Hz wide, centered about a known resonance frequency. At the completion of the sweep, the force was set approximately equal to zero, as shown in Figure 10. This type of excitation acts as an impulse which has its predominant effect on the central resonance.

Visual Analysis of Decay Curves. Although the damping could be extracted from the input and response by a number of spectral analysis techniques, it was immediately evident during experimentation that a well-defined oscillatory decay pattern occurred as a response following cessation of the input. Whenever possible, this decay pattern was used to calculate damping and frequency because the necessary analysis of the signal could be performed without special equipment. The damping ratio ζ, expressed as a fraction of critical damping, was calculated from the relation

$$\zeta = \frac{\ln(y_1/y_2)}{\omega \Delta t}$$

---

[10] Skingle, C.W., "A Method for Analyzing the Response of a Resonant System to a Rapid Frequency Sweep Input," RAE TR 66379 (Dec 1966).

[11] Kandianis, F., "The Effects of Extraneous Noise on the Measurement of the Frequency Response of Structures under Transient Excitation," I.S.V.R. Technical Report 20 (Nov 1969).

[12] Kandianis, F., "Frequency Response of Structures Excited by Transient or Random Forces using Cross Correlation and its Laplace Transform," I.S.V.R. Technical Report 47 (Aug 1971).

[13] White, R.G., "Measurement of Structural Frequency Response by Transient Excitation," I.S.V.R. Technical Report 12 (Jan 1969).

[14] White, R.G., "Use of Transient Excitation in the Dynamic Analysis of Structures," RAS Aero. J., Vol. 73, pp. 1047-1050 (Dec 1969).

[15] White, R.G., "Use of Transient Excitation in the Measurement of the Frequency Response of Systems with Nonlinearities Arising from Large Deflections," I.S.V.R. Technical Report 27 (Feb 1970).

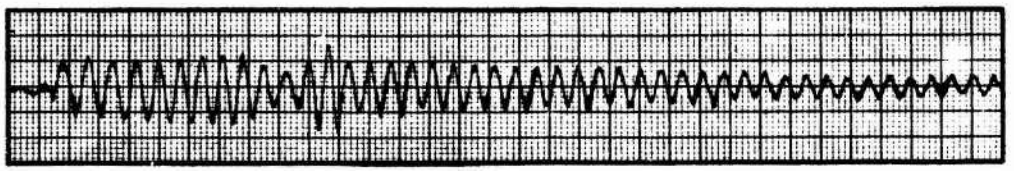

STRAIN DUE TO STRUT BENDING

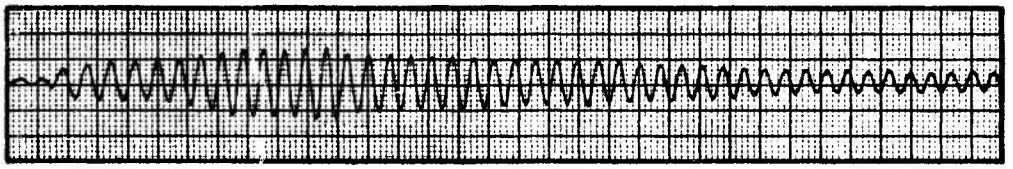

STRAIN DUE TO STRUT TORSION

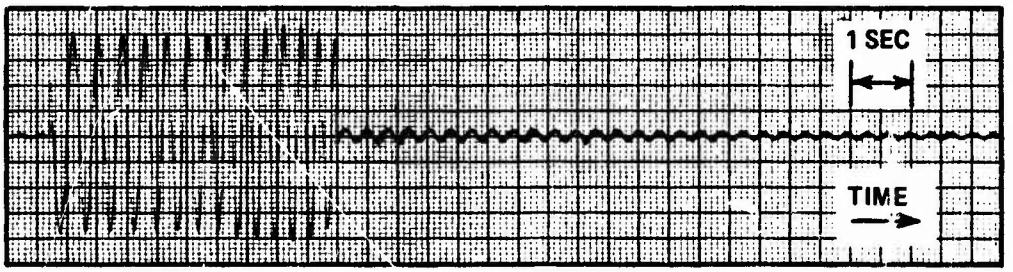

RAPID SWEEP EXCITING FORCE (2.25 Hz TO 3.75 Hz)

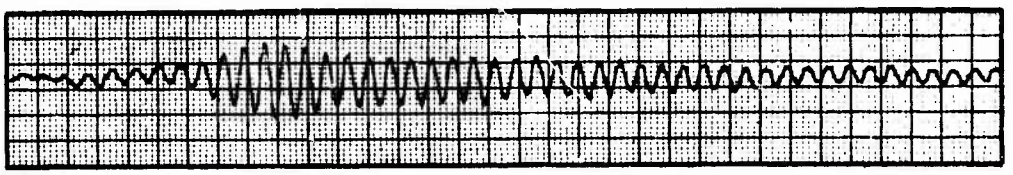

STRUT DISPLACEMENT, NORMAL TO PLANE OF UNDEFLECTED STRUT

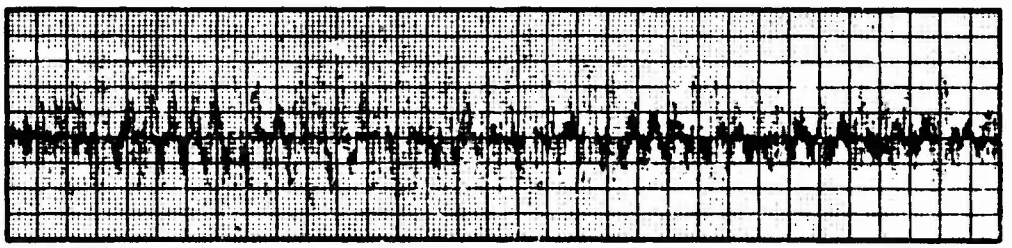

STRUT VELOCITY, NORMAL TO PLANE OF UNDEFLECTED STRUT

Figure 10 - Sample Oscillograph Records of Rapid Sweep Excitation and Subsequent Decay below the Flutter Inception Speed

Better decay patterns for direct visual measurement of amplitudes were obtained by using a shorter sweep time and a narrower frequency range than recommended by White[14] when performing a Fourier transformation analysis. With these changes, the model was released while the oscillation amplitude was still near its maximum, thereby yielding a longer usable decay signal.

This method of determining damping was used to obtain most of the torsional flutter inception speeds for Models Alpha and Beta. The torsional strain gages provided the best signals for this purpose. Part of the velocity data were unsuitable for visual analysis because of distortions caused by operation of the transducer magnetic core in and out of the working range of the winding. It was found that damping ratios above about 10 percent could not be determined in this manner because oscillations damped out too quickly. Consequently, the bending flutter mode, characterized by a precipitous drop in damping just prior to the inception speed, could not be sufficiently excited for visual analysis.

The variety of decay patterns that occured will now be described, together with the rationale for identifying flutter inception. At speeds below flutter inception, the struts exhibited positive damping in the form of decaying oscillations. All oscillations showed an increase in damping with time. Damping values were taken from near the beginning of the oscillation and, where possible, from at least one later interval in order to approximate the range of values that occurred. As the speed approached flutter inception, oscillations that occurred after rapid sweep excitation followed one of two decay patterns:

1. Initially decaying oscillations were followed by "bursts" of oscillations of increasing and decreasing amplitude. For the most part, these bursts were triggered by carriage vibration; as the steel wheels of the carriage moved over irregularities in the steel tracks, the "clacking" sounds coincided with the beginning of many bursts. Flow perturbations may have caused some oscillations as well.

2. There was an immediate growth in oscillation amplitude at a rate that indicated substantial negative damping. When this second decay pattern occurred, the carriage was immediately slowed to prevent model damage.

The oscillation bursts typically became longer and of larger amplitude as speed increased. Flutter inception was considered to occur just below the speed at which an oscillation burst contained enough well-defined cycles to enable a negative value of ζ to be calculated. Thus the beginning of the oscillation burst was interpreted as a valid negative damping point and not merely a response to carriage vibration. The subsequent decaying oscillations yielded a positive damping value. The shift of damping from negative to positive was considered to be an amplitude limitation often observed in hydrofoil flutter experiments.

Flutter inception speeds were obtained from plots of ζ as a function of speed by linear interpolation across the zero damping axis between adjacent positive and negative values of ζ. The speed intervals between these damping values are included in Table 4. Subsequent spectral analysis showed that one flutter inception speed determined in this manner was about 10 percent above the actual inception speed. This delay occurred for a gradually decreasing damping curve and is expected to have been less significant when damping decreased rapidly.

Direct Fourier Transform Analysis. Damping and frequency measurements were also obtained from spectral analysis of tape-recorded excitation and response. This type of analysis has been extensively developed in the literature.[10-15] Specialized equipment is required, but the method may permit damping measurements to be made when various complicating effects interfere with direct observation of individual oscillation mode amplitudes. The technique used by the authors generated accurate damping and frequency values and appeared to be capable of detecting flutter inception precisely.

The simplest spectral analysis method--direct Fourier transform analysis--was used. This method requires calculation of the transfer

TABLE 4 - SUMMARY OF FLUTTER DATA

Strut Model	Strut Profile	Pod	Foil	Strut Submergence ℓ/L	Flutter Speed knots	Possible Flutter Speed Range knots	Flutter Frequency Hz	Flutter Mode
A	Parabolic	-	No	0.894	35.6	<35.6	1.1	Bending
		-		0.667	39.8	<39.8	1.0	Bending
2T	Blunt Based	C		0.79*	37.0	36-38	8.0	Torsion
		D		0.793	27.7	26-28	7.9	
		G		0.793	18.3	18-19	6.4	
				0.40	17.0	16-17	7.6	
				0.30	19.6	18.7-19.6	7.9	
				0.20	25.0	24-25	8.0	
Alpha	Parabolic	A		0.50	6.5*	6.25-6.75	3.7	
				0.50	7.3	7.25-7.5	3.7	Torsion
		B		0.50	>13*	-	-	-
				0.50	18.6	17-19	4.7	Torsion
Beta	NACA	A		0.52	6.6	6.5-6.75	2.9	
	16-005	B		0.52	8.4	8.0-8.5	3.5	
	Blunt Based	A		0.52	5.9	5.0-6.0	3.0	
		B		0.52	7.0	6.5-7.5	3.5	
		C		0.52	12.7	12-14	5.0	
	Blunt L.E.	A		0.52	6.2	6.0-6.25	2.9	
		B		0.52	7.5	7.0-8.0	3.5	
		C		0.52	8.2	7.0-9.0	5.0	
		D		0.52	10.7	10.5-11	5.7	
		E		0.52	12.2	12-12.25	7.7	
			No	0.28	12.1	12-12.5	7.9	
		DF	Yes	0.52	11.2	11-11.25	4.9	Torsion
			Yes	0.28	9.5	9.5-9.75	1.3	Bending
		EF	Yes	0.52	11.5	11.5-11.75	6.1	Torsion
			Yes	0.28	9.7	9.5-9.75	1.3	Bending

*Fourier analysis.

function of the input and response. The analysis was performed by using the exciting force and both velocity and displacement forms of response. The spectral content of a sample excitation and response is shown in Figures 11a and 11b, respectively. The transfer function of these quantities, defined as the vector quotient of the Fourier transform of each, was calculated electronically and plotted in the complex plane; see Figure 11c. The indicated calculation gives a damping value of 1.2 to 1.6 percent for the condition shown in the example.

Damping values obtained from the spectral analysis were in fair-to-good agreement with visually determined values. The frequencies agreed nearly exactly. The spectral analysis results were obtained for the two pod configurations of Model Alpha and are explicitly given along with the flutter characteristics of that model.

A notable characteristic of the measured transfer function was the occurrence of a relative phase shift between input and response at a speed of 6 1/2 knots for the Pod A configuration, about 3/4 knot below the flutter speed obtained by visual analysis. The phase shift occurred as a reflection of the circle plot about the imaginary axis shown in Figure 11c. Such a phase shift would be expected when damping changes from positive to negative. The delay in exhibiting negative damping during visually analyzed decay might have been caused by the small amount of damping produced by the vibration generator in its zero-current mode of operation. It is concluded that the true flutter inception speed was indicated by the phase shift. The same criterion confirmed that the Pod B configuration of Model Alpha had positive damping to a speed of at least 13 knots, which was consistent with a flutter speed of 18.6 knots determined by visual analysis.

Several factors contributed to the inaccuracy of the direct Fourier transform analysis. The accuracy was generally reduced by the narrow sweep range and short sweep duration which had been chosen to produce optimum decay curves for visual analysis. These sweep characteristics introduced larger errors due to truncation and ripple than were necessary.[14] At low values of damping--below 0.5 percent--the maximum

Figure 11 - Direct Fourier Analysis of Rapid Sweep Excitation and Response for Model Alpha with Pod B at 7.5 Knots

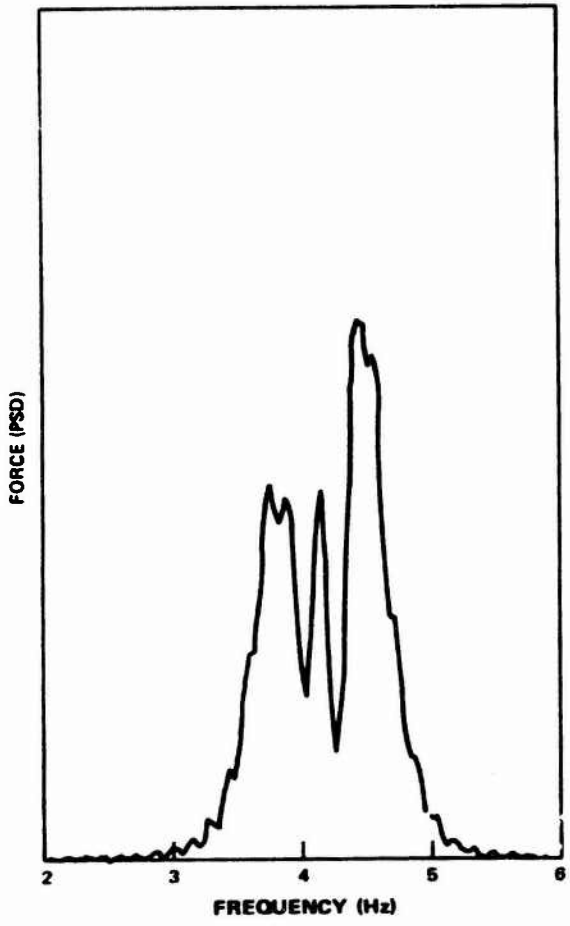

Figure 11a - Power Spectral Density of Excitation Force (Sweep Range = 3.5 to 5.0 Hz; Sweep Rate = 0.2 Hz/sec)

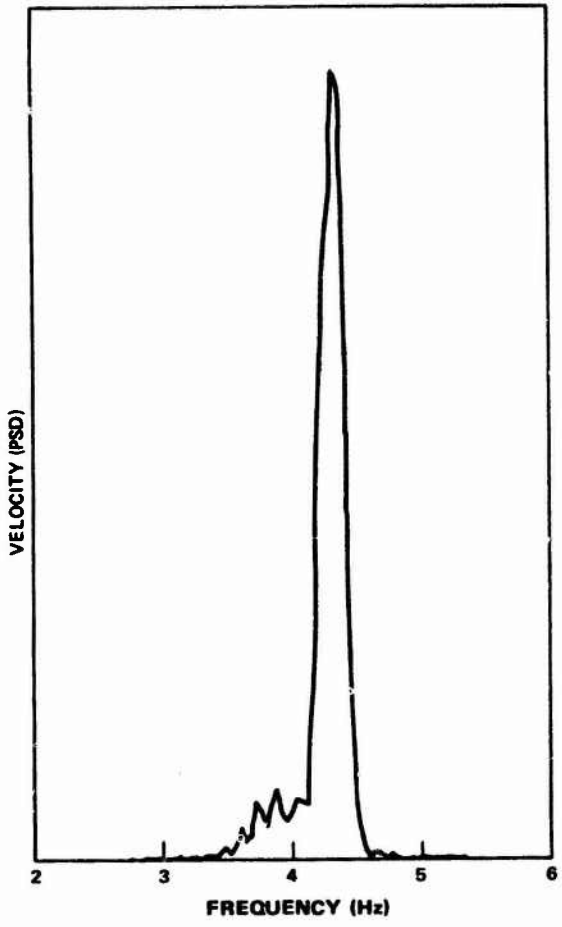

Figure 11b -- Power Spectral Density of Response Velocity at Forward Velocity Transducer

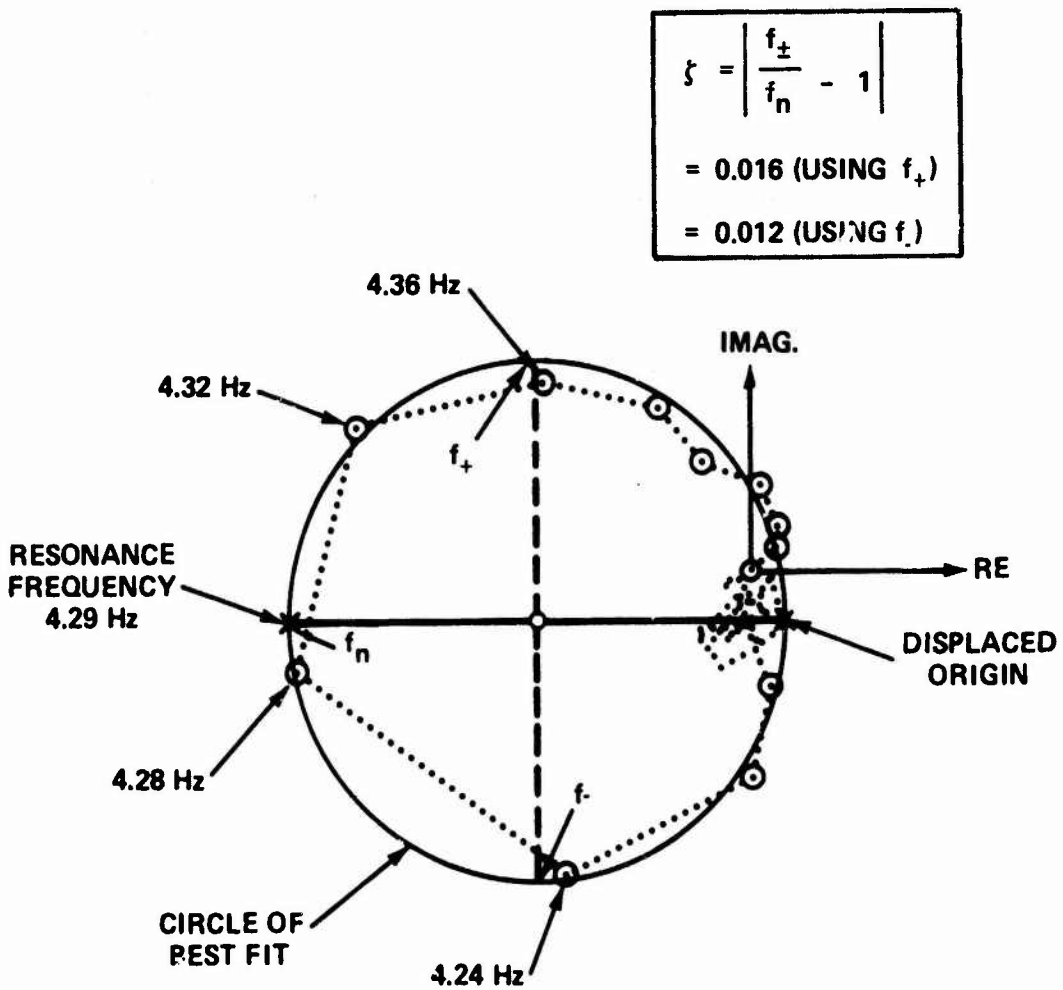

Figure 11c - Complex Plane Plot of Transfer Function of Force and Velocity

available frequency resolution (0.04 Hz) generated too few values of the transfer function to define a circle. The resolution could be slightly but not indefinitely improved by optimum sweep characteristics. Flow-induced noise prevented application of the analysis at speeds above 10 knots. The noise produced random shifts in the transfer function values, making it impossible to fit a circle to the points. At sufficiently high levels of damping, the small circle diagrams generated would be effectively rendered meaningless by even low noise levels.

By eliminating the need for visual measurement of oscillation amplitudes, spectral analysis techniques potentially can achieve higher accuracy than direct measurement techniques when multiple frequencies, noise, and even nonlinear effects are present. The present "direct" method is suitable when vibration modes are close in frequency. "Indirect" spectral analyses, through the use of crosscorrelation and autocorrelation procedures, offer promising approaches in the presence of noise[10,11] and nonlinear effects.[15] When single modes can be excited without the above complications, however, spectral analysis has the disadvantage of requiring specialized equipment and longer data acquisition times than for the decay curve method.

It is concluded that rapid sweep excitation is a valid and useful technique for flutter experimentation. Because of the potentially greater accuracy and range obtained from spectral analysis methods as compared to visual analysis, the advanced spectral analysis methods should be evaluated for use in future model and full-scale flutter experimentation.

Line Cut Excitation

Most of the models were also excited with an attached line, as previously described, and the resulting oscillations were analyzed visually. Only hydroelastic modes with damping ratios below about 10 percent produced sufficient cycles to permit analysis. As a result, the torsional flutter mode could be studied readily, but the first bending mode could be detected only at zero speed.

Damping values for Model 2T were determined exclusively by line cut excitation, and a number of damping points were determined for Models Alpha and Beta for comparison with other methods. Results agreed with rapid sweep measurements, but this technique did not have the versatility to excite more than one mode at speeds other than zero.

Mechanical Impedance Determination

Mechanical impedance, a complex quantity obtained by vector division of applied force and velocity, has a magnitude equal to the damping of the model system at resonance. The quantity was determined by making a long, slow frequency sweep at 0.01 to 0.03 Hz/sec, using the vibration generator and recording force and velocity signals from the appropriate transducers. The resulting impedance, generated with the impedance-measuring system previously described, were plotted on graphs which showed resonances as minimum values. Damping values obtained in this manner (dimensional quantities) were converted to damping ratios by comparing the values to the results of the other techniques at zero speed.

The resulting damping values showed fair-to-poor agreement with previous results. However, substantial data scatter and lack of sufficient data prevent a reliable evaluation of the technique. Only the frequency measurements obtained from mechanical impedance measurements are presented in this report.

FLUTTER CHARACTERISTICS OF THE MODELS

Twenty-three flutter inception conditions were determined for various configurations of the four strut models. In many cases detailed damping and frequency measurements were made for the unstable hydroelastic mode and other modes. Flutter inception parameters are included in Tables 1 and 2 in dimensional and nondimensional form, respectively, and are summarized in Table 4. Results for each model will be described separately in the following sections.

MODEL A

Model A was flutter tested at both the 89.4-percent submergence previously studied by Squires[3] and at 66.7-percent submergence. Observed damping and frequency characteristics are shown in Figure 12. Flutter inception for this strut was approximated by the occurrence of oscillation bursts, indicated as zero damping in Figure 12. No positive damping values below flutter inception were obtained.

Bending flutter occurred at both submergence depths. The flutter mode had a clearly visible first bending mode shape and a frequency much lower than the torsional mode. The flutter speed of 35.6 knots at 89.4-percent submergence agreed with a 35- to 36-knot flutter speed obtained from Figure 7 of Squires. However, the flutter inception frequency of 1.1 Hz was 40 percent higher than the 0.78 Hz previously obtained. This discrepancy may be due to the Squires procedure of accelerating through flutter inception. The increase in flutter speed (from 35.6 to 39.8 knots) that occurred when submergence was decreased to 66.7 percent was consistent with all previous data obtained from bending-type struts.[1]

At the deeper submergence, a ventilated cavity spontaneously appeared over approximately the upper one-third of the submerged span during test runs at 35.6 and 36.5 knots. The cavity caused no deflection of the strut and therefore was symmetrical.

Very large amplitude oscillations occurred when Model A was 1 to 2 knots above flutter inception. Despite the fact that a surprisingly large amplitude in bending was reached before deceleration of the carriage took effect, the strut suffered no damage. This type of oscillation had destroyed the first production model of Model A early in the Squires experimental program.

Figure 12 - Damping Ratio and Frequency of Oscillation as Functions of Speed for Model A

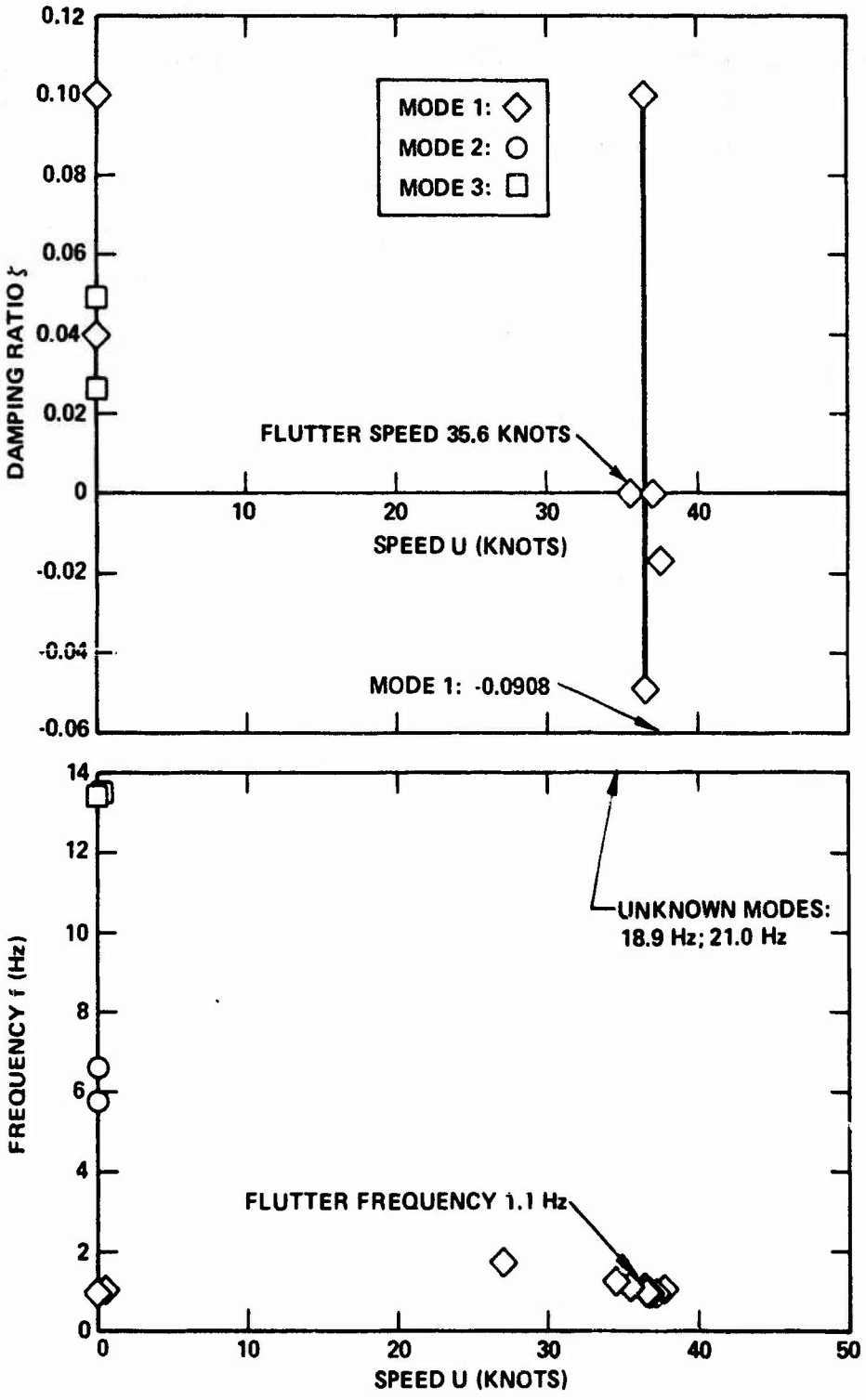

Figure 12a - Strut Submergence ℓ/L = 0.894

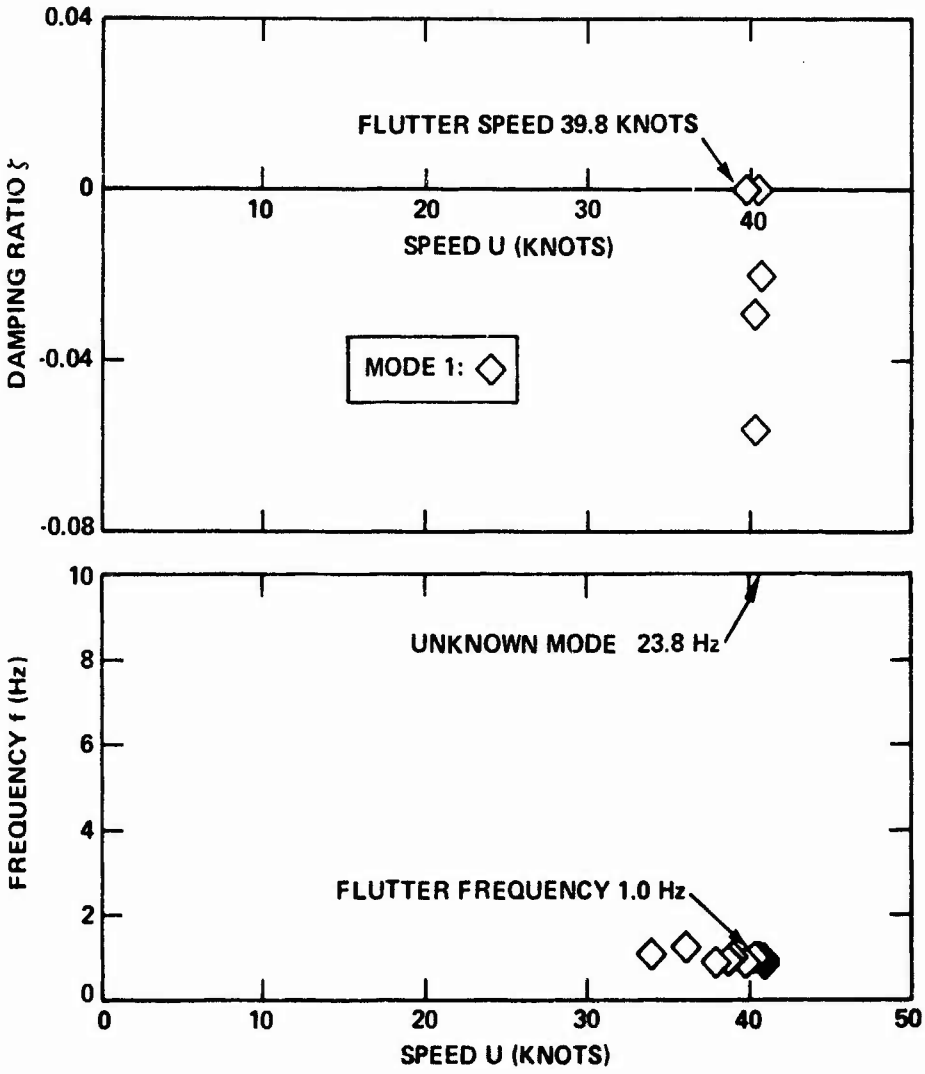

Figure 12b - Strut Submergence $\ell/L = 0.667$

MODEL 2T

Flutter test configurations of Model 2T consisted of three pod ballast configurations at one depth (previously studied by Baird et al.[4]) as well as one of the earlier pod configurations at several additional strut submergence levels.

Detailed measurements of the damping and frequency as functions of speed are shown in Figure 13 which indicates the maximum and minimum values of damping obtained at each speed. Flutter occurred in the second hydroelastic mode. Based on visual observation, the unstable oscillation had a first torsion mode shape. The damping ratio ζ of the second mode was about 2 percent at zero speed and increased by varying amounts before gradually decreasing to zero at flutter inception. Both pod inertia and strut submergence strongly affected the damping and the flutter speed. These effects will be discussed below.

Effect of Pod Moment of Inertia

As already indicated, the damping ratio ζ was about 2 percent at zero speed for all pod configurations and increased by varying amounts before gradually decreasing to zero at flutter inception. The maximum value of ζ decreased monotonically as pod moment of inertia $I_{y,\ pod}$ increased, ranging from about 20 percent for Pod C to about 5 percent for Pod G.

The flutter inception speed decreased sharply as $I_{y,\ pod}$ increased, ranging from 37 to 18.3 knots. Corresponding flutter frequencies changed only slightly, from 8.0 to 6.4 Hz. The dependence of these quantities on pod moment of inertia is illustrated in Figure 14.

These results were in reasonably close agreement with the earlier Baird results (included in Figure 14) except for the Pod D configuration which was reported to have a 55-knot flutter speed compared to the present 27.7 knots. The earlier value, corresponding to model failure during flutter, is believed to have represented a deep penetration into the negative damping region during which amplitude-limiting effects prevented any substantial buildup of oscillation amplitude. Such an

Figure 13 - Damping Ratio and Frequency of Oscillation as Functions of Speed for Model 2T

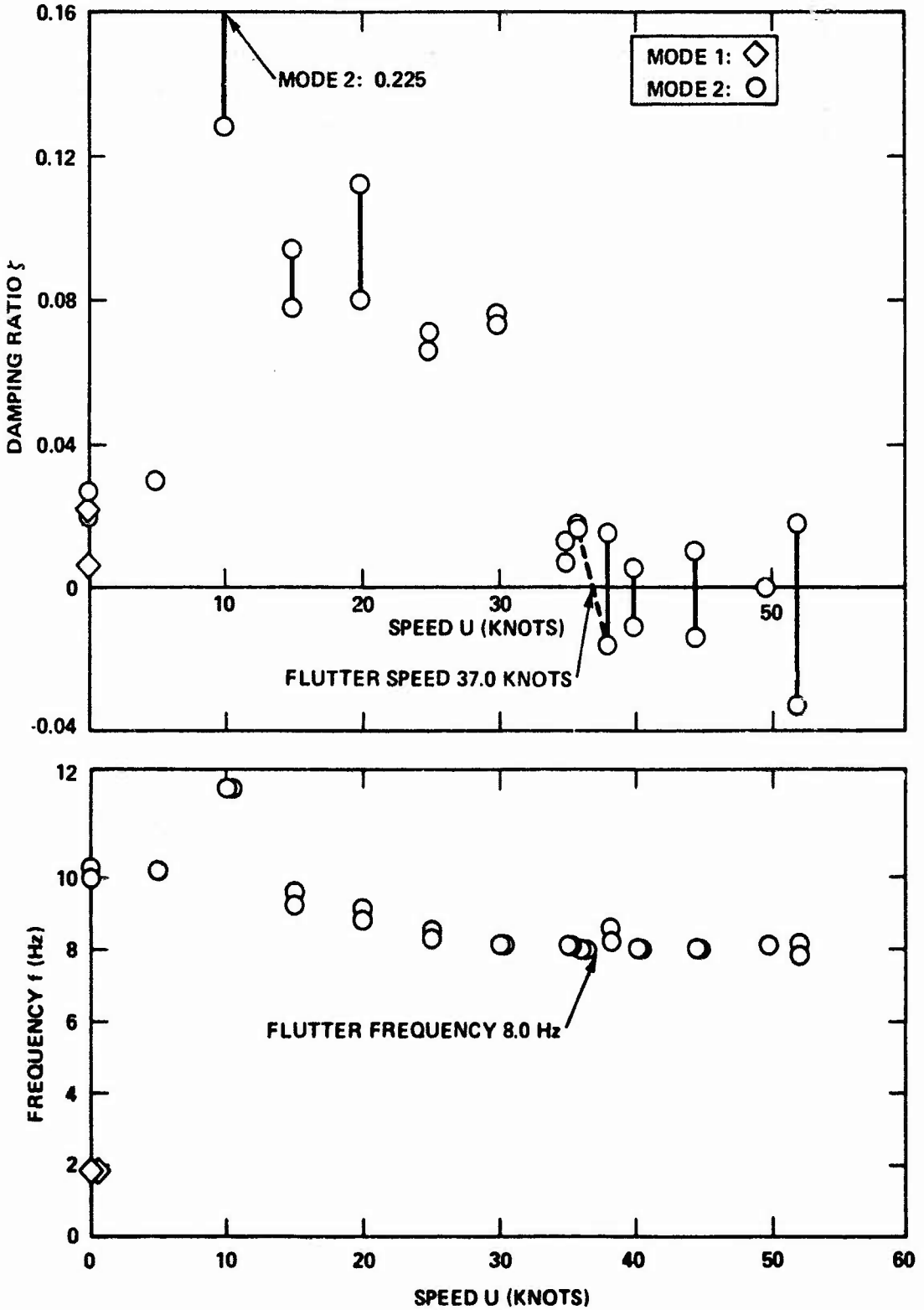

Figure 13a - Model 2T with Pod C, Strut Submergence ℓ/L = 0.793

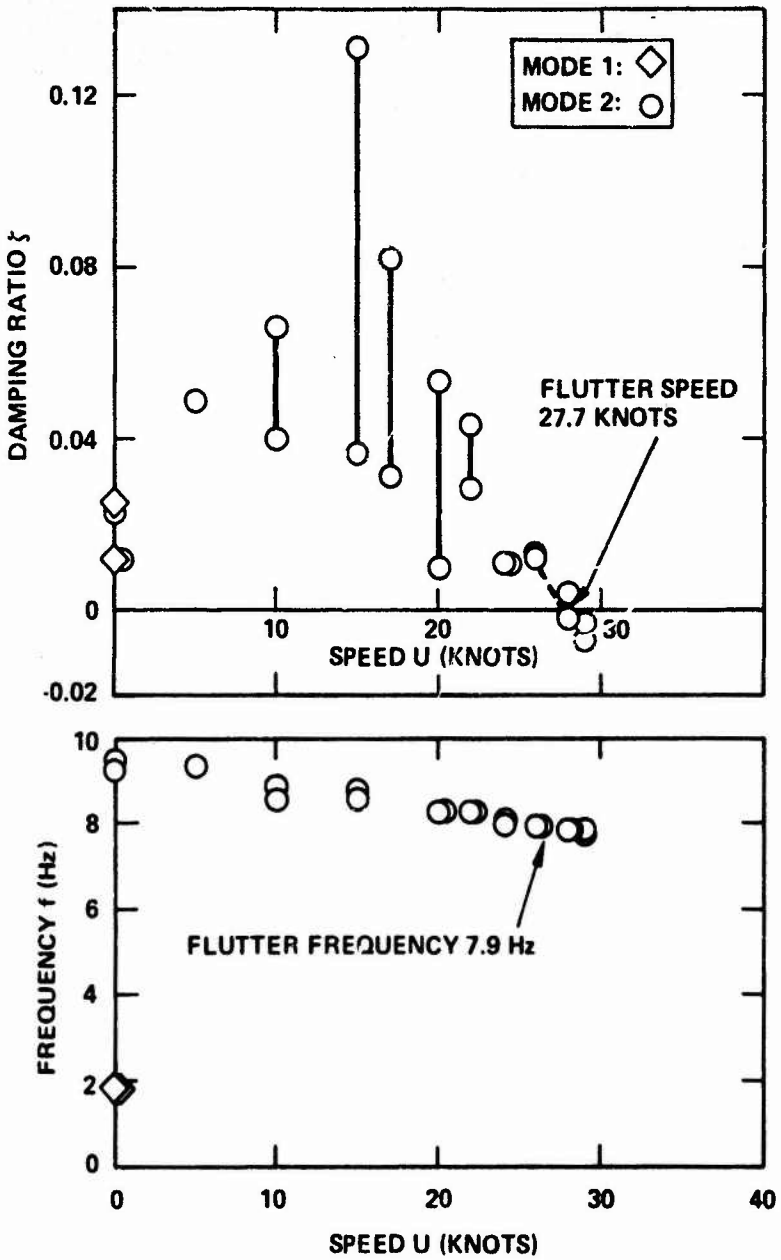

Figure 13b - Model 2T with Pod D, Strut Submergence
$\ell/L = 0.793$

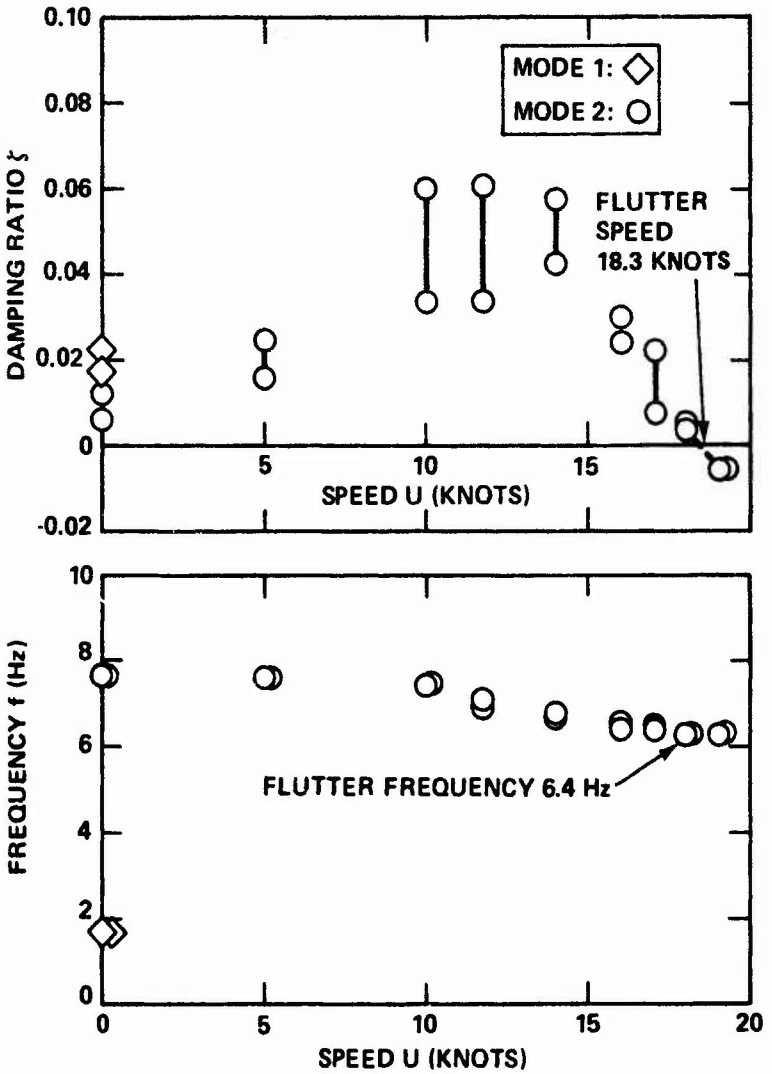

Figure 13c - Model 2T with Pod G, Strut Submergence $\ell/L = 0.793$

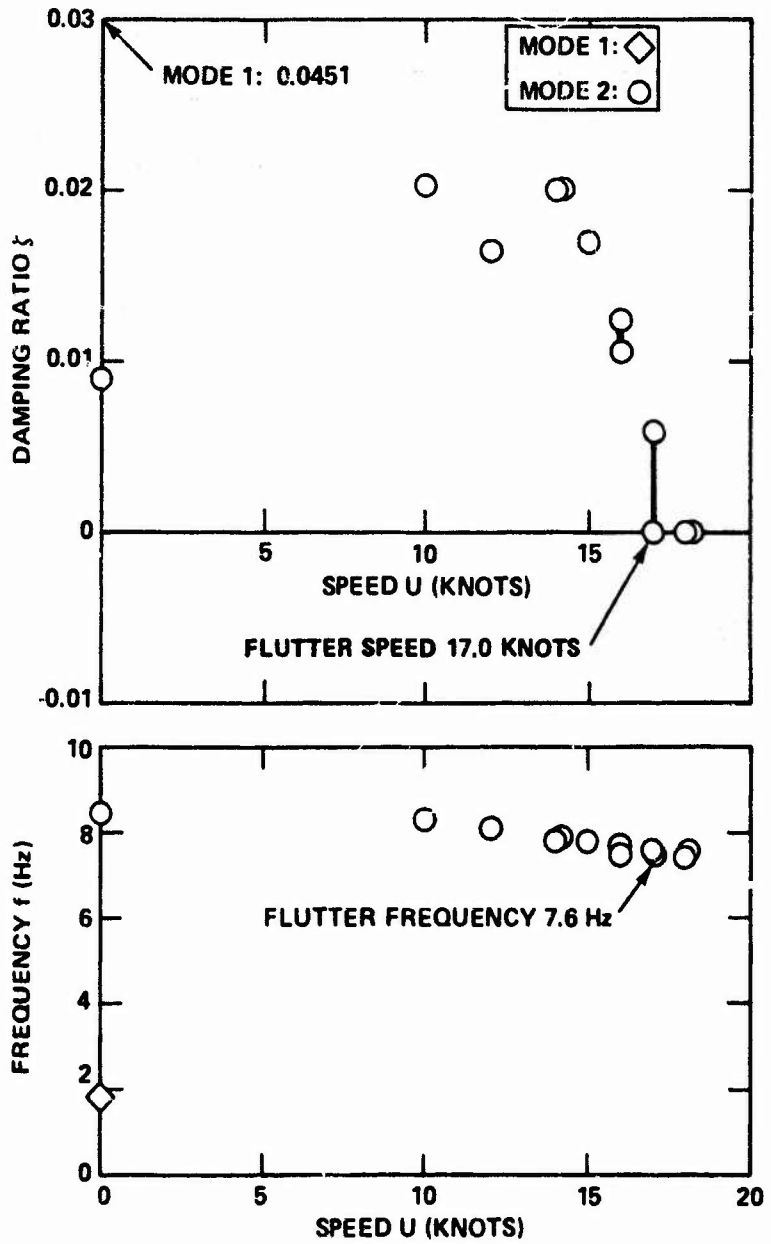

Figure 13d - Model 2T with Pod G, Strut Submergence
$\ell/L = 0.40$

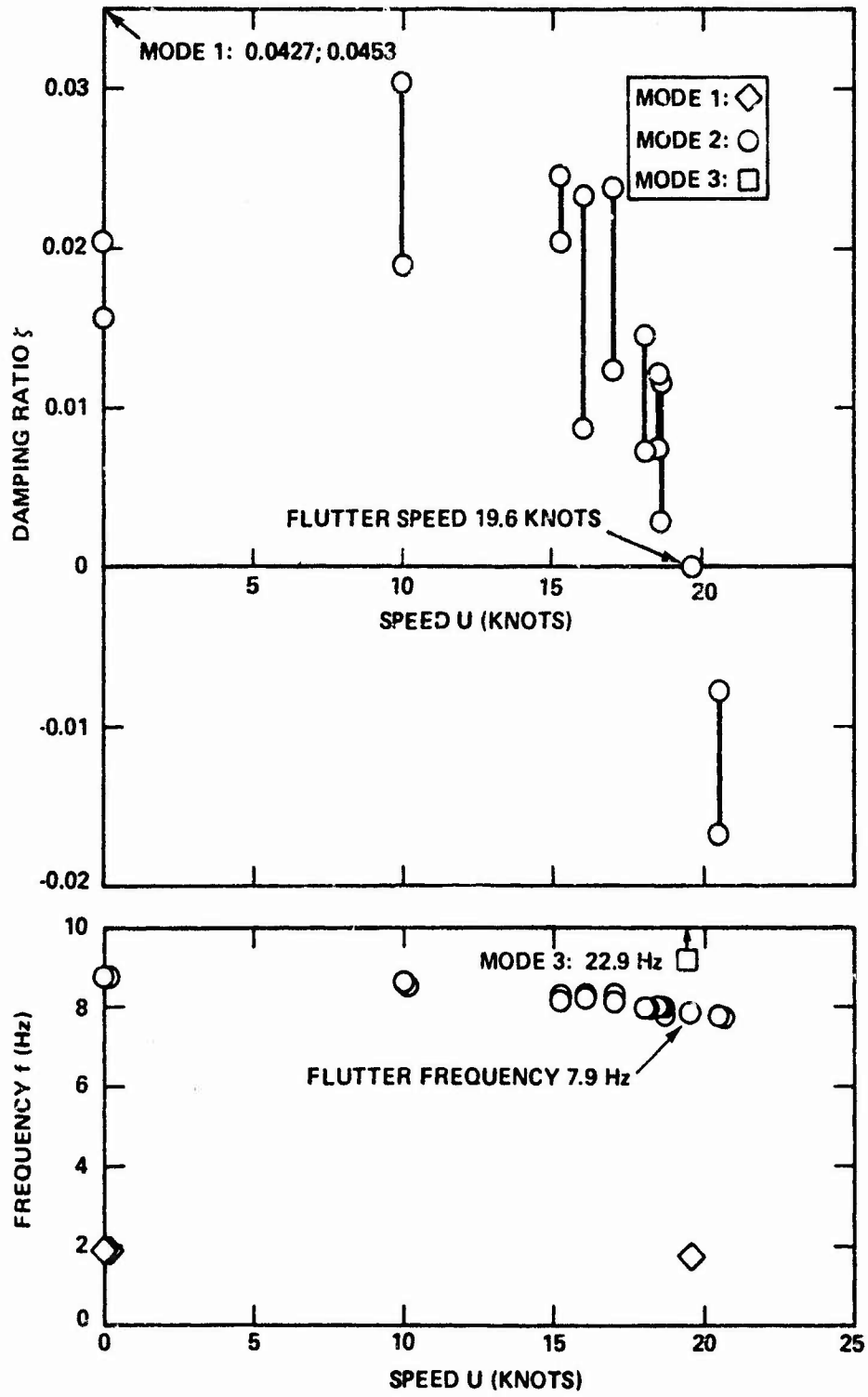

Figure 13e - Model 2T with Pod G, Strut Submergence
$\ell/L = 0.30$

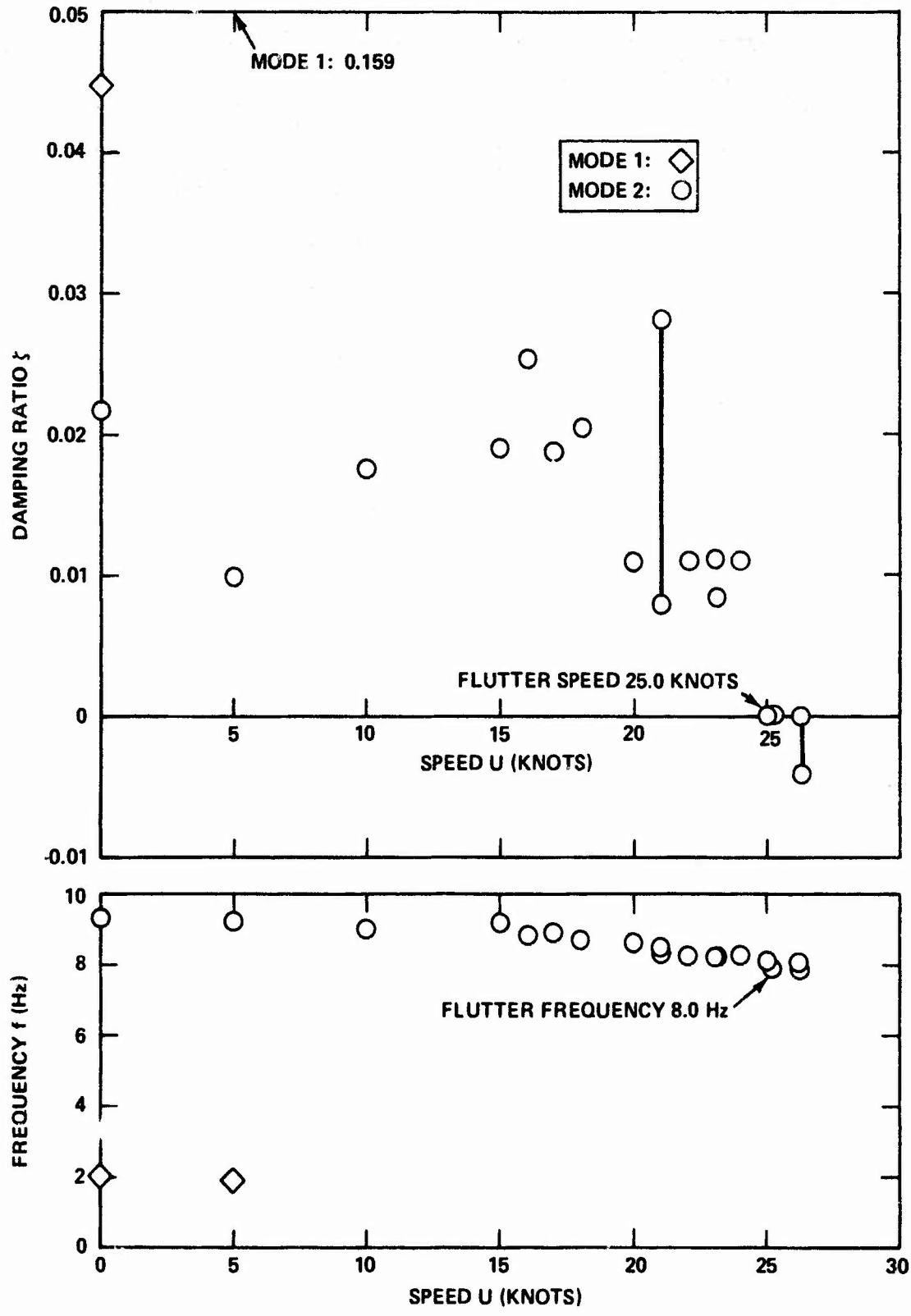

Figure 13f - Model 2T with Pod G, Strut Submergence
$\ell/L = 0.20$

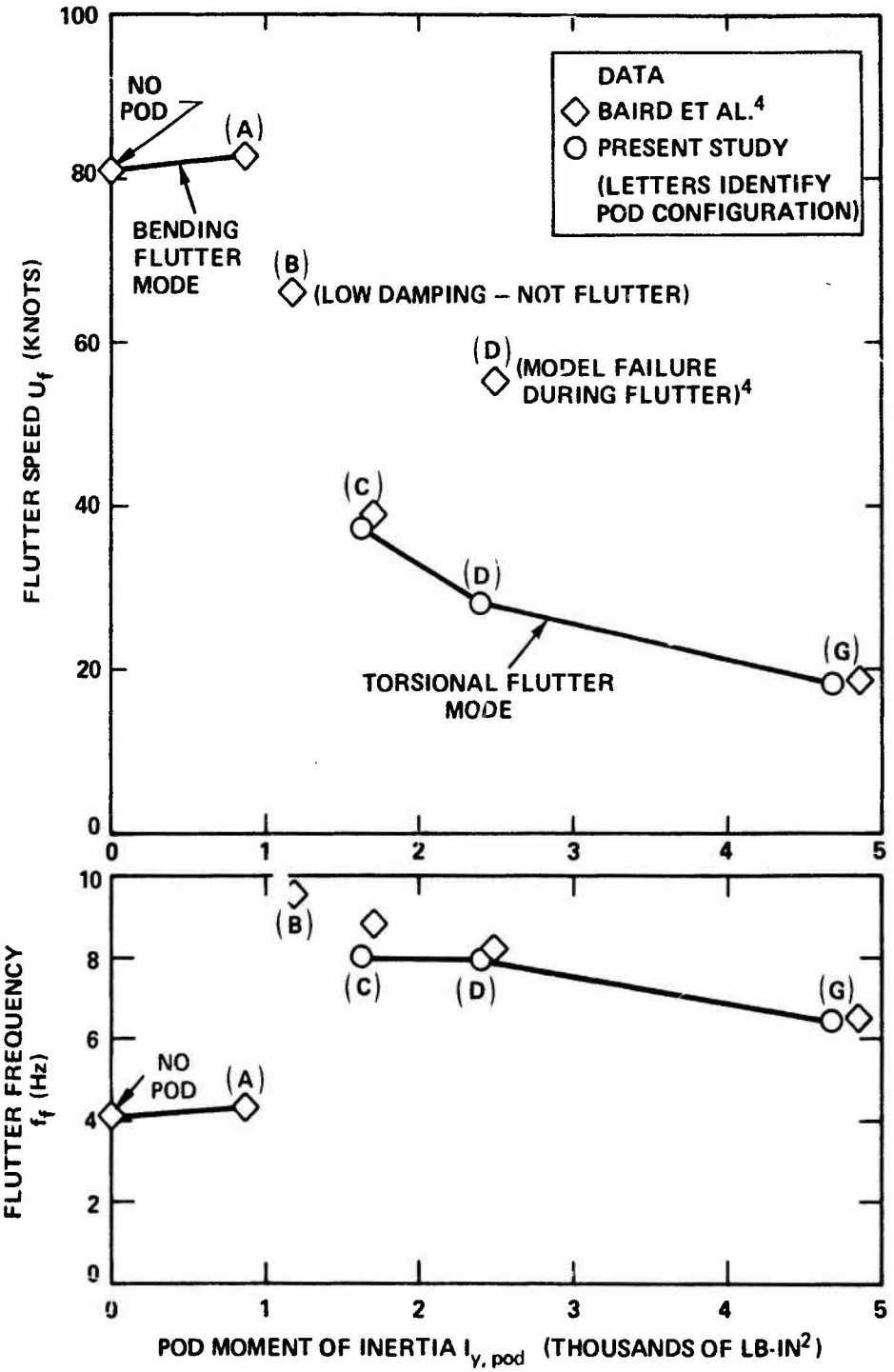

Figure 14 - Effect of Pod Moment of Inertia on Flutter Speed and Flutter Frequency for Model 2T at Strut Submergence $\ell/L = 0.793$

explanation can be confidently advanced because the Pod C configuration was operated in the present experiment up to 52 knots (more than 15 knots above flutter inception) without displaying excessively large oscillations.

Effect of Strut Submergence

For the Pod G configuration, decreasing strut submergence steadily decreased the maximum value of ζ until the damping peak at intermediate speed completely disappeared. Flutter speed first decreased and then increased, exhibiting a minimum value at about 55-percent submergence, as shown in Figure 15. The minimum flutter speed was estimated to be 16 knots. Flutter frequency, also shown in Figure 15, gradually increased as submergence decreased.

Spontaneous Ventilation

Ventilation occurrences similar to those experienced with Model A also occurred on Model 2T. On two occasions, spontaneous, symmetrical vents appeared aft of the leading edge within a short speed interval of flutter inception. The vents occurred at 18 knots when the strut was 40-percent submerged (inception of flutter at 17 knots) and at 19 knots at 30-percent submergence (compared to a 19.6-knot flutter speed) in both cases with the Pod G configuration.

MODEL ALPHA

Damping and frequency data for the two pod configurations of Model Alpha are shown in Figure 16. Flutter occurred in the second hydroelastic mode, in a first torsion mode shape, at speeds of 6.5 and approximately 18.6 knots.

These data showed a strong dependence of damping and flutter speed characteristics on pod moment of inertia $I_{y,\ pod}$. Gradually decreasing, well-behaved damping values occurred in the unstable mode when the more massive Pod A was used. Flutter inception was indicated to have occurred at 6.5 knots by spectral analysis and at 7.3 knots by visual

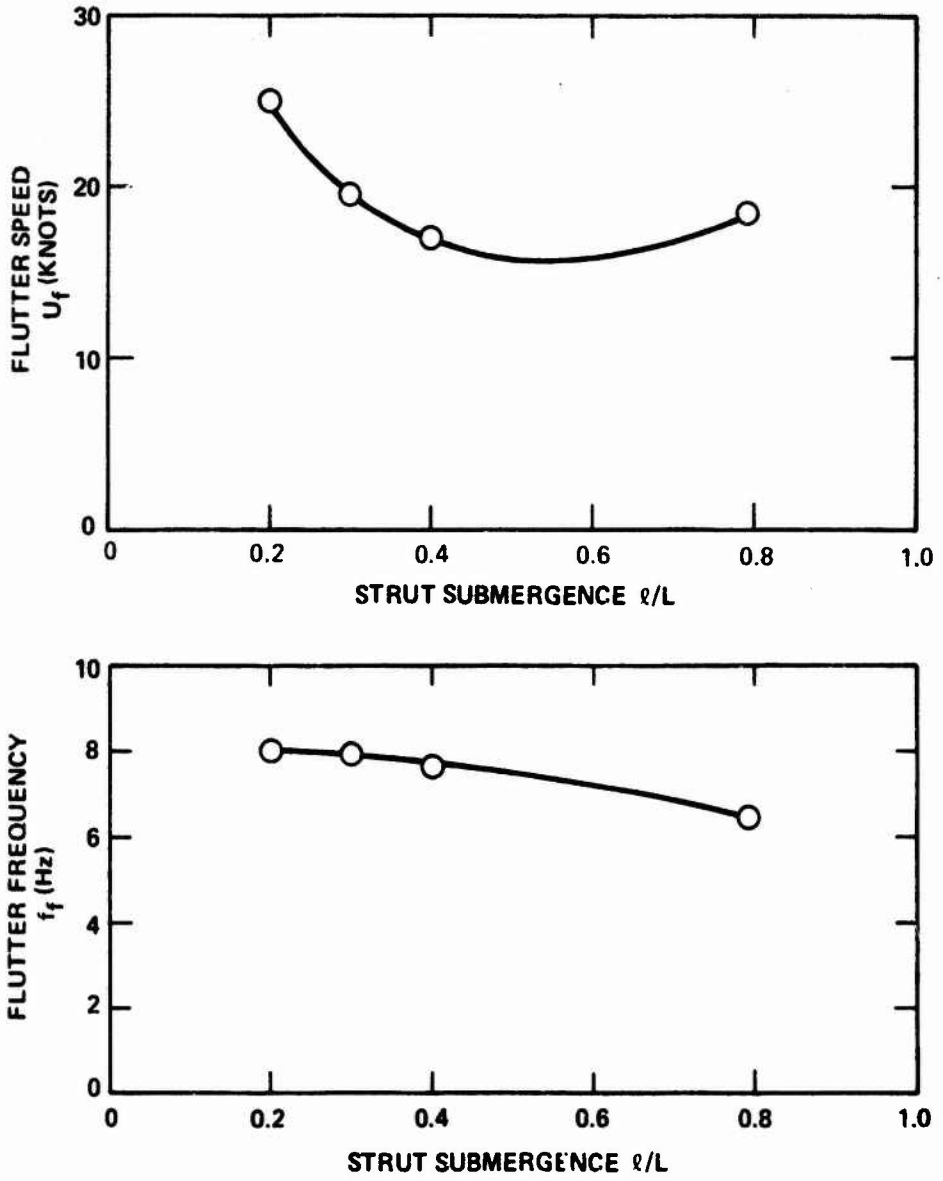

Figure 15 - Effect of Strut Submergence on Flutter Speed and Flutter Frequency for Model 2T with Pod G

Figure 16 - Damping Ratio and Frequency of Oscillation as Functions of Speed for Model Alpha

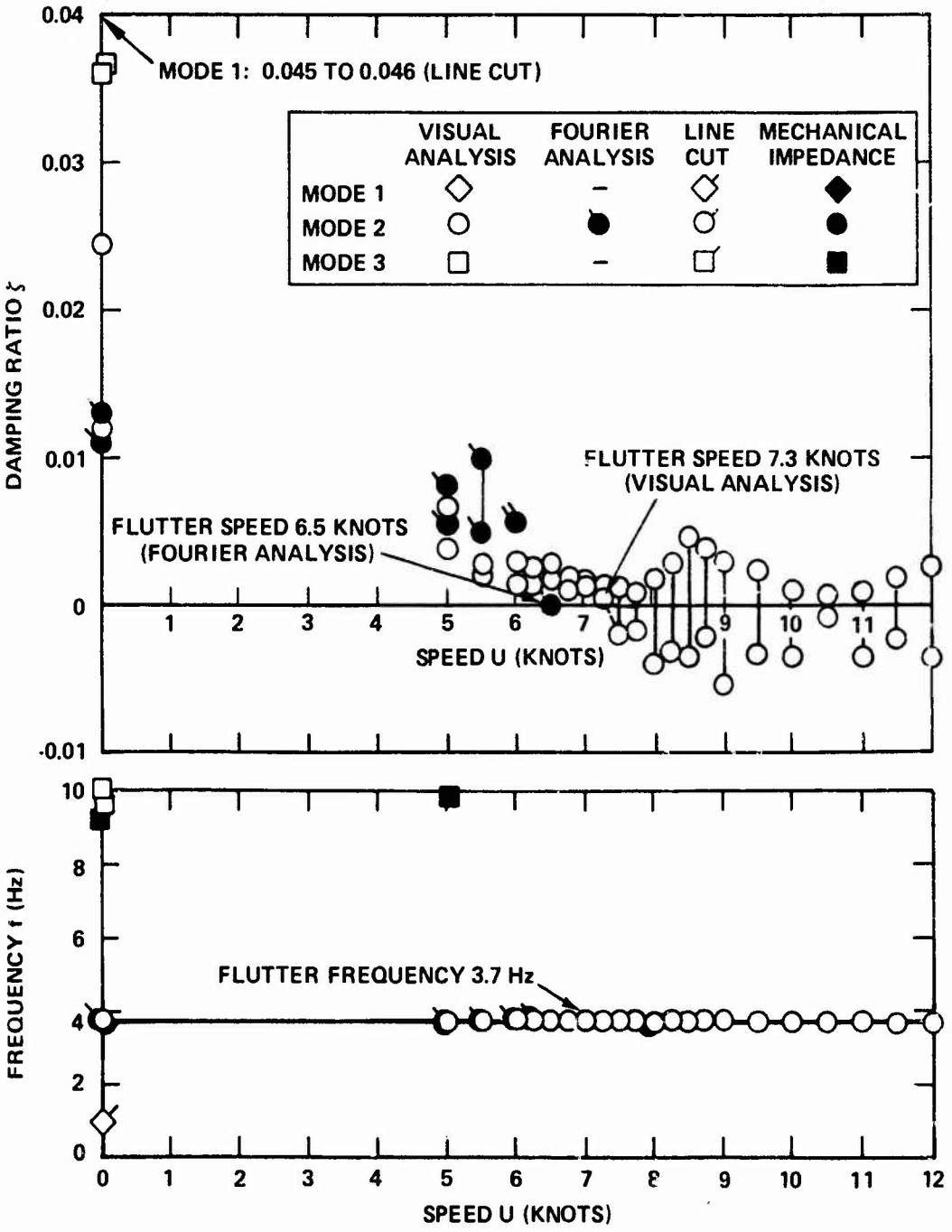

Figure 16a - Model Alpha with Pod A, Strut Submergence $\ell/L = 0.50$

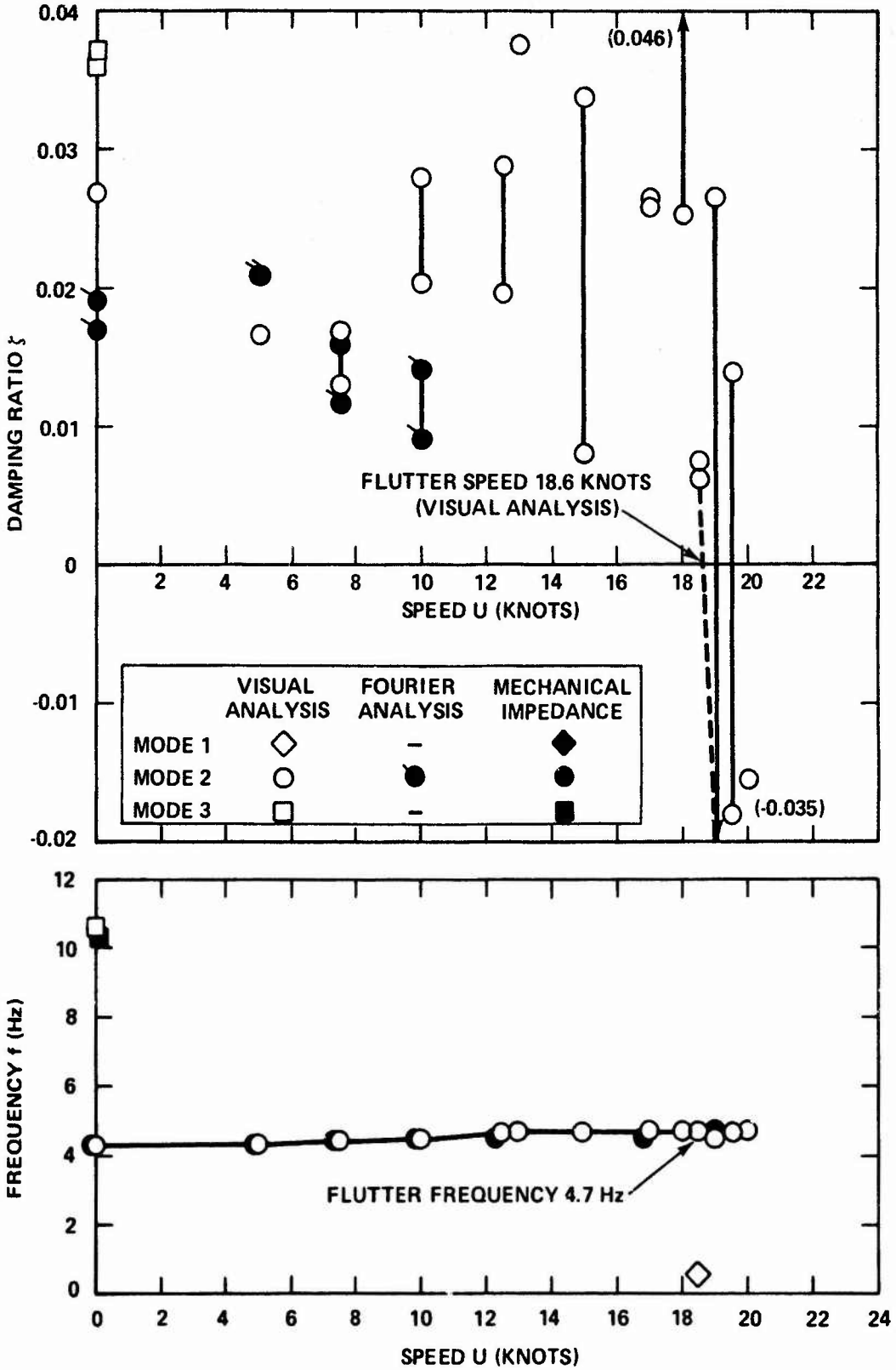

Figure 16b - Model Alpha with Pod B, Strut Submergence
$\ell/L = 0.50$

decay curve analysis. Damping measurements were not made between 0 and 5 knots and so the presence or absence of an initial rise in damping was not determined.

In contrast, damping values with the lighter Pod B remained high until a much higher speed was reached. There were indications of an increase in damping at intermediate speeds and a rapid decrease near flutter inception; these were estimated to have occurred at 18.6 knots, but considerable data scatter made the exact trend unclear. Positive damping was found by spectral analysis to occur up to at least 13 knots in the torsional mode.

There are several reasons for data scatter in the higher speed range. Flow-induced random oscillations, appearing as noise in the transducer response, began to reduce the readability of the already limited number of torsional oscillations at speeds above 10 knots. Further degradation in the decay curve was produced by a first-bending-mode oscillation which appeared at about 15 knots and increased in amplitude, possibly because of decreasing damping, up to 20 knots. The bending oscillation had a triangular rather than a sinusoidal waveform with an approximate frequency range of 0.3 to 0.6 Hz. Only one such frequency is shown in Figure 16b because frequent disruptions in the oscillation usually prevented a precise frequency from being obtained. No damping values were found.

MODEL BETA

Flutter characteristics of Model Beta were obtained for three strut profile configurations, two pod lengths, several values of pod moment of inertia, and two strut submergence levels for the model with and without an attached foil. Damping and frequency measurements are plotted in Figure 17.

Most flutter instabilities occurred in the second hydroelastic mode and had a first torsion mode shape. Variations in damping of this unstable mode followed the same pattern described for the previous

Figure 17 - Damping Ratio and Frequency of Oscillation as Functions of Speed for Model Beta

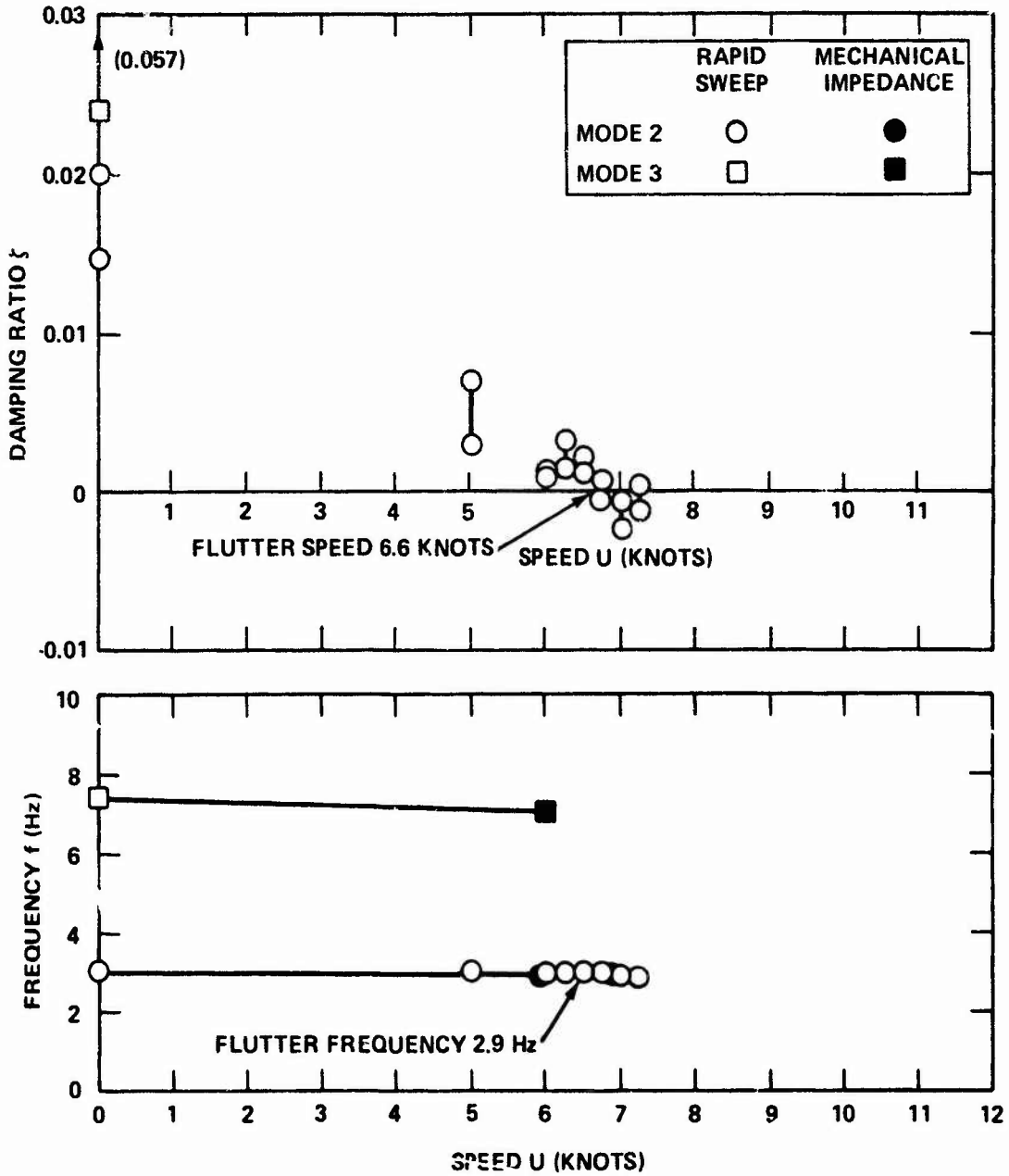

Figure 17a - Model Beta with NACA Profile, Pod A, Strut Submergence $\ell/L = 0.52$

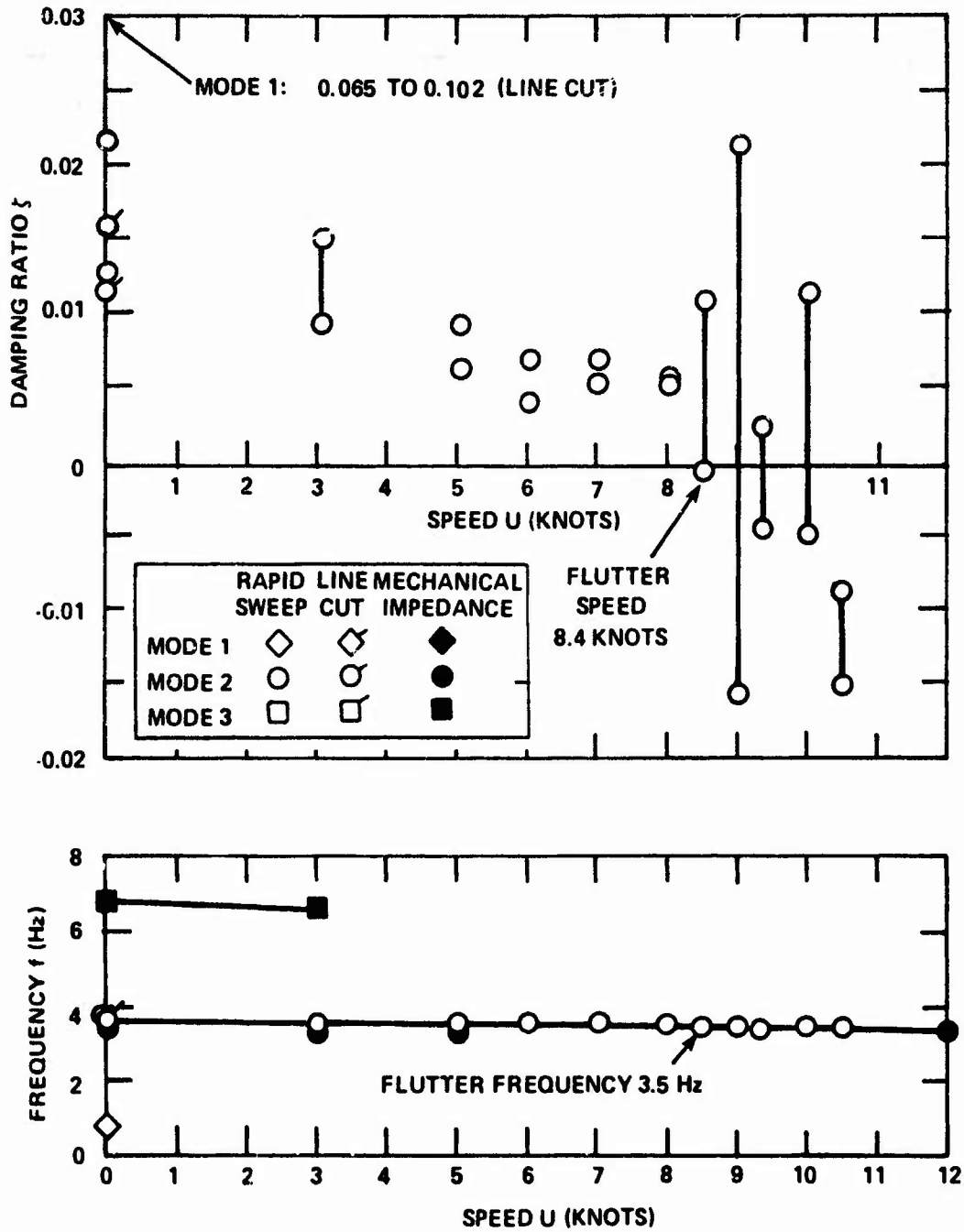

Figure 17b - Model Beta with NACA Profile, Pod B, Strut Submergence ℓ/L = 0.52

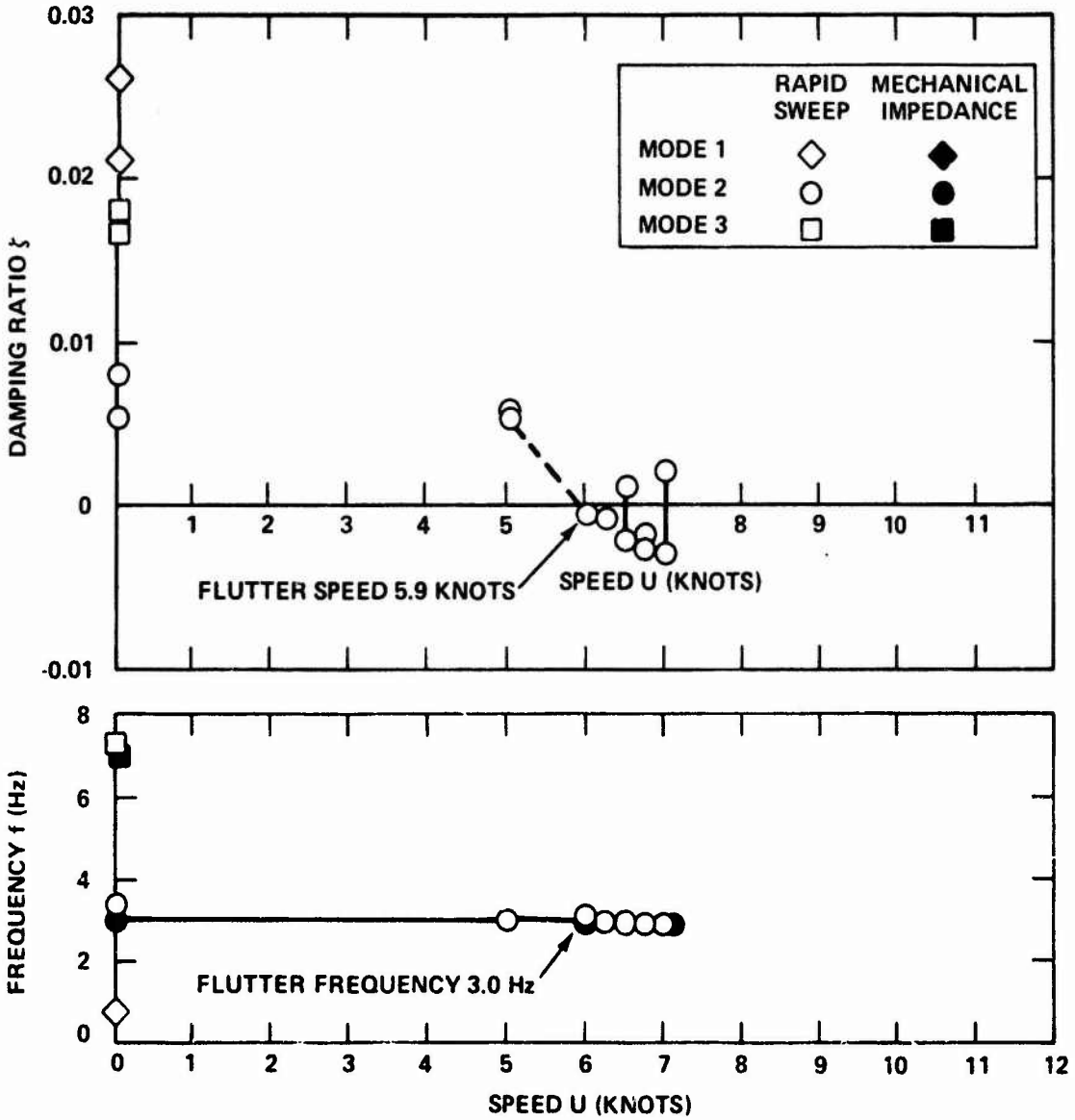

Figure 17c - Model Beta with Blunt Base Profile, Pod A, Strut Submergence $\ell/L = 0.52$

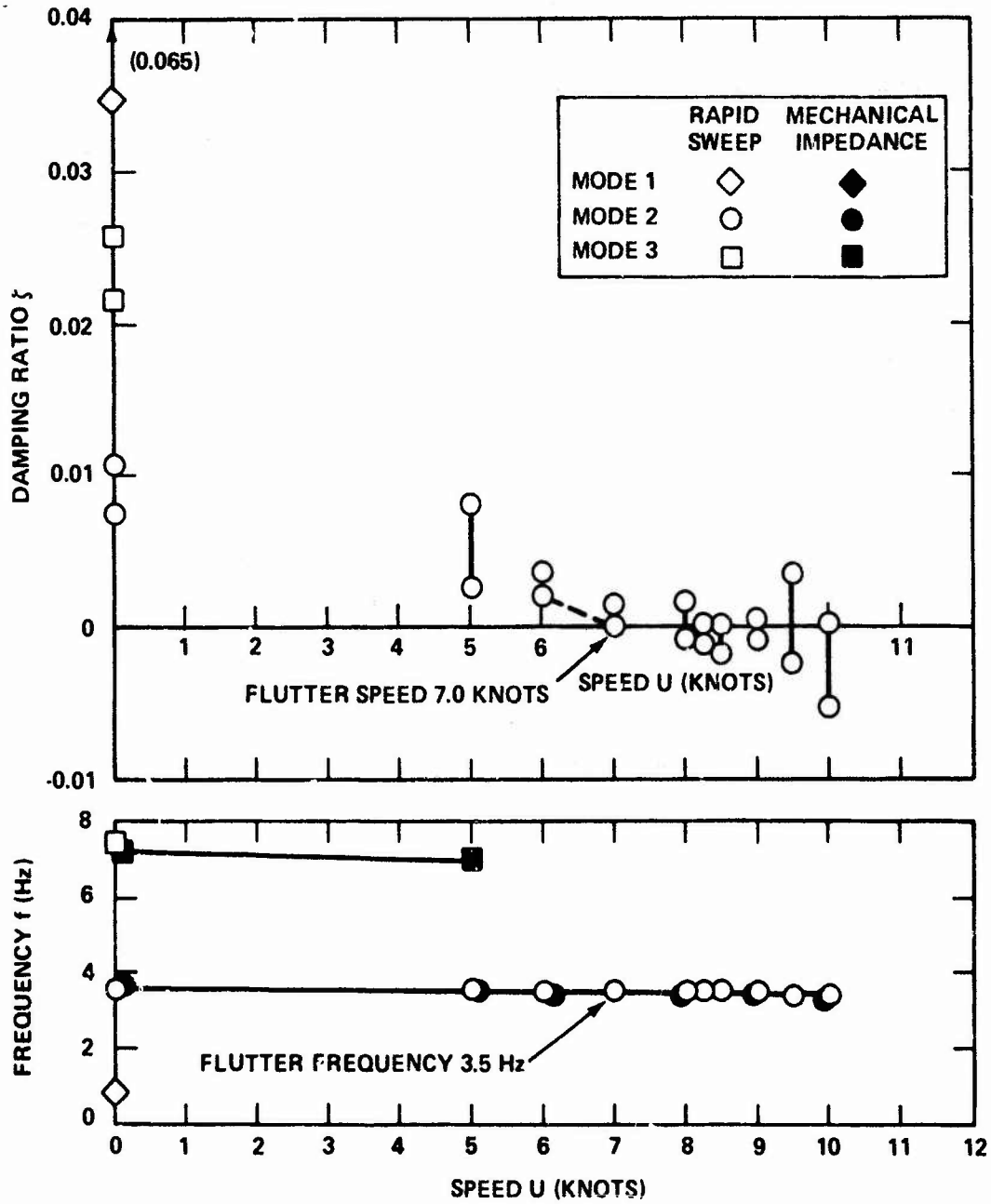

Figure 17d - Model Beta with Blunt Profile, Pod B, Strut Submergence $\ell/L = 0.52$

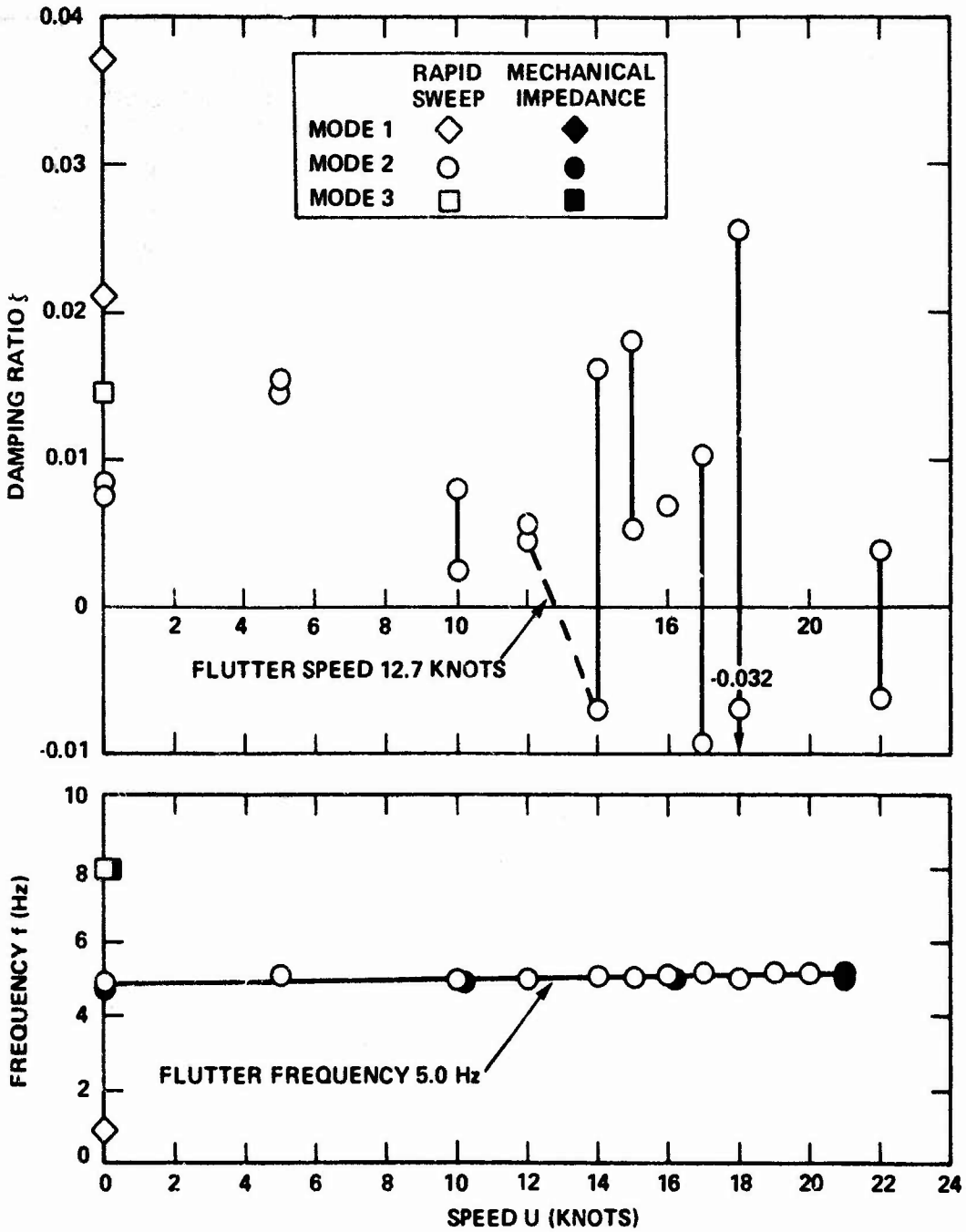

Figure 17e - Model Beta with Blunt Base Profile, Pod C, Strut Submergence $\ell/L = 0.52$

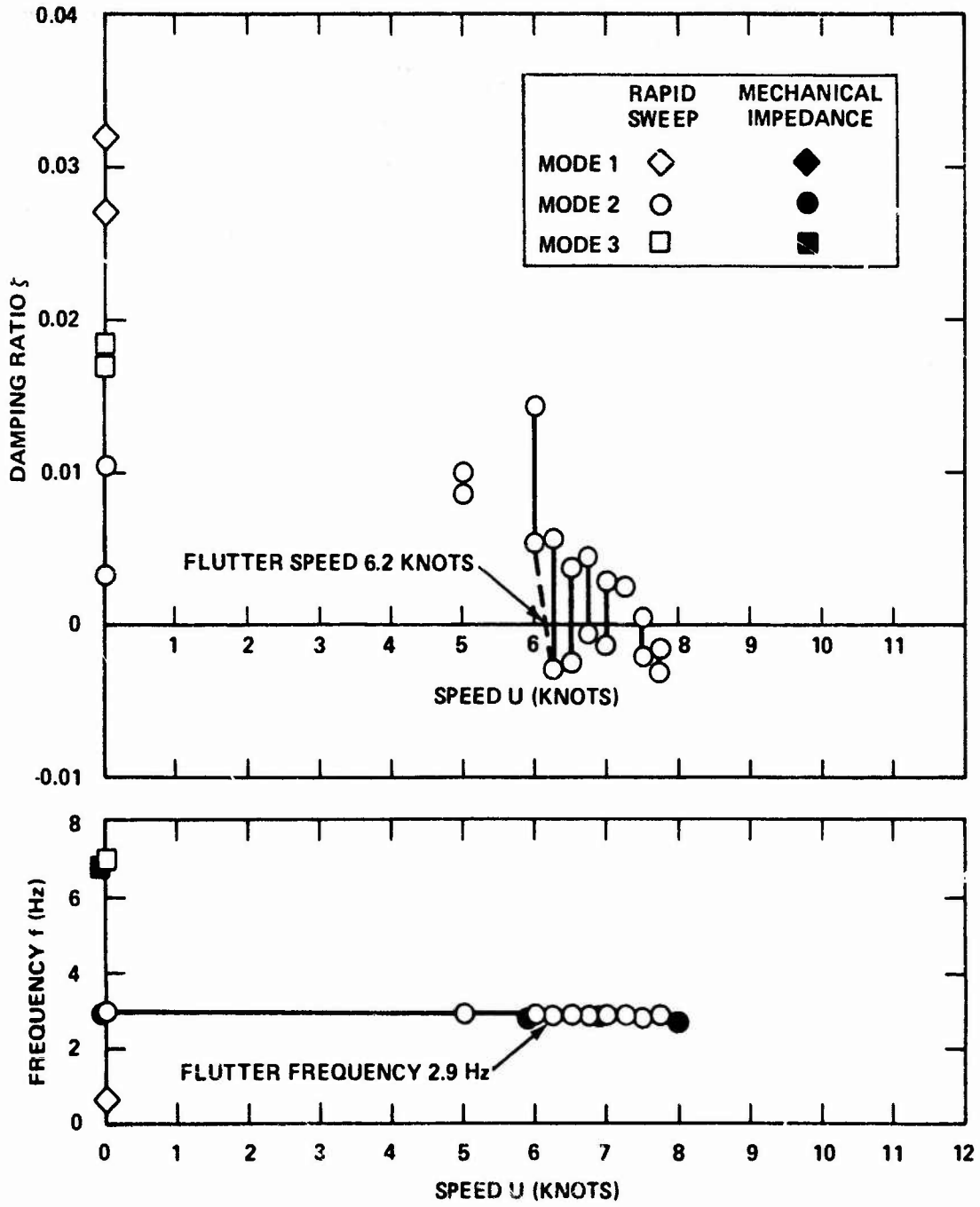

Figure 17f - Model Beta with Blunt Leading Edge Profile, Pod A, Strut Submergence ℓ/L = 0.52

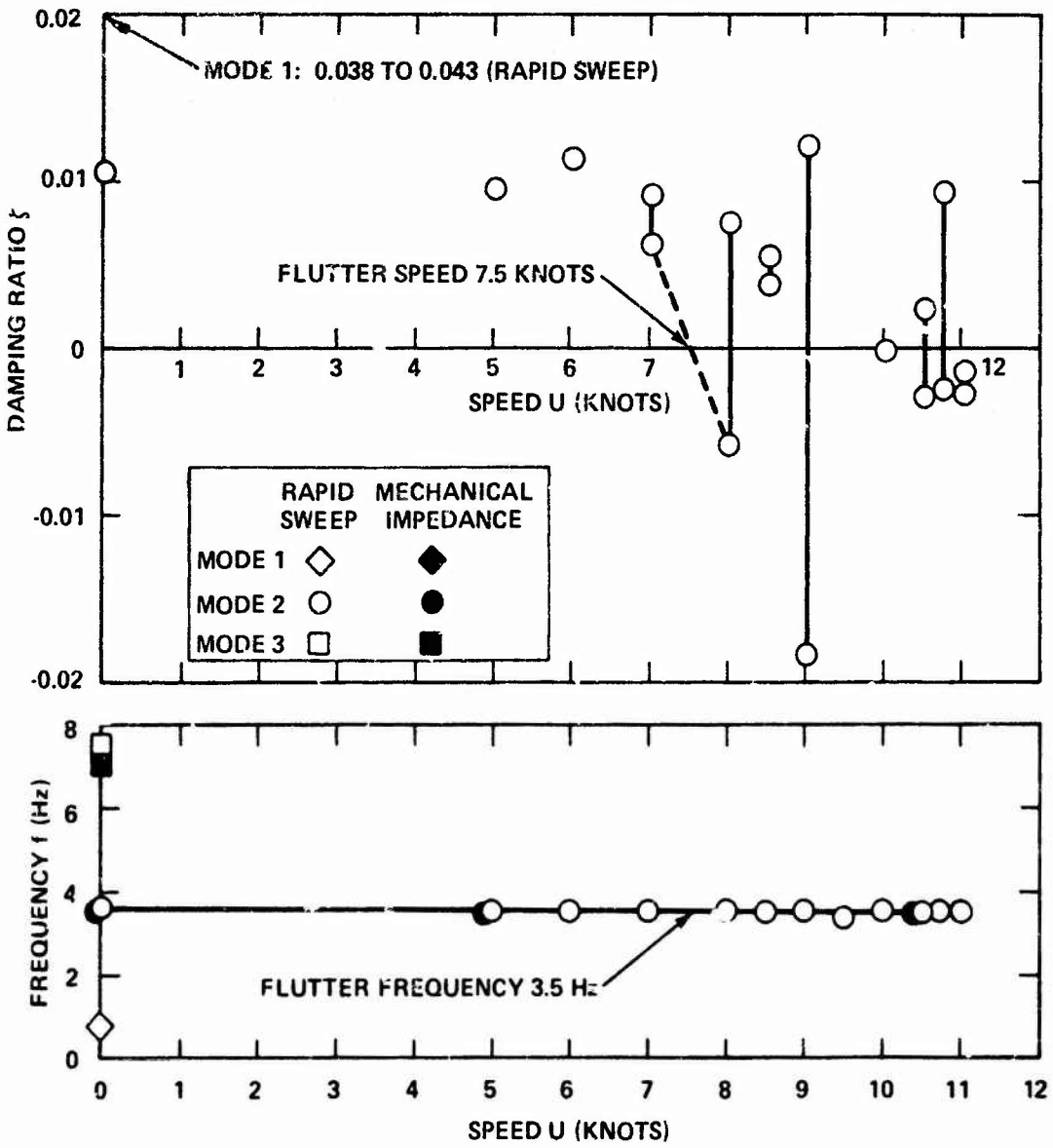

Figure 17g - Model Beta with Blunt Leading Edge Profile, Pod B, Strut Submergence S/L = 0.52

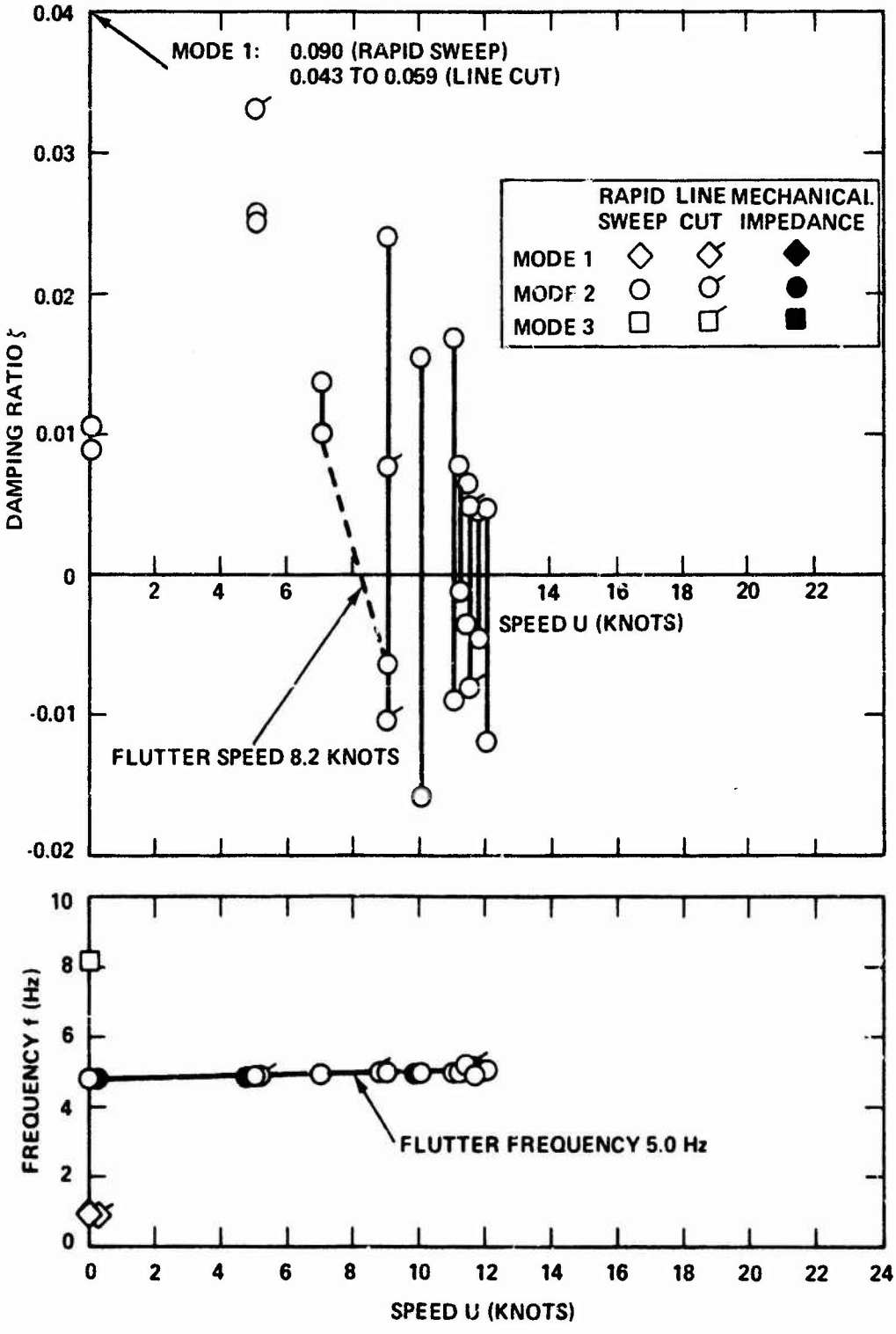

Figure 17h - Model Beta with Blunt Leading Edge Profile, Pod C, Strut Submergence $\cdot$/L = 0.52

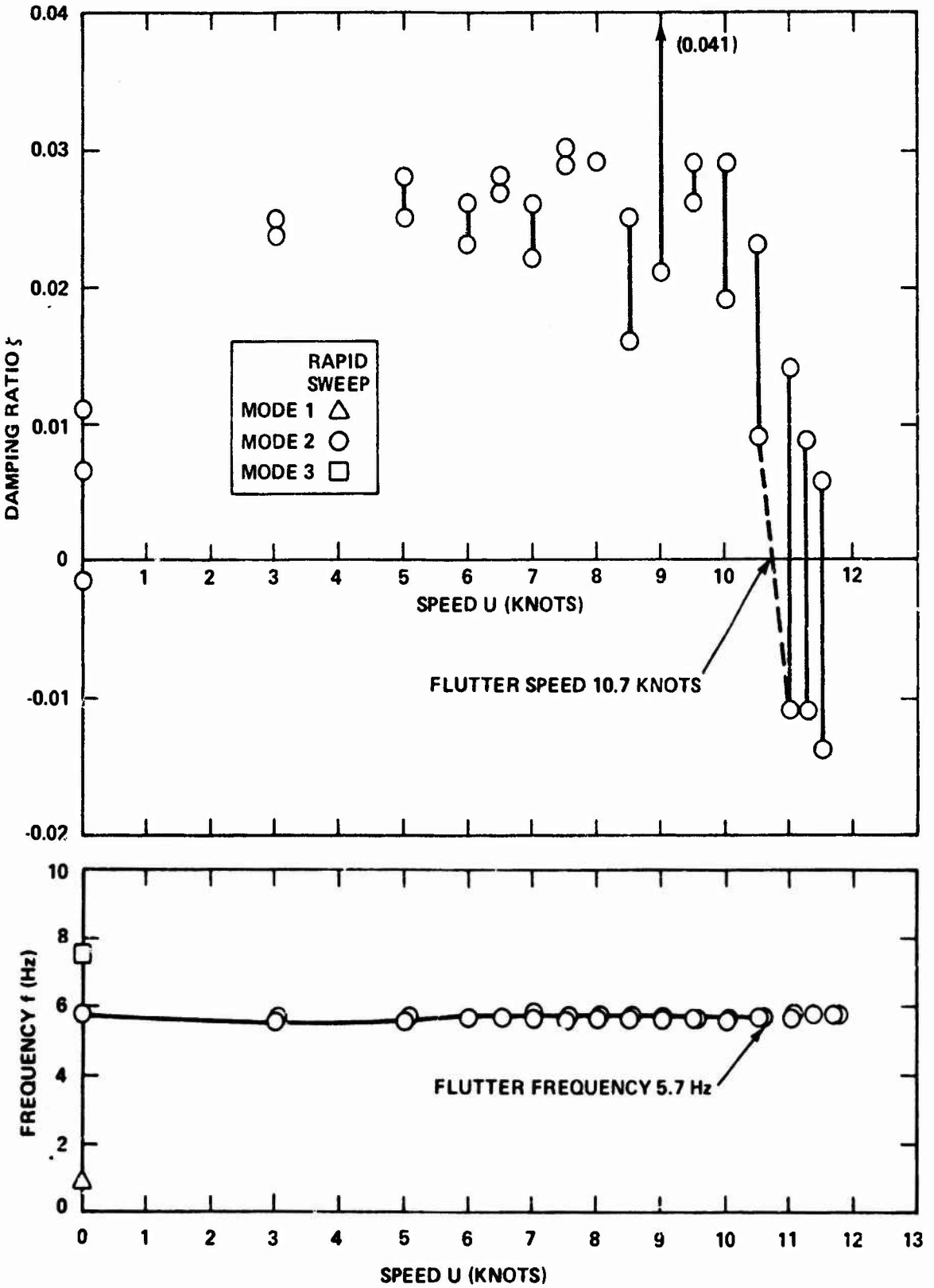

Figure 17i - Model Beta with Blunt Leading Edge Profile, Pod D, Strut Submergence $\ell/L = 0.52$

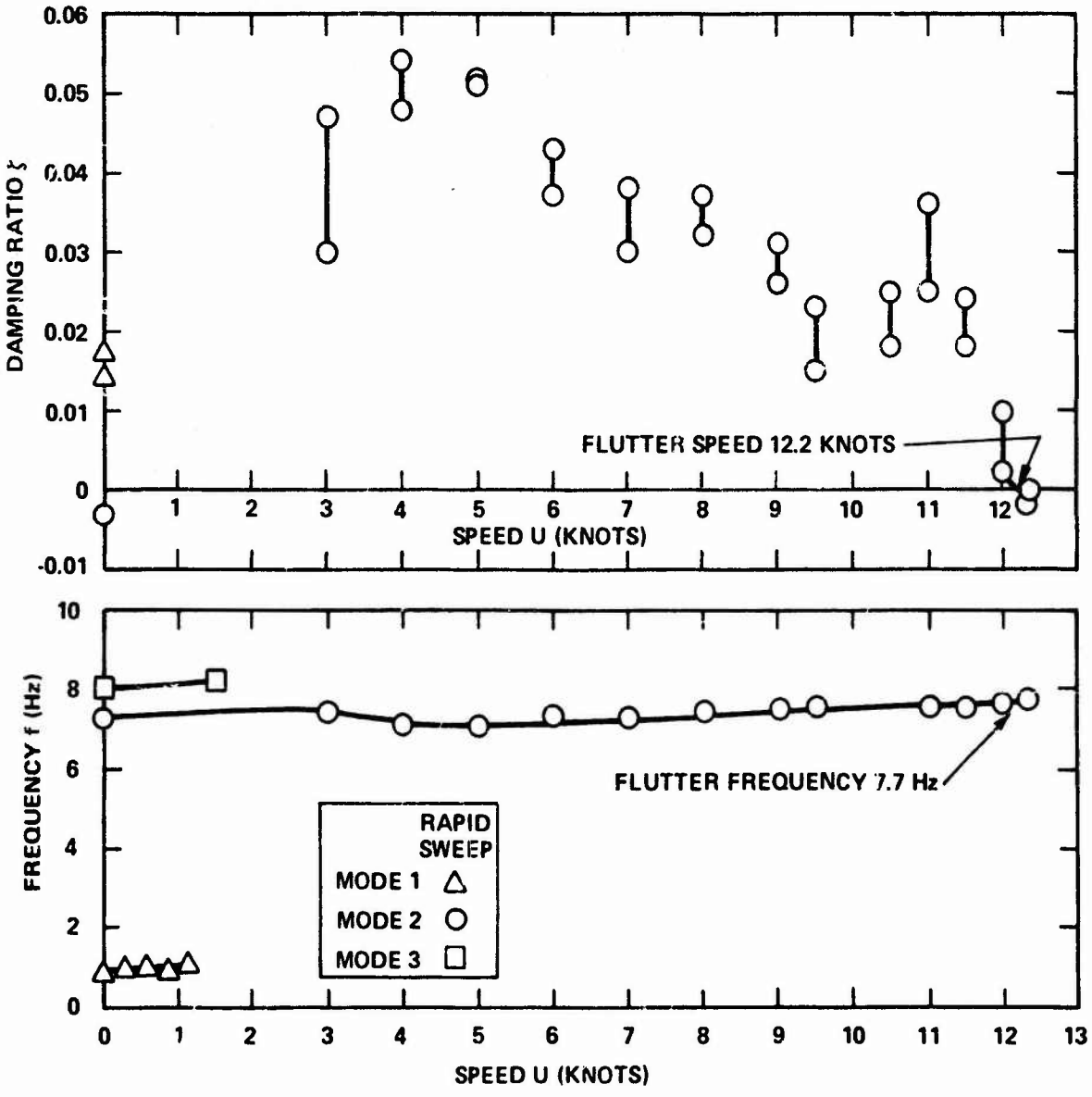

Figure 17j - Model Beta with Blunt Leading Edge Profile, Pod F, .
Strut Submergence ℓ/l. = 0.52

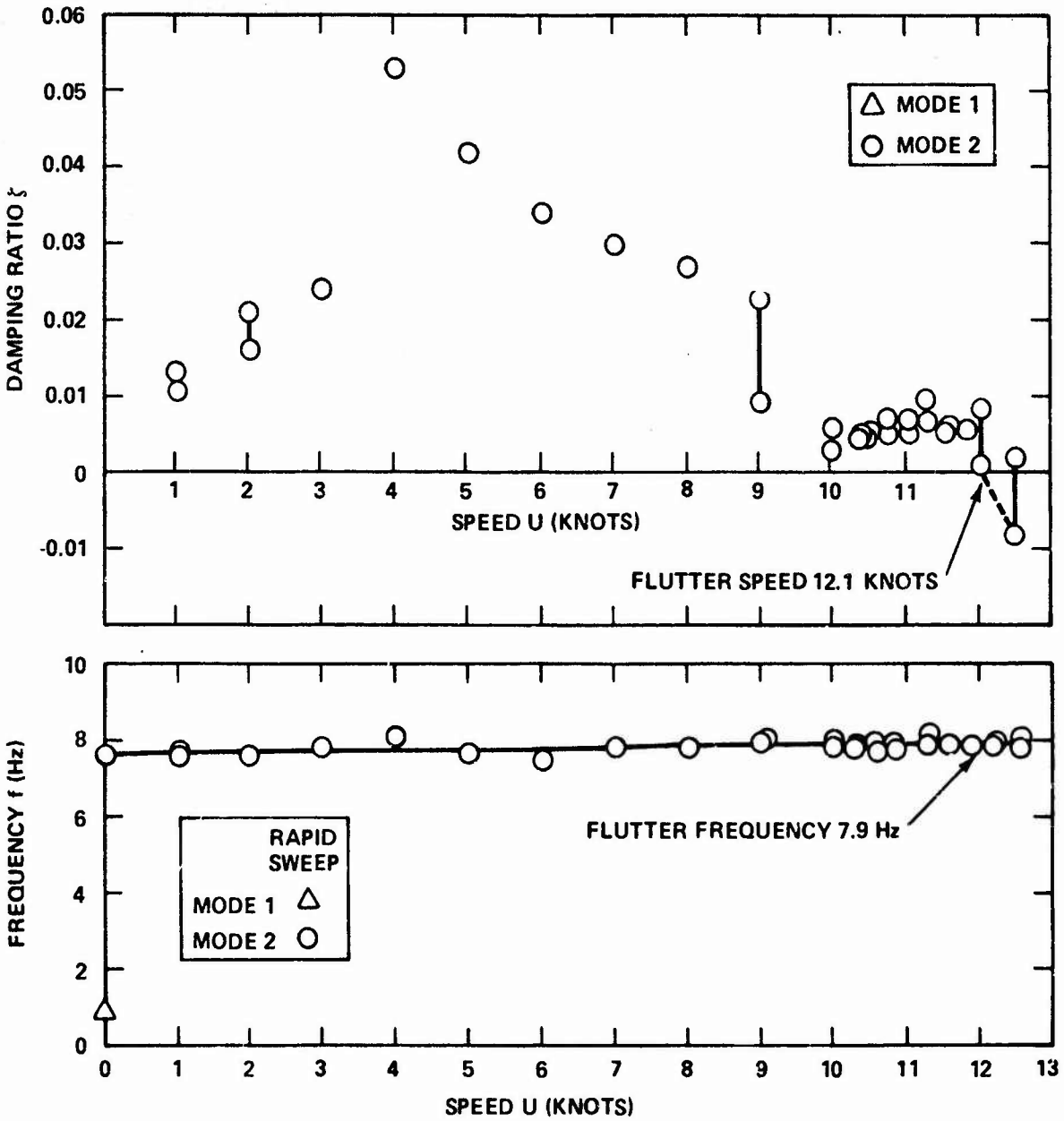

Figure 17k - Model Beta with Blunt Leading Edge Profile, Pod E, Strut Submergence $\ell/L = 0.28$

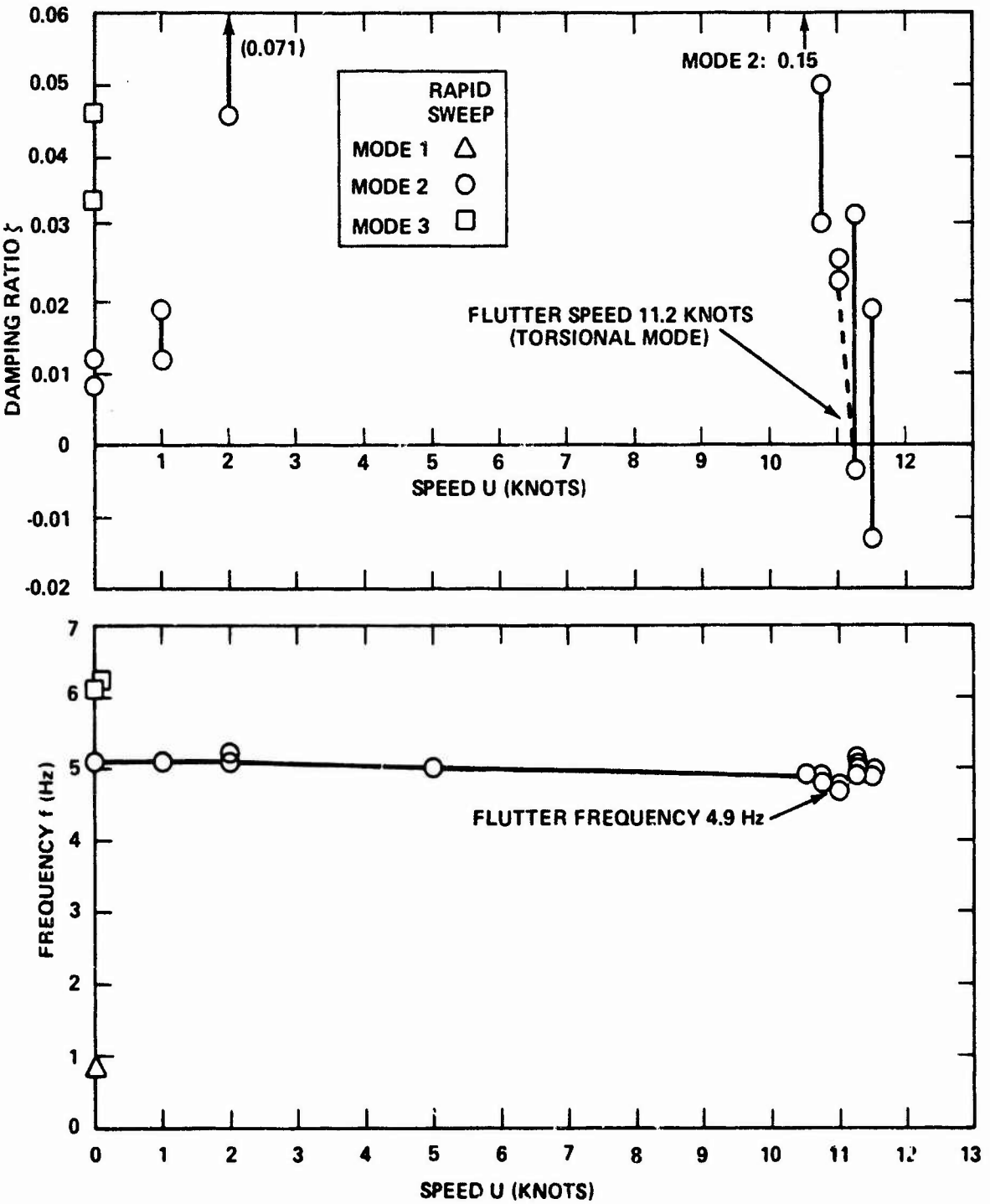

Figure 171 - Model Beta with Blunt Leading Edge Profile, Pod DF and Foil, Strut Submergence $\ell/L = 0.52$

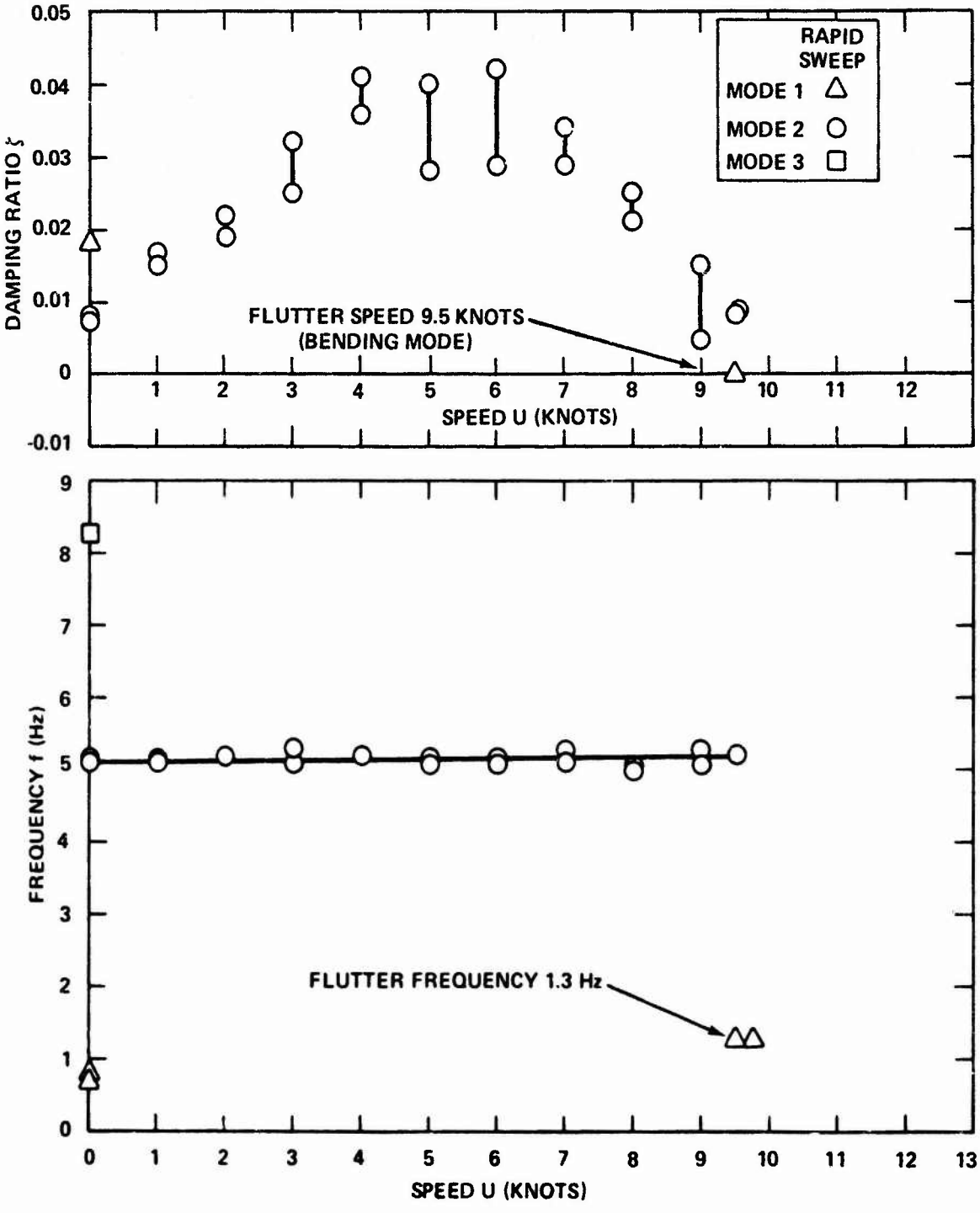

Figure 17m - Model Beta with Blunt Leading Edge Profile, Pod DF and Foil, Strut Submergence ℓ/L = 0.28

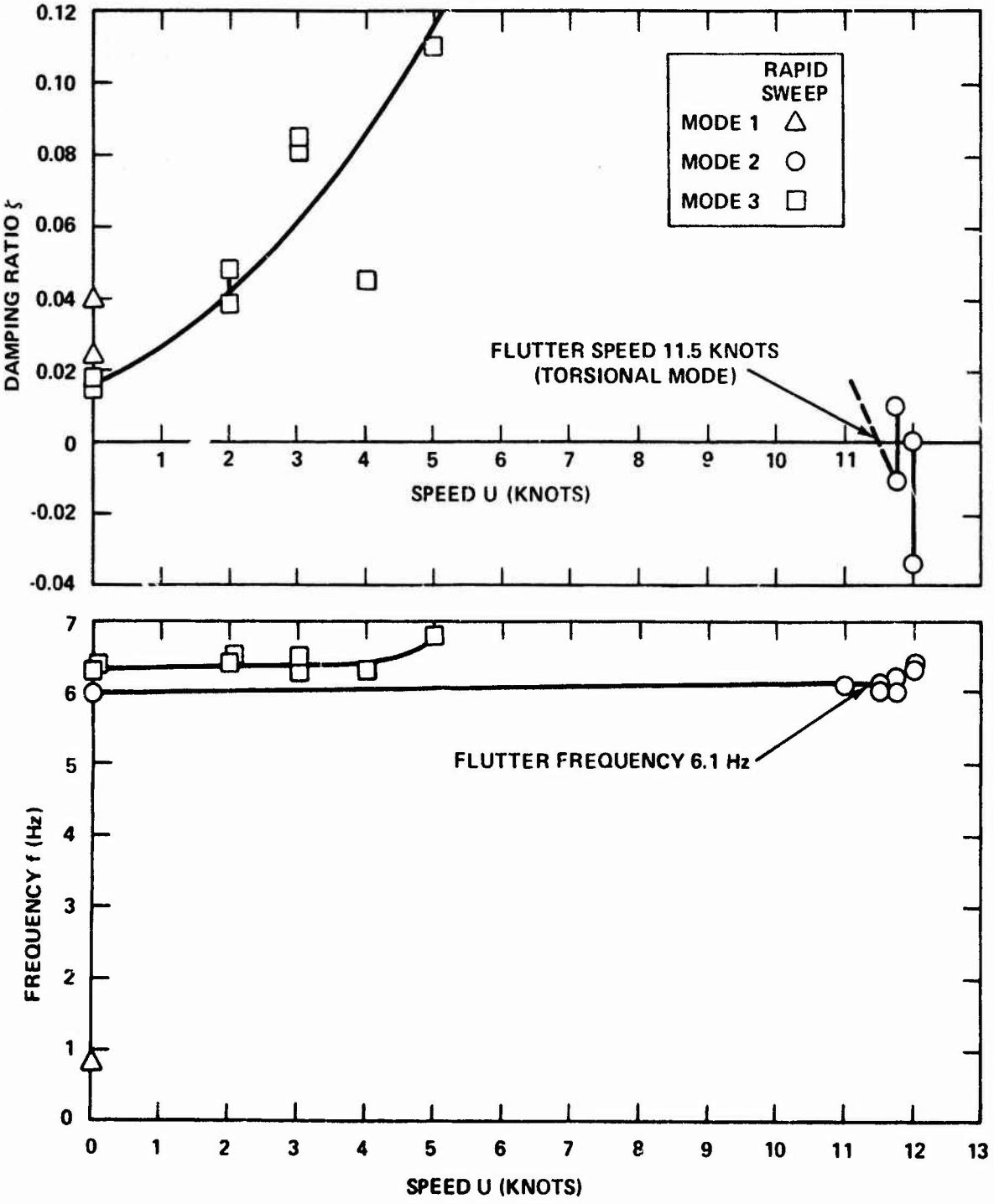

Figure 17n - Model Beta with Blunt Leading Edge Profile, Pod EF and Foil, Strut Submergence ℓ/L = 0.52

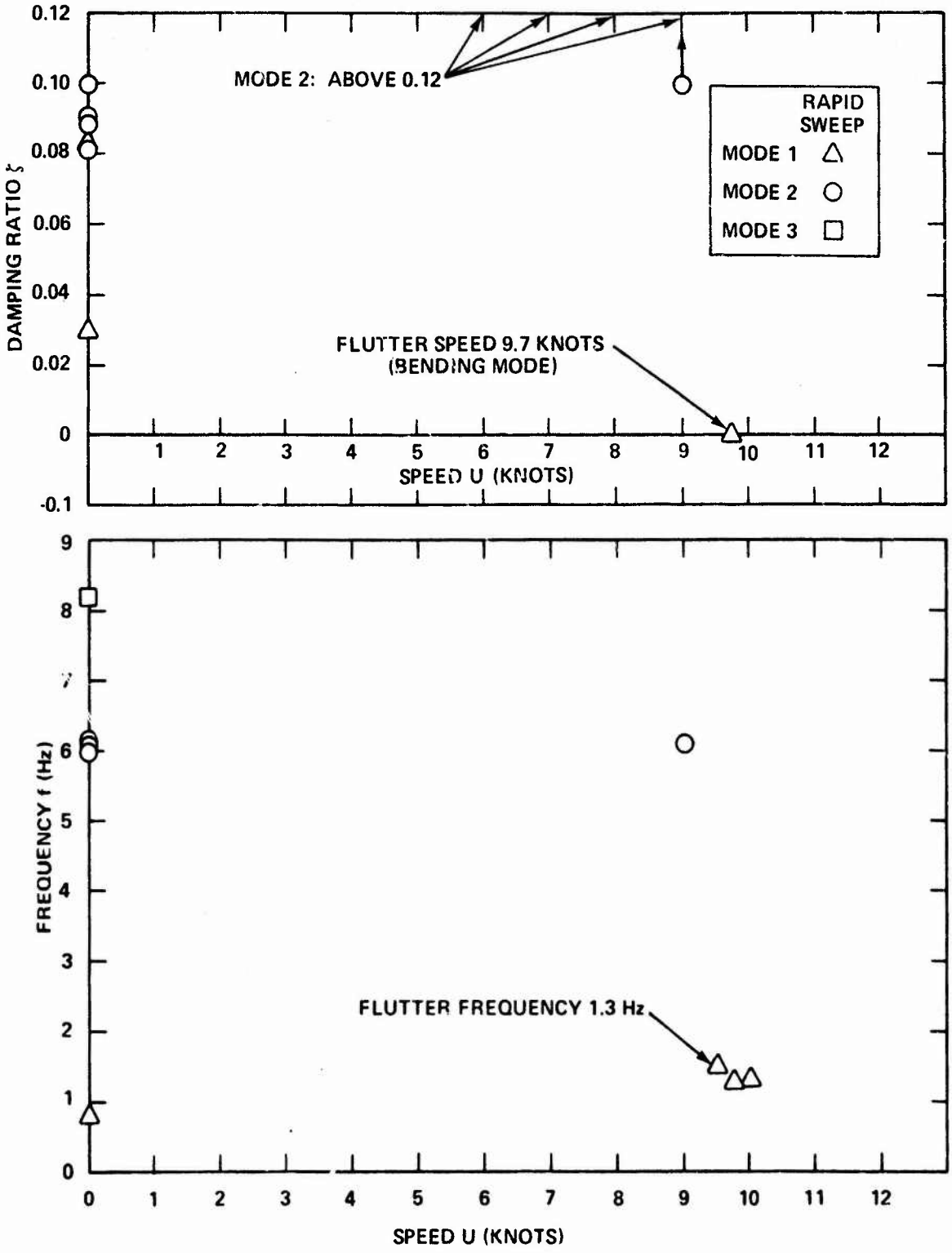

Figure 17o - Model Beta with Blunt Leading Edge Profile, Pod EF and Foil, Strut Submergence ℓ/L = 0.28

models. Zero-speed damping values ζ ranged from 0.5 to 2 percent of critical damping. As speed increased, damping initially increased, reached a peak at intermediate speeds, and then decreased to zero. Some peak damping values were as high as 15 percent but most were much lower. Second-mode frequencies remained nearly unchanged over the entire speed range.

Visual observations indicated that two model configurations (those with pod-foils DF and EF) underwent flutter in a first bending mode shape. Damping and frequency in this mode could not be accurately measured at speeds below flutter inception, but values of damping are known to have been well above 10 percent. The sudden appearance of unstable bending oscillations indicated that damping had decreased more than 10 percent over a speed interval of less than 1/2 knot. The bending instability did not interfere with measurement of the torsional mode characteristics, however. Damping and frequency values of the torsional (second) hydroelastic mode were measured for the pod-foil DF configuration over the entire speed range up to flutter inception of the bending mode; see Figure 17m. Moreover, the second mode itself appeared to be on the verge of experiencing torsional flutter when bending flutter intervened at 9.5 knots. It is estimated that torsional flutter would have occurred at approximately 10.5 knots. Frequencies in the unstable bending mode were slightly above zero-speed values for the first hydroelastic mode but far below second-mode frequencies.

Flutter speeds varied widely as system parameters were changed. The effects of strut, pod, and foil parameters on flutter speed are detailed in the following sections.

Effect of Strut Cavitation

The Pod A, B, and C configurations were flutter tested with either two or three of the strut profiles previously described. Two of these profiles produced significant amounts of cavitation. The blunt leading edge profile produced a ventilated cavity originating at the leading edge and enveloping more and more of the strut as speed increased.

The cavity covered about one-third of the submerged strut area at 8 knots and enveloped about three-quarters of the strut at 11.75 knots; see Figure 18. The blunt-base profile produced a ventilated base cavity aft of the strut but had no cavitation forward of the trailing edge. The NACA profile was noncavitating, as were both the longer and shorter pods themselves.

Flutter speeds were obtained for all three strut profiles with the heavier Pods A and B. The NACA profile configuration was slightly more stable than the two cavitating profiles, which did not differ significantly in flutter speed. Very little cavitation occurred in the 5.9- to 7.5-knot speed range involved.

With the lighter weight Pod C, a difference in strut profile had a much greater effect on flutter speed. This pod configuration was evaluated with the blunt base and blunt leading edge profiles only. Flutter occurred at 12.7 knots with the blunt base profile and at 8.2 knots (a decrease of 35 percent) with the blunt leading edge profile.

Effect of Strut Submergence

Changes in strut submergence had very little effect on flutter speed in the torsional mode, but data obtained for the blunt leading edge strut profile indicated that these changes did affect the bending flutter speed. When submergence decreased from 52 to 28 percent, the torsional flutter speed of 12.2 knots for the Pod E configuration remained virtually the same. Similarly, the torsional mode for pod-foil DF decreased only from 11.2 knots to an estimated 10.5 knots. This difference might have been even less but, as noted, the occurrence of bending flutter prevented further measurements.

By contrast, the bending flutter speed was strongly influenced by the change in strut depth. At the shallower submergence of 28 percent, bending flutter occurred at 9.5 and 9.7 knots for pod-foil configurations DF and EF, respectively. At 52-percent submergence, bending flutter for the same configurations did not occur at speeds up to 11.2 and 11.5 knots, respectively, (corresponding to an increase in the bending flutter speed of at least 1.7 knots, or 18 percent).

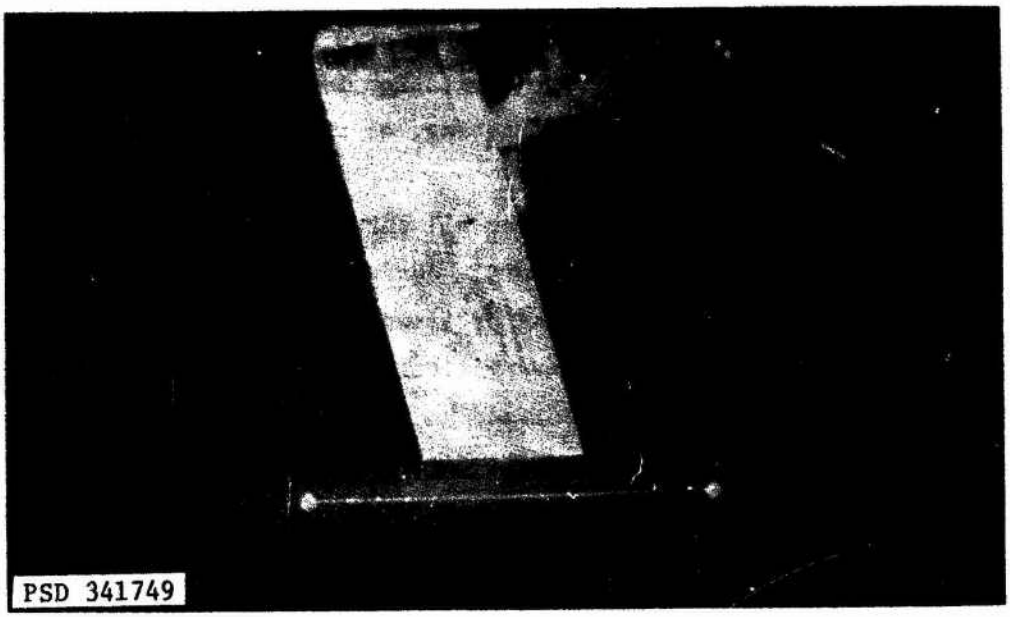

Speed U = 8 Knots; Strut Submergence ℓ/L = 0.52

Speed U = 11.75 Knots; Strut Submergence ℓ/L = 0.52

Figure 18 - Underwater Photographs of Model Beta with Blunt Leading Edge Profile and Pod C in the High Speed Basin

Within the range of available data, the net effect of a decrease in submergence on the pod-foil configuration was a decrease in the maximum stable operating speed. Furthermore, the submergence change reversed the relative stability of the two flutter modes.

Effect of Pod Moment of Inertia

Reducing pod moment of inertia $I_{y,\ pod}$ invariably increased flutter speed. However, the increases were relatively small except for the blunt base profile configuration. With that strut profile, changing from Pod A to Pod C raised the flutter speed in the torsional mode from 5.9 to 12.7 knots, a huge increase of 115 percent. In contrast, a similar pod change with the blunt leading edge profile raised U_f only 32 percent. Increases in U_f were even less pronounced in changing from Pod D to Pod E and from the related pod-foil configuration DF to EF, in data obtained with the blunt leading edge strut profile. Flutter speeds in the bending mode did not significantly vary when pod inertia was changed.

Effect of Pod Length

Comparison of data for Pod C and the shorter Pods D and E indicated that reducing pod length increased the flutter speed of the torsional flutter mode for the blunt leading edge strut profile. Flutter occurred at 8.2 knots for Pod C and at 10.7 and 12.2 knots for Pods D and E, respectively. It is believed that a configuration intermediate between Pods D and E would give a flutter speed between 11 and 12 knots. Therefore, a substantial increase in flutter speed accompanied the increase in pod length from 28.5 to 44 in. Figures 19 and 20 show that the strut was largely enveloped in cavitation and that the pods were for the most part fully wetted when flutter occurred.

Effect of Attaching Foil

The foil was attached horizontally to the tip of the strut, with all components of the pod-foil system configured for maximum cavitation.

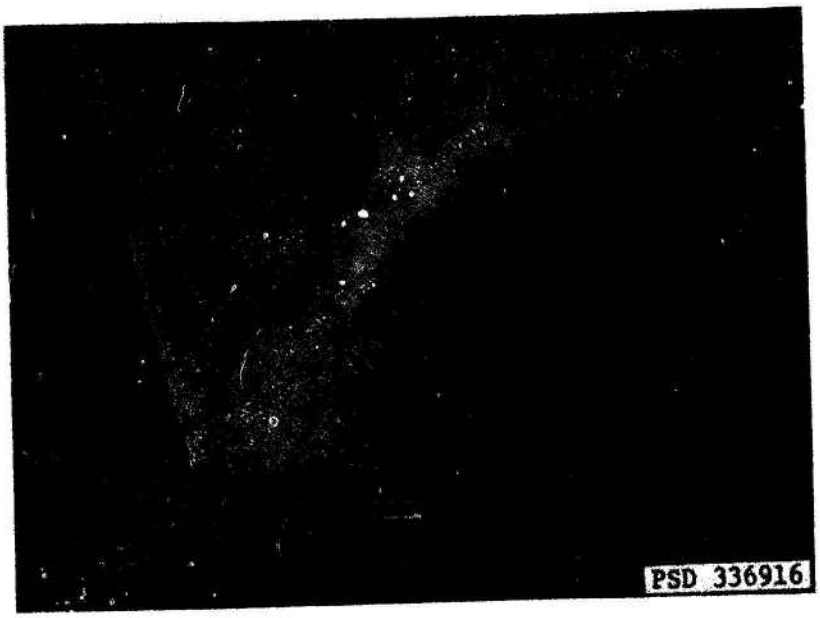

Speed U = 11.5 Knots; Strut Submergence ℓ/L = 0.52

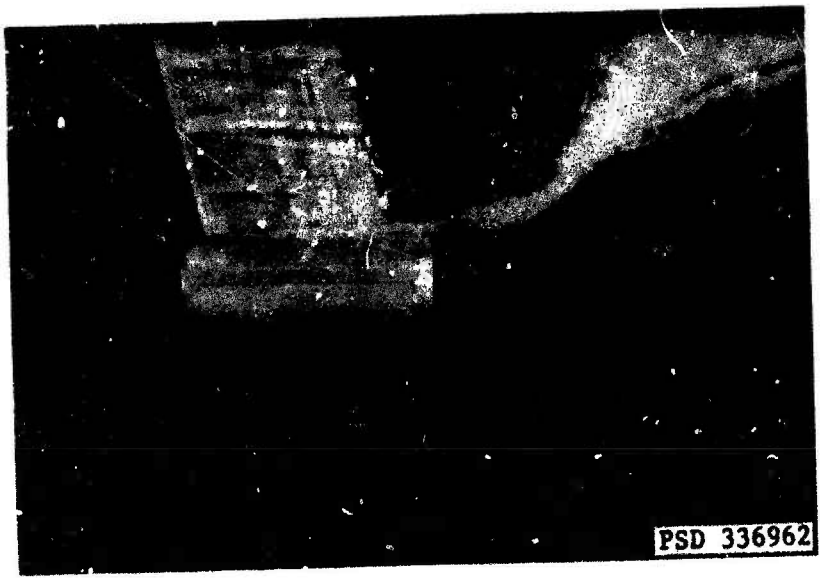

Speed U = 11.8 Knots; Strut Submergence ℓ/L = 0.28

Figure 19 - Underwater Photographs of Model Beta with Blunt Leading Edge Profile and Pod E in the High Speed Basin

Figure 20 - Photographs of Model Beta with Blunt Leading Edge Profile and Attached Pod and Foil, at Speeds near Flutter Inception in the High Speed Basin

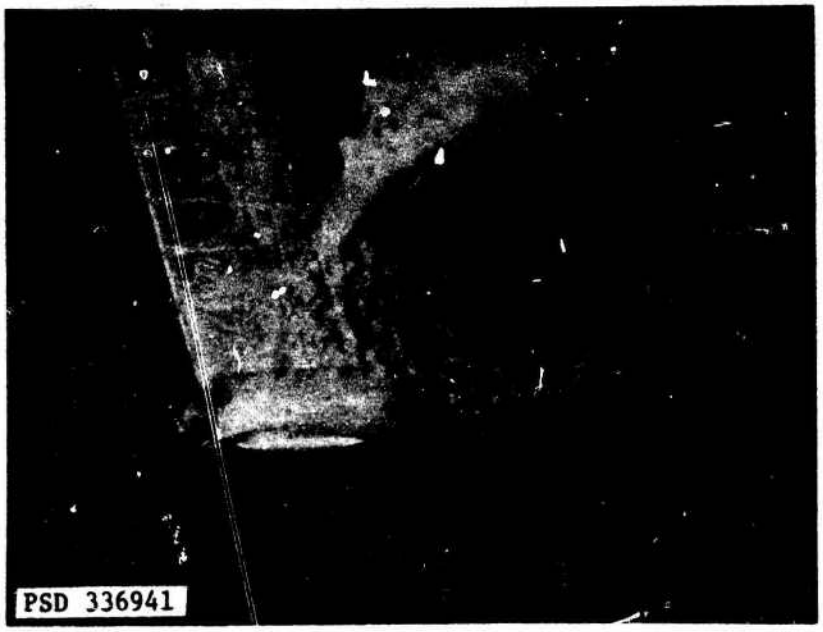

Figure 20a - Underwater View at Speed U = 12 Knots with Pod EF and Foil, Strut Submergence ℓ/L = 0.52

Figure 20b - Above-Water View at Speed U = 9.5 Knots with Pod DF and Foil, Strut Submergence ·/L = 0.28

The blunt leading edge profile was used on the strut, the ventilation trips were in place on both pod and foil, and the ventilating air supply was on. In all instances of flutter, the strut was almost entirely enveloped by a ventilated cavity and the upper surfaces of the pod and foil were covered by a combination of ventilation and air-water mixture. These conditions are shown in Figure 20b. Even though a positive foil angle of attack would have increased the amount of foil cavitation, the foil was operated at zero incidence because the available angle settings produced excessive side deflections of the strut.

Attaching the foil reduced the bending flutter speed substantially while changing the torsional flutter speed very little. Bending flutter did not occur at speeds up to 12.1 knots for the Pod E configuration, but it appeared at 9.7 knots when the foil was attached, constituting a decrease of 20 percent and possibly more in bending flutter speed. Torsional flutter speeds for Pods D and E at a deeper submergence changed by no more than 6 percent when the foil was attached. The foil can also be interpreted as a parameter which both inverted the relative stability of the bending and torsional modes and reduced the maximum stable speed of operation of the strut system.

DISCUSSION

As detailed in the foregoing sections, many parameters governing the occurrence of flutter were identified and several qualitative trends were noted. Of particular interest was the demonstration, for the first time, of the simultaneous existence of two different unstable modes in the same strut system. It is clear that both modes must be well understood to ensure stability of a given strut system.

The flutter characteristics of the four models are now summarized in terms of parametric trends for each flutter mode, the relative stability of the two modes is discussed, and experimental flutter testing techniques are evaluated.

BENDING FLUTTER MODE

General Characteristics

The hydroelastic mode associated with bending flutter could not be traced from zero speed up to flutter inception. Calculations[1] have shown that the unstable mode first appears at intermediate speeds, critically damped and with zero frequency. At a speed only slightly different, the lowest frequency hydroelastic mode also becomes critically damped and of zero frequency. This correlation suggests that the unstable mode may be a continuation of the first hydroelastic mode. The unstable mode was predicted to decrease rapidly in damping as the flutter inception speed approached.

The present bending flutter modes did show a rapid decrease in damping just prior to flutter inception. Flutter consequently appeared with very little or no warning since high values of damping were not measured. The flutter mode shape was predominantly first bending. Frequencies at flutter were very close to the first bending frequency of the strut at zero speed. In the low-speed range, damping of the first hydroelastic mode rose quickly to a value that was too high to be measured.

Important Flutter Speed Parameters

Important changes in the bending flutter speed were produced by variations in two parameters, namely, strut submergence and the presence or absence of a foil attached to the tip of the strut. However, bending flutter speed was not significantly affected by a third parametric variation which involved simultaneous variation of both pod mass and pod moment of inertia.

Changing strut submergence produced opposite effects for different strut systems. A base-cavitating strut (Model A) exhibited an increase in flutter speed as submergence was decreased. A similar trend has been found for other struts without attached pods or foils.[1] On the other hand, decreasing the submergence of a strut enveloped in cavitation (Model Beta) lowered the bending flutter speed by at least

18 percent. In addition to the cavitation pattern, the reversal in trend might also have been caused by pod or by foil effects, or by some interaction of the three.

Attaching a foil to a strut-pod system significantly decreased bending flutter speed; the reduction was at least 20 percent for Model Beta. Although a large proportion of the submerged strut was enveloped in cavitation, cavitation on the foil was limited to a region of air-water mixture on the upper surface of pod and foil; the exact extent of the region is unknown.

One remaining comparison (pod-foils DF and EF of Model Beta) showed that the bending flutter speed was virtually insensitive to a large change in pod mass and pod moment of inertia.

Additionally, there was some indication that symmetrical, leading-edge ventilation of a strut decreased bending flutter speed relative to a base-vented strut. This possibility was raised by the occurrence of spontaneous ventilation on Models A and 2T at speeds near some flutter inception speeds.

Flutter speeds of strut systems of different size and stiffness can be compared by using nondimensional parameters, provided in theory that all such parameters are equal for both systems. Available bending flutter data correspond in part to struts which are not nondimensionally equivalent. Two parameter ratios are customarily used to compare flutter characteristics: mass ratio and a nondimensionalized flutter speed. For bending motion, the mass ratio of a strut might be approximated as

$$\mu_{bending} = \frac{mL}{\pi \rho b^2 \ell}$$

Following a common approach to nondimensionalizing flutter speed, the parameter

$$\frac{2U_f}{c\omega_h}$$

serves to incorporate to some extent both strut inertia and strut bending stiffness.

When available bending flutter data for struts without pods or foils are plotted using these parameters, one trend is clear (see Figure 21):[16,17] the flutter speed ratio rises monotonically as $\mu_{bending}$ increases. Comparisons of data for specific models further show that the flutter speed ratio rises as sweep parameter κ increases. Data obtained by Huang[16] and Baird et al.[4] for nondimensionally equivalent (i.e., scaled) models show good agreement. Other data, corresponding to struts having a number of differences including elastic axis location, do not correlate with respect to κ. It is concluded that although these data can provide a rough estimate of flutter speed for certain strut classes, they are insufficient to establish any broadly applicable quantitative stability boundaries for simple struts. The two bending flutter conditions obtained for a strut with pod and foils may require more exact analysis procedures and therefore are not included in this nondimensionalization.

TORSIONAL FLUTTER MODE

General Characteristics

Torsional flutter was an instability of a different hydroelastic mode than bending flutter. The instability occurred in the hydroelastic mode which had the second lowest frequency, and had a predominantly first torsion mode shape at zero speed. Torsional rather than bending flutter always occurred when those zero-speed characteristics existed except when a foil was present.

---

[16] Huang, T.T., "Experimental Study of a Low Modulus Flutter Model for Strut-Foil-Pod Configurations," Hydronautics, Inc. Technical Report 459-2 (Jul 1967).

[17] Hilborne, D.V., "The Hydroelasticity of Struts," Admiralty Research Laboratory (Great Britain) Report ARL/R1/G/HY/5/3 (1958).

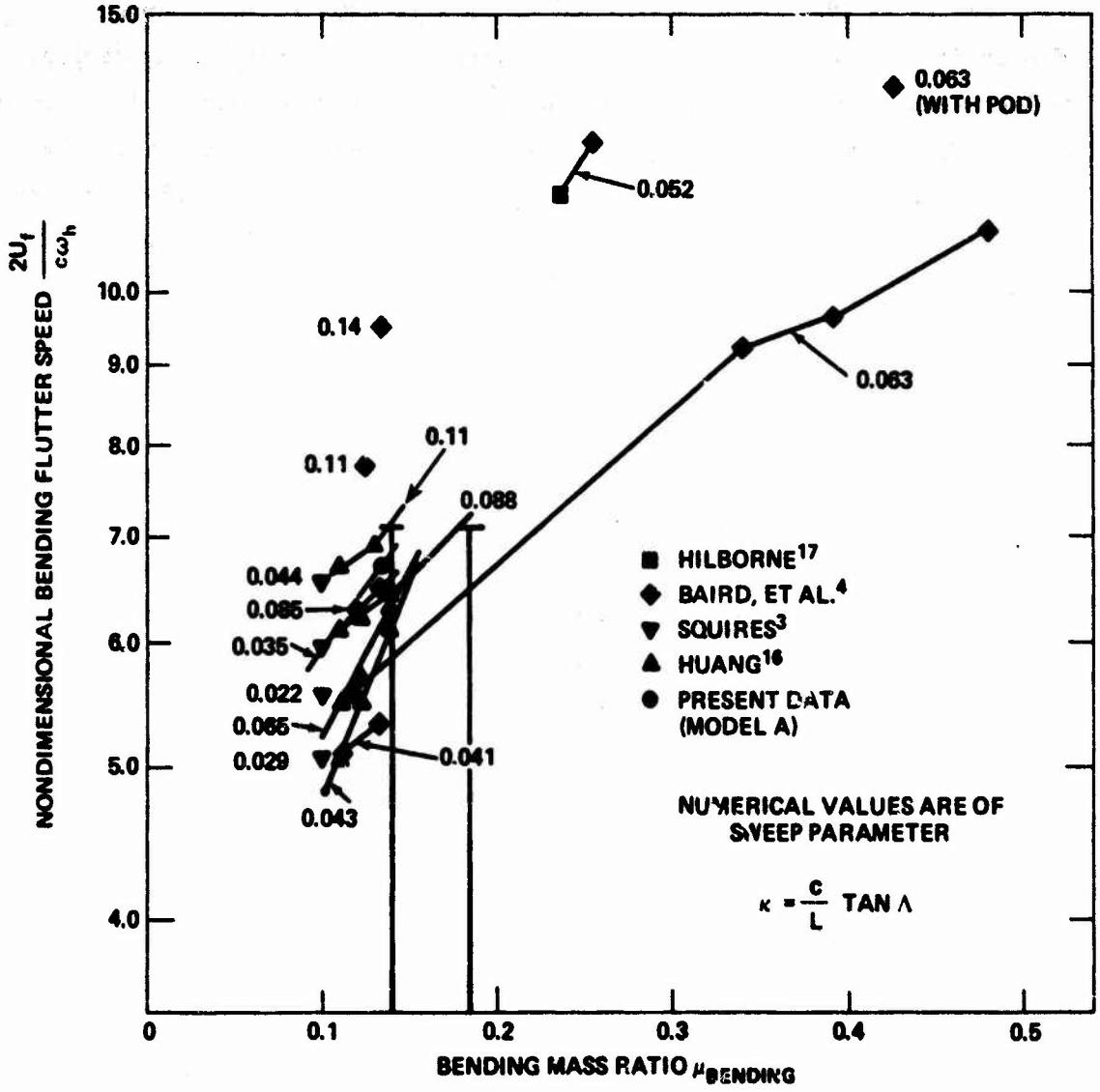

Figure 21 - Nondimensional Flutter Speed as a Function of Bending Mass Ratio for the Bending Flutter Mode of Hydrofoil Strut Systems

The torsional flutter mode displayed distinctively different damping and frequency characteristics from those of the bending flutter mode. As speed increased, damping initially increased for lightweight pod systems, remained constant for moderate weight pod systems, and decreased for heavy pod systems. Peak damping values were as high as 15 percent for the lighter weight systems, but the peaks were usually much lower. Higher flutter speeds were associated with initially increasing damping, higher peak values, and more rapid decreases to zero damping. An attached foil produced a rapid initial increase in damping, a high damping peak, and a rapid decrease to zero, similar to the behavior of lightweight pod systems. The frequency of the unstable mode remained almost unchanged from its zero-speed value throughout the speed range up to flutter.

Important Flutter Speed Parameters

All parameters investigated for the torsional flutter mode had an important effect on flutter speed: strut cavitation, strut submergence, pod moment of inertia, pod length, and presence or absence of a foil.

The largest variation of flutter speed was produced by changing pod moment of inertia $I_{y,\ pod}$. The effect of this parameter was exemplified by the behavior of Model 2T, as shown in Figure 14. Increasing $I_{y,\ pod}$ monotonically decreased the torsional flutter speed. The rate of decrease became less as $I_{y,\ pod}$ increased. For values of $I_{y,\ pod}$ smaller than those used in the present study, previously obtained data[4] (also shown in Figure 14) suggest a continual rise in torsional flutter speed until flutter occurred in the bending mode, which had become less stable than the torsional mode. A qualitatively similar trend in flutter speed as a function of $I_{y,\ pod}$ was found for all other torsional flutter data. From a comparison of the Pod C and D configurations of Model 2T, $I_{y,\ pod}$ is seen to be the parameter that governs torsional flutter speed of strut-pod systems rather than pod weight which usually also varied. The moment of inertia I_y of the foil appears to act additively with that of the pod.

The second strongest effect on torsional flutter speed was produced by varying the strut cavitation pattern. A cavity originating at the leading edge of one strut lowered the flutter speed 35 percent compared to the same strut with a base cavity aft of the strut. Comparisons for another configuration of the same strut (Model Beta) showed that a base-cavitating strut was 17 percent less stable than a noncavitating strut. It was further noted that the flutter inception speeds for two configurations of Model 2T virtually coincided with the occurrence of symmetrical leading-edge ventilation. These results suggest that the greater the amount of cavitation on a strut, the less stable it will be. Cavitation which originates at the leading edge and completely envelopes a strut on both sides may be particularly destabilizing.

Strut submergence also had a strong effect on torsional flutter speed. A blunt-based strut (Model 2T) had a minimum flutter speed at about 50-percent submergence; see Figure 15. Flutter speed increased rapidly at 20-percent submergence and would have disappeared had some shallower depth been investigated. A less strong variation would be expected for the deeper submergences. However, a strut enveloped in cavitation was quite insensitive (with respect to torsional flutter) to a change in submergence from 52 to 28 percent. This result suggests that the following mechanism governs the effect of strut submergence on torsional flutter. When both sides of a strut are in full contact with the flow, all submerged areas of the strut strongly participate in the hydroelastic behavior, along with the pod wetted area. When the strut is fully cavitating, the hydrodynamic effect of the strut is much weaker and the pod may play a dominant role. It was noted that the bending flutter speed did vary with submergence; an explanation might be found in a detailed analysis of the strut, pod, and foil hydrodynamics.

When increasing pod length decreased flutter speed by approximately 29 percent for Model Beta, the importance of this parameter and of

pod hydrodynamics in general was established. As suggested above, pod length may be of greater importance when strut loading is decreased by cavitation (or other considerations).

The presence of an attached foil was of least importance to the torsional flutter mode. The slight change in flutter speed that did occur might have been due to the increase in combined pod-foil moment of inertia I_y rather than to any effect of the increase in wetted area of the strut system or to the increase in a second component of moment of inertia I_ϕ.

Nondimensionalization of the torsional flutter speed boundaries can be carried out in a manner similar to that used for bending flutter. An approximate form for the mass ratio of a torsionally vibrating strut-pod system is

$$\mu_{torsion} = \frac{I_{y,\ strut} + I_{y,\ pod}}{I^*_{y,\ strut} + I^*_{y,\ pod}}$$

where

$$I^*_{y,\ strut} = \frac{\pi \rho c^4 \ell}{16} \left(1/8 + \left(\frac{2 x_{ea}}{c} - 1\right)^2\right)$$

A corresponding dependent stability parameter is

$$\frac{2 U_f}{c \omega_\alpha}$$

in which flutter speed is nondimensionalized by the in-air torsional frequency.

The nondimensional flutter speed, based on measured values of ω_α, is plotted as a function of $\mu_{torsion}$ for all existing torsional flutter data in Figure 22.[18,19] Cavitating struts were treated the same as non-cavitating struts in calculating $\mu_{torsion}$. Many of these data correspond to strut systems which were not equivalent in one or more nondimensional parameters. Systems which were similar exhibited a minimum value of 2 $U_f/c\ \omega_\alpha$ near $\mu_{torsion} = 2$. There was a marked tendency for the flutter speed ratio to rise at low and high values of $\mu_{torsion}$. The minimum value for 2 $U_f/c\ \omega_\alpha$ was 0.71 for fully wetted or base cavitating struts and 0.62 for cavitating struts. At present, these values constitute lower bounds for the flutter speed of the torsional flutter mode for a strut with an attached pod. However, the data base for these bounds is inadequate to establish general stability rules, and additional data could well indicate a downward revision.

The destabilizing influence of cavitation can be much larger than the above values indicate. In a direct comparison between base cavitating and cavity-enveloped strut systems at $\mu_{torsion} = 1.1$, the larger amount of cavitation produced a 35-percent decrease in flutter speed. Future experimentation should emphasize variations in parameters which are known to affect flutter speed strongly, e.g., strut cavitation.

Data for struts with foils, included in Figure 22, are too sparse to permit inferring any general stability trends. $\mu_{torsion}$ for these models was calculated by adding the foil moment of inertia $\bar{I}_y$ to that of the strut and foil in the given expression. This calculation may not be sufficiently accurate to permit comparison with struts without foils but is included for reference.

---

[18] Abramson, H.N. and G.E. Ransleben, Jr., "An Experimental Investigation of Flutter of a Fully Submerged Subcavitating Hydrofoil," Journal of Aircraft, Vol. 2, No. 5, pp. 439-442 (1965).

[19] Besch, P.K. and Y.-N. Liu, "Flutter and Divergence Characteristics of Four Low Mass Ratio Hydrofoils," NSRDC Report 3410 (Oct 1970).

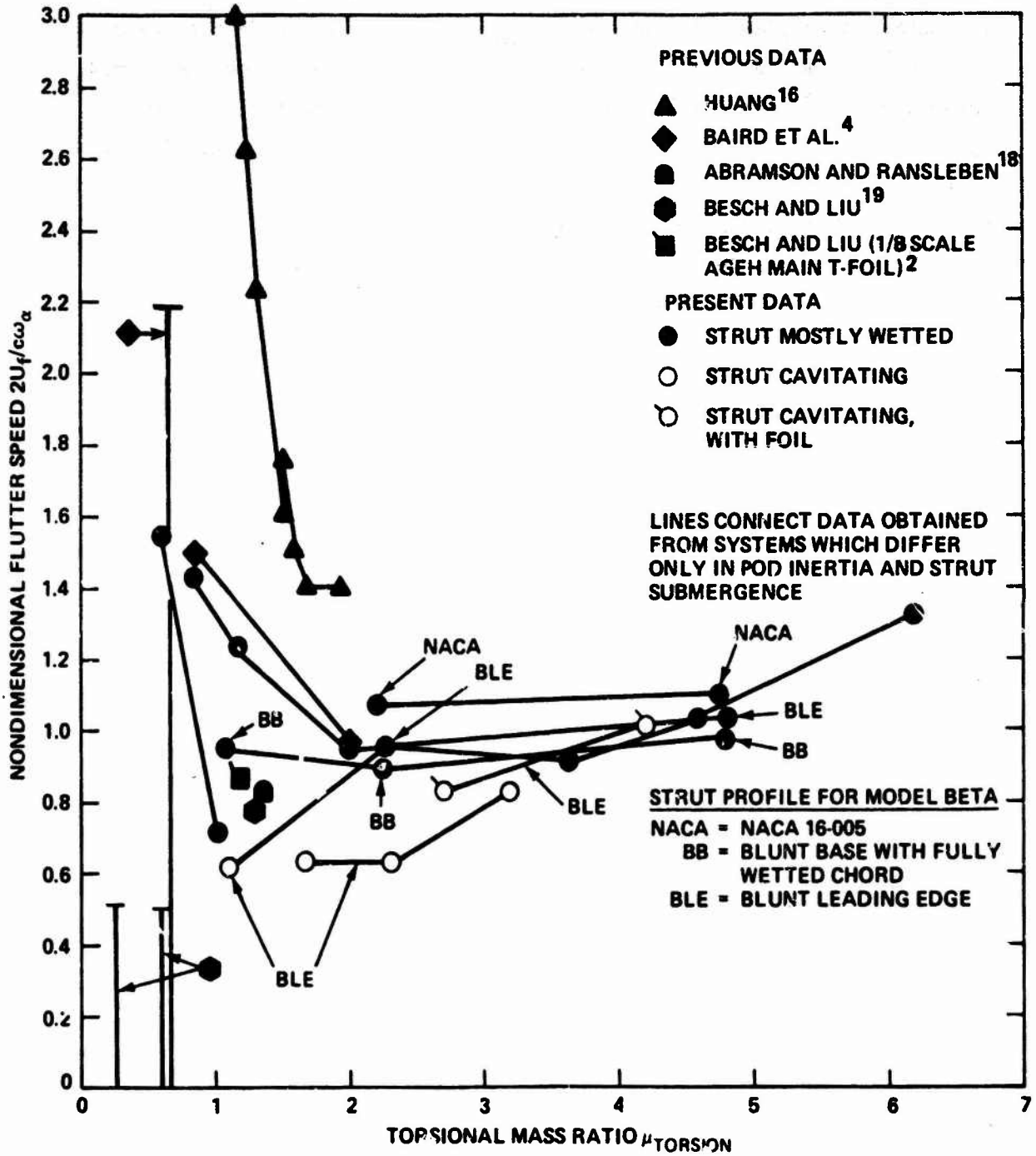

Figure 22 - Nondimensional Flutter Speed as a Function of Torsional Mass Ratio for the Torsional Flutter Mode of Hydrofoil Strut Systems

RELATIVE STABILITY OF BENDING AND TORSIONAL FLUTTER

As pointed out earlier, the mode shape of the second vibration mode can be used to predict which mode of flutter will occur at a lower speed. No exceptions to this method have been found for simple struts and struts with pods. Even Model Beta, which had very closely spaced second and third mode frequencies, behaved as a torsion-type strut when no foil was attached.

When the second and third modes are strongly coupled, however, it might be difficult to determine the predominant components of the second mode. Two observations may be helpful in such an instance:

1. Torsional flutter is believed to correspond to in-phase deflection of the strut leading edge due to bending and torsion components of the second vibration mode.

2. Such strong coupling indicates that bending and torsional flutter speeds are relatively close to each other; thus it is less important that they be differentiated.

It was not possible to predict the less stable mode of flutter when a foil was added to a strut-pod system. Use of the second vibration mode for this purpose, as for strut-pod systems, was questionable because of the extremely small amount of data available on strut systems with foils. The present data for Model Beta, given in Table 3, show that bending flutter can occur for a strut-pod-foil system even when the second vibration mode is predominantly first torsion. Separation into bending-type and torsion-type struts is therefore not feasible in the presence of a foil.

Although the relative stability of the two flutter modes could not be determined confidently, it was clear that both modes became unstable at nearly the same speed in the presence of a foil. This result contrasts markedly with those for struts without foils where bending flutter had always occurred at much higher speeds than torsional flutter.

EVALUATION OF EXPERIMENTAL TECHNIQUES

Zero damping must be detected in order to determine flutter speeds experimentally. The present data show that damping which decreases very rapidly prior to flutter produces large-amplitude oscillations, indicating flutter speed with very little "overshoot" into the speed range above flutter. No special provision for exciting strut oscillations need be provided, but a method for restricting oscillation amplitude might be required to prevent model failure. This type of damping behavior occurred for bending flutter and in some instances of torsional flutter wherein damping became high before decreasing to zero. This behavior helps to explain the close agreement obtained with the Squires result for Model A in bending flutter. A further evaluation of either the rapid sweep excitation technique or the mechanical impedance technique would be required in order to measure damping and frequency of such hydroelastic modes prior to flutter inception.

External excitation is required for detecting flutter inception when damping decreases gradually because amplitude-limiting effects keep oscillation amplitude at very low levels. Both line cut excitation and rapid sweep excitation appear to be satisfactory for this purpose. More advanced methods of analyzing rapid sweep data may be required under some conditions but have not yet been evaluated for flutter testing.

CONCLUSIONS

1. Flutter of cantilevered strut systems occurs in two independent hydroelastic modes, having predominantly first bending and first torsion mode shapes, respectively. The damping and frequency behavior of each mode is different.

2. Flutter inception speed of the bending flutter mode is affected by strut submergence and the presence or absence of a foil.

3. Flutter inception speed of the torsional flutter mode is affected by strut cavitation pattern, strut submergence, pod moment of inertia, pod length, and the presence or absence of a foil.

RECOMMENDATIONS

Now that a great deal of qualitative information is available on strut flutter characteristics, it would be desirable to obtain more quantitative information. Additional flutter experiments should be performed by using models which closely resemble existing strut systems on operational or conceptual hydrofoil craft. Since extensive cavitation has been found to be destabilizing, specific attention should be given to strut systems which may operate under cavitating conditions.

ACKNOWLEDGMENTS

This work was performed by the Special Systems Branch of the Ship Performance Department. Detail design and construction of the experimental apparatus were carried out by the Central Instrumentation Department and the Industrial and Facilities Directorate, respectively. Measurements of strut stiffness were made by the Structures Department. Spectral analyses were done by the Ship Acoustics Department. The report was published by the Technical and Administrative Services Department.

The authors gratefully acknowledge the helpful suggestions given by Mr. D.S. Cieslowski and Mr. K.R. Todack regarding the experimental approach, and the assistance of Mr. C.D. Bradley in designing the rapid sweep excitation system.

REFERENCES

1. Besch, P.K. and Y.-N. Liu, "Bending Flutter and Torsional Flutter of Flexible Hydrofoil Struts," Ninth Symposium on Naval Hydrodynamics, Paris, France (20-25 Aug 1972); also available as NSRDC Report 4012 (Feb 1973).

2. Besch, P.K. and Y.-N. Liu, "Hydroelastic Design of Subcavitating and Cavitating Hydrofoil Strut Systems," NSRDC Report 4257 (Apr 1974).

3. Squires, C.E., Jr., "Hydrofoil Flutter, Small Sweep Angle Investigation--Final Report," Grumman Aircraft Engineering Corporation Report DA Nonr-3989.3 (Nov 1963).

4. Baird, E.F. et al., "Investigation of Hydrofoil Flutter--Final Report," Grumman Aircraft Engineering Corporation Report DA 10-480-3 (Feb 1962).

5. Olson, R.E. and W.F. Brownell, "Facilities and Research Capabilities--High Speed Phenomena Division, David Taylor Model Basin, Langley Field, Va.," David Taylor Model Basin Report 1809 (Apr 1964).

6. Duncan, W.J., "The Flexural Centre or Centre of Shear," J. Royal Aeronautical Society, Vol. 57, pp. 594-597 (Sep 1953).

7. Caporali, R.L. and E.J. Brunelle, "Hydrofoil Instability at Low Mass Density Ratios," Princeton University Aerospace and Mechanical Sciences Report 670 (Mar 1964).

8. Rowe, W.S. and T.G.B. Marvin, "A Program of Theoretical Research on Hydroelastic Stability," The Boeing Company, Contract N00014-67-C-0248 (Nov 1968).

9. Brownell, W.F. and M.L. Miller, "Hydromechanics Cavitation Research Facilities and Techniques in Use at the David Taylor Model Basin," Symposium on Cavitation Research Facilities and Techniques, American Society of Mechanical Engineers (May 1964); also available as David Taylor Model Basin Report 1856 (Oct 1964).

10. Skingle, C.W., "A Method for Analyzing the Response of a Resonant System to a Rapid Frequency Sweep Input," RAE TR 66379 (Dec 1966).

11. Kandianis, F., "The Effects of Extraneous Noise on the Measurement of the Frequency Response of Structures under Transient Excitation," I.S.V.R. Technical Report 20 (Nov 1969).

12. Kandianis, F., "Frequency Response of Structures Excited by Transient or Random Forces Using Cross Correlation and Its Laplace Transform," I.S.V.R. Technical Report 47 (Aug 1971).

13. White, R.G., "Measurement of Structural Frequency Response by Transient Excitation," I.S.V.R. Technical Report 12 (Jan 1969).

14. White, R.G., "Use of Transient Excitation in the Dynamic Analysis of Structures," RAS Aero. J., Vol. 73, pp. 1047-1050 (Dec 1969).

15. White, R.G., "Use of Transient Excitation in the Measurement of the Frequency Response of Systems with Nonlinearities Arising from Large Deflections," I.S.V.R. Technical Report 27 (Feb 1970).

16. Huang, T.T., "Experimental Study of a Low Modulus Flutter Model for Strut-Foil-Pod Configurations," Hydronautics, Inc. Technical Report 459-2 (Jul 1967).

17. Hilborne, D.V., "The Hydroelasticity of Struts," Admiralty Research Laboratory (Great Britain) Report ARL/R1/G/HY/5/3 (1958).

18. Abramson, H.N. and G.E. Ransleben, Jr., "An Experimental Investigation of Flutter of a Fully Submerged Subcavitating Hydrofoil," Journal of Aircraft, Vol. 2, No. 5, pp. 439-442 (1965).

19. Besch, P.K. and Y.-N. Liu, "Flutter and Divergence Characteristics of Four Low Mass Ratio Hydrofoils," NSRDC Report 3410 (Oct 1970).

INITIAL DISTRIBUTION

Copies		Copies	
1	WES/LIBRARY	1	NAVSHIPYD CHASN/LIB
1	ONR 438/R. Cooper	1	NAVSHIPYD LBEACH/LIB
2	Chief of Naval Material (MAT 033)	1	NAVSHIPYD MARE 250
		1	NAVSHIPYD NORVA/LIB
1	NAVOCEANO 1640	1	NAVSHIPYD PEARL/LIB
1	NRL 2627 LIB	1	NAVSHIPYD PHILA 240
2	USNA 1 LIB 1 Van Mater	1	NAVSHIPYD PTSMH/LIB
		1	NAVSHIPYD BREM/LIB
1	NAVPGSCOL LIB	5	NAVSEC 1 SEC 6034B 2 SEC 6110 1 SEC 6114 1 SEC 6136
1	NROTC & NAVADMINU, MIT		
1	NAVWARCOL		
8	NAVSEA 1 SEA 032 1 SEA 0322/Schuler 1 SEA 03221/Benen 1 SEA 033 1 SEA 034 1 SEA 035 1 SEA 037 1 PMS-303	1	AFFDL/FYS/Olsen
		12	DDC
		1	HQS COGARD
		1	COGARD/MERCH MARINE SAFETY
		1	LC/SCI & TECH DIV
1	FAC LIBRARY	1	MARAD
1	NAVAIRDEVCEN ADL	1	MMA LIB
1	NELC LIB	1	NASA LANGLEY RES CEN/E. Yates
1	CIVENGRLAB L31 LIB	1	NASA STIF
1	NSWC DAHLGREN/LIB	1	NSF ENGR DIV LIB
1	NPTLAB NUSC/LIB	1	U BRIDGEPORT/Uram
1	NLONLAB NUSC	1	U CAL BERKELEY/DEPT NAME
		1	U CAL NAME/Paulling

Copies		Copies	
1	U CAL NAME/Schade	1	U MICHIGAN NAME/Ogilvie
1	U CAL NAME/Wehausen	1	U MINNESOTA SAFHL
3	CIT 1 Acosta 1 Plesset 1 Wu	1	U MINNESOTA SAFHL/Killen
		1	U MINNESOTA SAFHL/Schiebe
		1	U MINNESOTA SAFHL/Song
1	COLORADO STATE U/Albertson	1	U MINNESOTA SAFHL/Wetzel
1	U CONNECTICUT/Scottron	1	NEW YORK U/Pierson
1	CORNELL U/Sears	2	NYU COURANT INST 1 Peters 1 Stoker
1	HARVARD U/Birkhoff		
1	U ILLINOIS/Robertson	1	NOTRE DAME/Strandhagen
3	U IOWA IHR 1 Kennedy 1 Landweber 1 Rouse	1	PENN STATE U ARL
		1	PENN STATE U/B. Parkin
1	KANSAS ST U ENGR EXP/ Nesmith	1	ST JOHNS U/Lurye
		3	SWRI 1 Abramson 1 Ransleben 1 Applied Mech Review
1	LEHIGH U FRITZ ENGR LAB LIB		
1	U MARYLAND/Cunniff	1	STANFORD U DEPT CIV ENGR/ Perry
1	MIT OCEAN ENGR/Abkowitz		
1	MIT DEPTH OCEAN ENGR/ Kerwin	1	STANFORD U/Street
		1	STANFORD U/Ashley
1	MIT OCEAN ENGR/Leehey	1	STANFORD RES INST LIB
1	MIT OCEAN ENGR/Mandel	3	SIT DAVIDSON LAB 1 Breslin 1 Tsakonas 1 Lib
1	MIT PARSONS LAB/Ippen		
1	U MICHIGAN NAME/Benford		
1	U MICHIGAN NAME/Couch	1	UTAH STATE U/Jeppson

Copies	
2	WEBB INST 1 E. Lewis 1 L. Ward
1	WPI ALDEN HYDR LAB LIB
1	SNAME
1	AEROJET-GENERAL/Beckwith
1	BELL AEROSPACE/ New Orleans/BACNOO
1	BELL AEROSPACE/ Buffalo/G.C.C. Smith
1	BETHLEHEM STEEL SPARROWS/ A. Haff
10	BOEING AEROSPACE GROUP 1 R. Barbar 1 H. French 1 R. Hatte 1 R. Hubard 1 T. Marvin 3 C. Ray 1 W. Rowe 1 F. Watson
2	BOEING ADV MAR SYS DIV 1 M. Kiehle 1 Longfelder
1	CORNELL AERO LAB APPL MECH
1	GEN APPL SCI LAB/F. Lane
1	GEN DYN ELEC BOAT/ Boatwright
1	GIBBS & COX
2	GRUMMAN AEROSPACE 1 W. Carl 1 Wright
2	HYDRONAUTICS 1 P. Eisenberg 1 M. Tulin

Copies	
4	LOCKHEED MISS & SPACE 1 R. Kramer 1 R. Lacy 1 R. Perkins 1 R. Waid
2	DOUGLAS AIRCRAFT 1 Hess 1 Smith
1	NEWPORT NEWS SHIPBUILDING LIB
1	OCEANICS/Kaplan
1	ROBERT TAGGART
1	ROHR SES DIV/E. Marmentini
1	TETRA-TECH Pasadena, Calif./E. James

CENTER DISTRIBUTION

Copies	Code	
3	1150	
1	1154	
1	1170	D. Jewell
1	1500	
1	1502	
1	1504	
1	1506	
1	1507	
1	1520	
1	1524	Y. Shen
2	1532	
1	1540	

Copies	Code	
1	1542	
1	1552	
32	1556	P. Besch (15) D. Coder E. Rood (15) R. Rothblum
1	1560	
2	1572	
1	1576	
2	1966	J. Caspar Y.-N. Liu
30	5211	Reports Distribution
1	5221	Library (C)
1	5222	Library (A)

DTNSRDC ISSUES THREE TYPES OF REPORTS

(1) DTNSRDC REPORTS, A FORMAL SERIES PUBLISHING INFORMATION OF PERMANENT TECHNICAL VALUE, DESIGNATED BY A SERIAL REPORT NUMBER.

(2) DEPARTMENTAL REPORTS, A SEMIFORMAL SERIES, RECORDING INFORMATION OF A PRELIMINARY OR TEMPORARY NATURE, OR OF LIMITED INTEREST OR SIGNIFICANCE, CARRYING A DEPARTMENTAL ALPHANUMERIC IDENTIFICATION.

(3) TECHNICAL MEMORANDA, AN INFORMAL SERIES, USUALLY INTERNAL WORKING PAPERS OR DIRECT REPORTS TO SPONSORS, NUMBERED AS TM SERIES REPORTS; NOT FOR GENERAL DISTRIBUTION.